Politecnico di Torino

Master’s degree: Energy engineering
A.y. 2021/2022
Degree session: October 2022

Energy assessment of a geothermal heat pump system in a residential context

Cooling season 2022

Supervisors:
Prof. Marco Barla
Prof. Davide Papurello
Ing. Alessandra Insana

Candidate:
Barotto Luca

Abstract

The main goal pursued by this thesis work was that of assessing the cooling performance of a novel shallow geothermal energy system, located on the north-east side of the Energy center (Turin).
From a technical point of view, the project laid its roots on the data provided by the sensors installed on the NIBE F1155 heat pump, which are reported on a ".txt" file generated by the electronic control unit.
This file was processed by a MATLAB script which, based on the hypothesis assumed, performed all the calculations with the aim of achieving the desired performance parameters, relying on CoolProp databases to derive the required thermodynamic quantities.
To achieve these results, different considerations were made in terms of the correct approach to obtain a good modelling for the heat pump system, also compensating for the lack of some fundamental data, as the pressure levels of the heat pump cycle.
This particular aspect led towards the consideration of two parallel methods, consisting in a fixed pressures approach and a variable pressures one, with the aim of performing a further step regarding the representation of the system operation. Specifically, the first provided few guidelines representing then the basis for the variable pressures one, defining the operative ranges and anticipating the expected results, finally arranged on daily basis and reported in the form of graphs.
To assess the reliability of the thermodynamic properties calculated, representing a key aspect to guarantee the convergence of the pressure calculation algorithm (variable pressures method), they were all verified with CoolPack by computing and analysing the related percentage deviation.
Final considerations were also reserved to the heating season, with a global overview of an experimental campaign led in October 2019, obtaining so a more complete set of results regarding both the heat pump modes of operation.
At the end, basing on the outputs derived from the large amount of experimental evidences, both the cooling and heating operation reported good performances, so the first one was further investigated through a more detailed analysis regarding the indicative volume that could be actually cooled.

Summary

Table of figures

1. Thesis structure and expected achievements

The performance evaluation to be carried out, regarding the GeothermSkin energy system installed in the Energy Center, aimed to test the operation of this prototype and to detect eventual drawbacks which may limit its application in a residential setting.

The pursuit of those results passed through the determination of the main thermodynamic quantities of the system: the thermal power exchanged at the evaporator/condenser, the compression work, the refrigerant flow circulating and finally the calculation of the COP. The starting point of the analysis was represented by the data acquired through the heat pump sensors, at a selected sampling rate of one minute.

This information was exploited to derive the thermodynamic quantities needed, first calculated as instantaneous values, employing a Matlab script realized to speed up the calculations, then averaged over selected periods of 24 hours to better handle the field measurements.

The calculation procedure was accompanied by many counterchecks, performed using the CoolPack software, to verify the consistency of the results obtained.

Regarding the structure of the thesis, it was conceived as a pathway which started from a general overview of the current energy and geopolitical situation, mentioning the main targets and policies involved on a more global scale, especially regarding the renewable energy penetration and the energy demand for buildings.

These first topics were reported in the introductory section, then followed by a deeper discussion concerning the origin of the geothermal energy source and its main applications.

As the NIBE F1155 heat pump played a central role in the energy system analysed, the general concept and the operating principle of these systems were explored in dedicated sections, which concluded with a general overview of the geothermal heat pumps field.

From that point on, the discussion focused on the experimental field description, presenting the main realization phases and both the user and ground side arrangement, with a special mention for the sensors location.

After the experimental setting characterization, and the illustration of the system operating principle, the following sections involved the main topic: the

assessment of the cooling performance during the summer season (considering June 2022 experimental campaign), which represented the actual starting point of this thesis work and the personal contribution to the ongoing study.
The two parallel methods adopted, with fixed and variable pressures levels, were then exposed in the relative sections, reporting the main results and discussing the main problems involved with the tested approaches, together with some final considerations about the trends.
After a shorter parenthesis regarding the coolable volume and the geothermal probes surface scalability, always for the cooling operation analysed, a general overview was provided for the heating operation too, based on the data coming from the previous years. The results coming from these last sections were then considered together with those obtained for the cooling operation, to broaden the point of view, concluding with a final discussion about the general performance of the Geothermskin system.

2. Introduction

Observing the global condition in recent years, the energy sector has been and still is affected by the COVID-19 pandemic, together with the current economic and geopolitical developments.
The aftershocks from pandemic upset the renewable supply chain, representing a transformative event which was accompanied by a rise in the commodity prices.
Unfortunately, the historical chance for a green recovery post-COVID-19 has been lost and the February 2022 invasion of the Ukraine exacerbated even more the crisis that we are experiencing.
This invasion carried out by the Russian Federation impacts on the prices for fossil fuels, that were already spiking in late 2021, rising discussions on the role of the renewables around the theme of energy security.
The current situation stands at a crossroads, requiring a necessary and urgent decision about continuing to support a fossil fuel-based energy order, or accelerating the development of modern renewables and energy efficiency.
A further delay from decision makers would lead to consequences regarding not only the climate change, but also economic and political vulnerability that could lead to the treat of energy poverty for billions of people.
Among these events, a record growth in renewable energy deployment was reached in 2021, with a penetration around 28,3% in the global energy mix and more than 314 GW added in terms of power capacity.
After the decline in 2020, a market rebound in solar thermal and biofuels has in fact improved the outlook for renewables in heating and transport sectors, boosting the investments in renewable power and fuels.
On the other side there are still factors which slow down the shift towards a renewables-based energy system, such as the rebound in worldwide energy demand of 2021.
This additional demand largely met with coal and natural gas, recalling again the problems of CO_2 emissions and the subsidies still reserved to fossil fuels.
Talking about global commitments, the International Energy Agency's (IEA) set the Net Zero by 2050 scenario, released in May 2021, stimulating higher ambitions among governments and corporations.

After the COP26, held in Glasgow in November 2021, seventeen countries promised to reach net zero emissions by 2050 or a later date, while some countries target 2025.
The European Commission increased the 2030 target for renewables in total final energy consumption (TFEC) first to 40% in 2021, then to 45% in early 2022.
The Glasgow Climate Pact emerged calls on countries to raise their ambition annually instead of every five years, and for the first time in history of UN climate agreements, it explicitly acknowledged the need to reduce fossil fuel use.

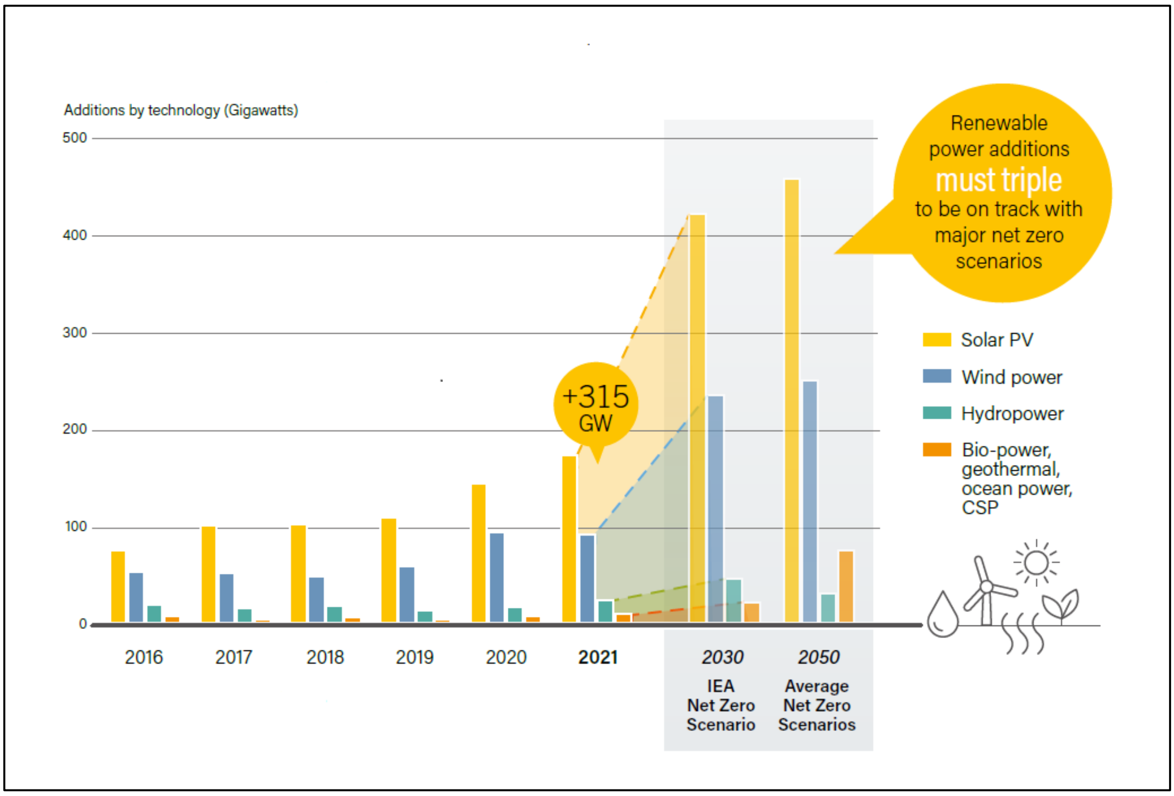

Figure 1: Renewable power capacity annual growth, Renewable 2022 Global status report

From *Figure 1* it is possible to get an idea about the IEA Net Zero Scenario, where the added capacity of almost 315 GW is highlighted for 2021, coming from a renewable power capacity additions growth of 17%.
Even if a growth of renewable energy capacity can be noticed over the years, these trends remain far from the deployment needed to keep the world on track to reach net zero emissions by 2050, which would require a yearly renewable additional capacity of almost 815 GW.
Anyway, an important fact is that most of the global power capacity newly installed in 2021 was renewable, continuing the trend since 2012 (reaching the record of 84% share in net power additions).

2.1 Renewables in buildings

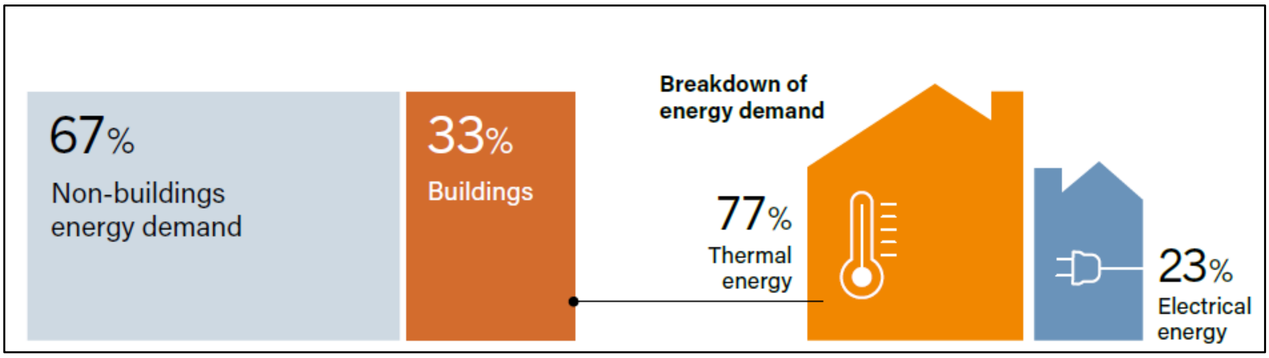

Figure 2: Energy demand for buildings (2019), Renewable 2022 Global status report

Moving from the production side to the consumption one, the global final energy use data shows that roughly one third of the total is reserved to buildings, then subdivided into thermal and electrical end-uses.

In 2019 almost 14,7% of building energy use was estimated to come from renewables, with a growth of 4% with respect to 2012.

The energy use in buildings rose of almost 1% per year between 2009 and 2019, while the situation changed in 2020 with the COVID-19 pandemic.

The effects led to a temporary decrease of the demand, as the pattern moved towards less energy intensive residential applications, instead of commercial buildings, but later it came back towards the previous values.

This increase observed in the energy use made building operations responsible for almost 27% of global greenhouse gas emissions in 2020, together with a negative air quality impact coming for example from the combustion of natural gas for cooking.

Talking about the end-uses of this energy demand, two main categories can be mentioned:

- **Thermal end-uses**: referring to space heating and cooling, water heating and cooking.
- **Electrical end-uses**: referring to major appliances such as lighting, refrigerators and washing machines.

Globally, around 77% of building energy use is thermal and 23% is electrical, while generally increasing the use of renewables tends to be more challenging from the thermal perspective.

In 2019 the share of modern renewables to supply heating and cooling was estimated around 10,7%, with an increase of almost 3% with respect to 2009.
The main portion of the thermal use in buildings is represented by the heating demand, even if the cooling demand has been growing too in the last years, but most of it is provided by electrical devices, linking to the electrical end-uses.
Among the renewable heating supply, the direct use of modern renewables supplies almost two-third of the total, while the rest comes from sources like electricity and district heating.
Most of the direct heat is represented by bioenergy, while sources such as solar and geothermal accounted for respectively 1,4% and 0,9% in 2019, but they annually increase their share.
Bioheat, both supplied by stand-alone systems and delivered through district heating networks, rose 10% in the EU between 2015 and 2020, and also the global market of solar thermal collectors expanded in 2021, recovering from a decline period experienced in the previous years.
Solar heat finds its application both in stand-alone systems used for water heating, or even providing space heating via district heating.
Notably, space heating accounts for around 39% of geothermal direct use, while the overall installed geothermal capacity for heating has followed a growing trend with an annual increase around 7-8% in recent years.
The market for renewable heat technologies (such as heat pumps) has been boosted also by the rising electrification of energy use in buildings, with a growth in the use of renewable electricity to generate heat around 5,3% per year between 2009 and 2019.
On the other end, especially looking at the emerging countries, a significant share of global heating demand in buildings continues to be satisfied through the traditional use of biomass.

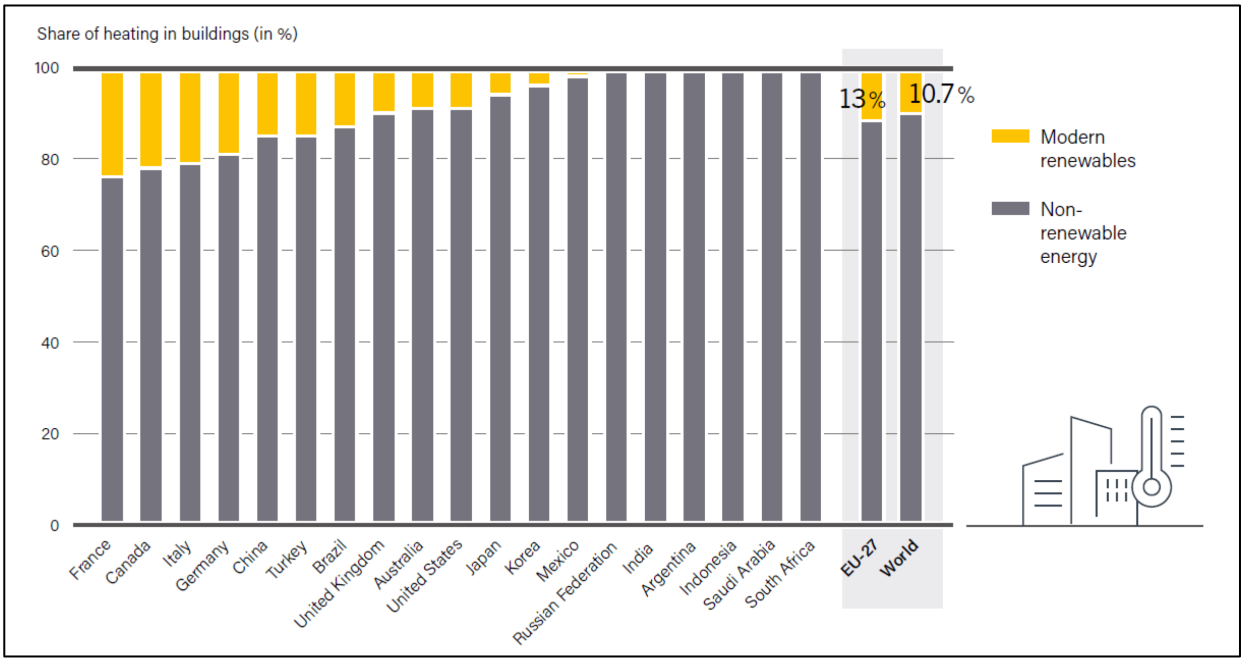

Figure 3: Share of Renewable Heating in Buildings, G20 Countries, 2019

A key factor to increase the renewables penetration in buildings consists in the mitigation of the total energy demand growth, both talking about heating and cooling.
Moving towards this direction, global policy efforts have been implemented to improve the energy efficiency and slow down the growing trend of the buildings energy demand.
Precisely, the slow growth of the renewable energy penetration in buildings and the consistent share of emissions in the building sector drew the attention of the governments to renewable heating and cooling, focusing in three main areas:

- **Pricing policies**: carbon pricing, emissions trading, taxation.
- **Financial support policies**: subsidies and rebates.
- **Regulatory policies**: targets, mandates, building codes and bans.

On the European scene there are many examples, such as the UK Heat and Buildings Strategy launched in 2021, offering grants to the householders for installing of renewable heat technology and moving towards the restriction of the sale of fossil fuel boilers.
Following the same trend, France announced in early 2022 an increase in the financing scheme, aimed at substituting fossil fuel heating systems with

renewable ones, while in Germany was introduced a national trading system applied to heating fuels.
Also at a global level, other countries have been involved, such as USA, Canada and China, aiming at the substitution of fossil fuel heating systems with the introduction of similar policies.
In Italy the Superbonus 110% scheme of 2021 introduced tax reductions up to 110% in the cost of replacement of the existing heating system with an efficient renewable-based one, regarding residential or commercial buildings.
In summary the measures adopted move towards new building energy codes, that promote electrification and high-level policy plans to address heat in buildings. Anyway, the bad aspect which undermines the effectiveness of this general policy development is that in many cases there still are incentives for fossil fuels appliances.

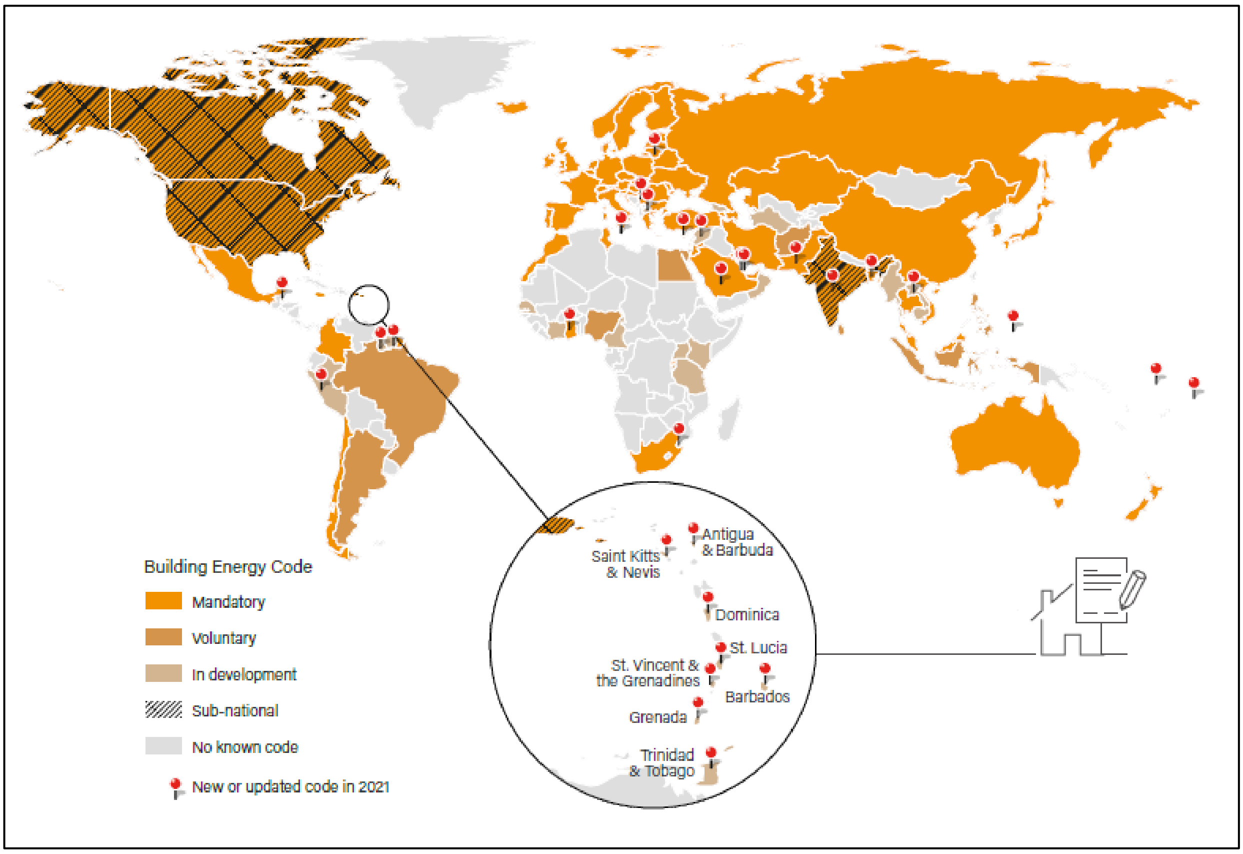

Figure 4: Coverage of Energy Codes for New Buildings, 2021, Based on GlobalABC and IEA

3. Geothermal energy

The geothermal energy is a form of renewable energy which derives from the heat of the Earth, harnessed by using the thermal and pressure differentials in the Earth's crust and meant either to supply thermal energy directly or to generate electricity.
The key resource for this kind of green energy is so represented by the Earth itself, as the geothermal heat derives from the original formation of the planet and from the nuclear decay of radioactive isotopes of uranium, thorium and potassium occurring in its nucleus, mantle and crust.

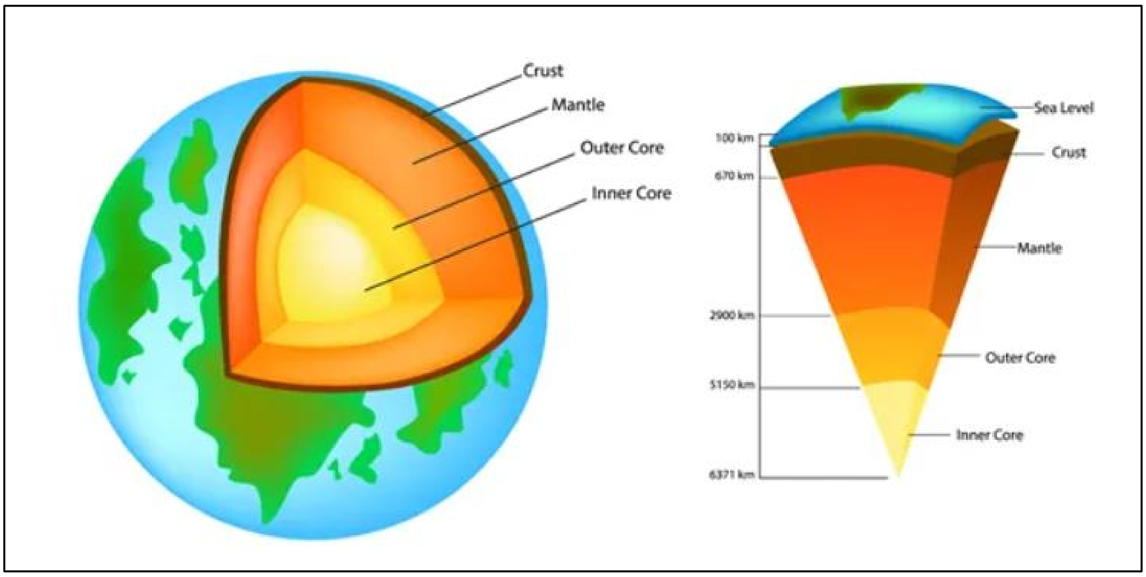

Figure 5: Structure of the Earth, from Shalom education

Compatibly with the observations and the tectonic theory, the Earth's structure can be subdivided into three main layers by <u>chemical composition</u>:

- **Crust**: the rigid outermost layer of the planet, segmented in different plates of two types, oceanic and continental. The first one is the youngest (<180 million years old), composed of basalts, while the second one is the oldest (>3,8 billion years old).
- **Mantle**: comprises almost 82% of the Earth's volume, being around 2900 km thick. It can flow plastically at very slow rates.
- **Core**: composed of iron, nickel and minor elements it can be subdivided into two additional shells, an inner one and an outer one.

The outer core is liquid and represents the source of the Earth's magnetic field, while the inner one is solid.

A similar layering of the Earth's structure can be realized by physical properties, deriving five main regions:

- **Lithosphere** (0 to 100 km): very stiff and fractured into a few large plates, whose movement can deliver heat to the surface, especially close to the spreading boundaries (plates moving apart).
- **Aesthenosphere** (100 to 600 km): hot region that flows like a molasses.
  The heat originated from the radioactive decay is carried away by the circulation of the Earth's interior, so it is delivered to the surface through convection mechanism.
- **Mesosphere** (660 to 2900 km): called also lower mantle, where the rock gradually strengthens with depth but can still flow.
- **Outer core** (2900 to 5170 km): liquid and composed of iron-nickel alloy, here the convective motion generates the Earth's magnetic field.
- **Inner core** (5170 to 6378 km): solid and composed of iron-nickel alloy, its solid state is due to the intense pressure which prevent it from melting.

The Earth's interior is so characterized by a progressive increase of temperature, pressure and density with the depth.
Notably, the increase of temperature with depth is called geothermal gradient, as most of the heat transport is vertical, except around hydrothermal and igneous intrusions.

$$\nabla T = \frac{dT}{dz}$$

Typical geothermal gradients in the Crust, depending on the site location and the geologic time, ranges between 25-30°C/km.
Unfortunately, the upwards heat transport caused by this gradient presents the problem that, in most areas, it reaches the Earth's surface in a diffuse state, making the exploitation of this resource uneconomical.
More in details this heat is believed to be transferred mostly by convection below the lithosphere, and mostly by conduction inside the lithosphere.

The geothermal systems able to exploit the heat form the Earth's interior can be distinguished depending on the temperature of the resource:

- **High enthalpy** resources (T>150°C): intended to produce electrical energy sending the geothermal fluid to the power plant, where it causes the rotating motion of a turbine, finally converted to electricity through an alternator.
- **Medium enthalpy** resources (90°C<T<150°C) and **Low enthalpy** resources (T<90°C): intended for the direct use of the heat from shallower soil (up to 100-200 m deep), such as SPA, building heating and cooling, district heating applications and more.

Focusing on the case of low enthalpy resources, the geothermal systems deal with the ground portion closest to the Earth's surface.
In addition to the geothermal gradient, the soil presents a seasonal zone of fluctuation in temperature.

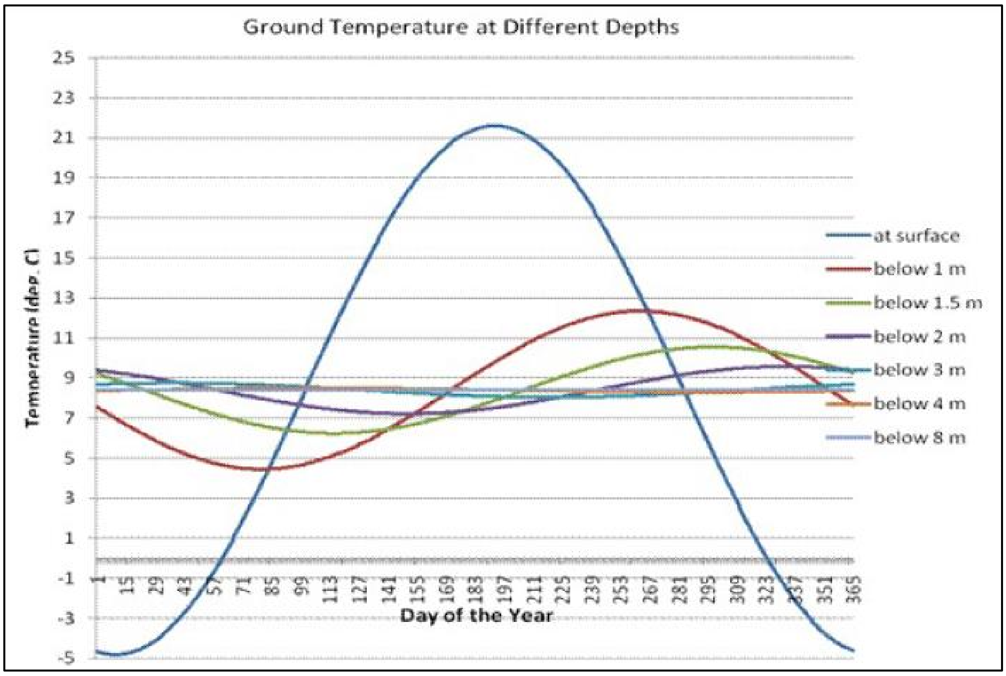

Figure 6: Temperature curves at different depths underground over the year

This layer partially reflects the trend of the external air temperature, which varies over the seasons, that is then progressively smoothed by going inside the ground. At a certain depth, typically around 10-15 m, the temperature becomes almost constant, becoming exploitable with suitable devices.

This is the case of the ground-source heat pump systems, able to couple a building with the ground, or a medium thermally connected to the ground, like groundwater.
The principal applications are space heating and cooling, even if hot water supply is also possible for domestic use, as the temperature of the water produced in that way makes it unexploitable for electricity production.
This kind of systems can be further distinguished between Closed-loop systems and Open-loop systems.

3.1 Open loop geothermal systems

The open loop geothermal systems involve the physical abstraction of water from a source by means of wells, this groundwater is sent to a heat pump for the extraction of the heat stored and then it is finally reinjected.

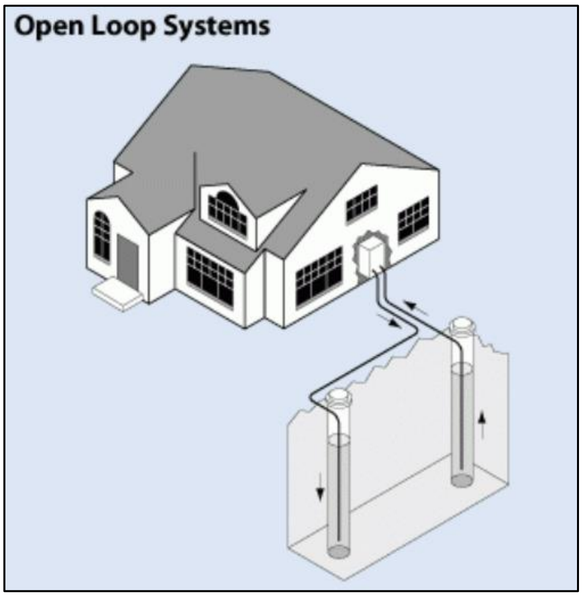

Figure 7: Example of open loop geothermal scheme (well doublet), from energy.gov

Many different technologies could be implemented:

- **Well doublet scheme**: requiring two separate wells, one for groundwater abstraction and the remaining one for the reinjection.
- **Standing column well**: requiring a single well both for abstraction and reinjection.
- **Single well**: requiring a well only for the groundwater abstraction, while the reinjection involves a lake, a pond or a river.

First, the construction of a ground-water open-loop heating or cooling system requires a suitable aquifer, able to yield enough water to support the required thermal load of the system.
In that situation there are some parameters which must be determined, such as the design depth of the well, its diameter and yield, together with information about the aquifer lithology.

If the groundwater is directly circulated through the evaporator or the condenser of the heat pump, a certain number of risks must be considered: the possible abrasion of the heat pump's pipework related to suspended particles, the possible precipitation of minerals such as calcite and the occurrence of corrosion phenomena linked to an excessive salinity.
Another crucial point is then represented by the disposal of the wastewater, that is a term adopted for the water at the outlet of the heat pump, which presents a different temperature.
The solution adopted must be preceded by a risk assessment and face several constraints from the authorities, often accompanied by a discharge fee.
The most typical options for water disposal involve:

- **Disposal to a surface water body**: the risk assessment must check the temperature variation caused by the injection, together with the geochemical compatibility and the flooding risk.
- **Re-injection to the abstracted aquifer**: attractive because of the few or no water resource implications, also minimizing any risk of ground settlement, but the wastewater may need to be sterilized and present a very low particle content.
  Another problem to be avoided is the reinjection of the wastewater too close to the abstraction well, as it would cause a short-circuit, increasing progressively the temperature of the water entering the heat pump.
- **Disposal to another aquifer**: particularly attractive if there is more than an aquifer below the site, allowing the abstraction of groundwater from an aquifer and the successive reinjection into another one.
  The main problems are related to the compromise of a resource or the negative impact on other users, such as the heat pollution in the form of a thermal plume (a body of warm or cold injected groundwater migrating with the natural groundwater flow).
- **Disposal to the abstraction well**: a portion of the wastewater is reinjected back into the upper part of the reinjection well, taking then a certain time to flow down and so being subjected to a temperature re-equilibration.
  Inside the well there will be a mix between new groundwater and wastewater, moving toward an equilibrium situation.
- **Disposal to the sewer**: it must have the excess capacity to accept the wastewater flow, and the permission of the sewer owner is required.

Among the main advantages of the open loop systems, can be mentioned the utilization of a natural medium (groundwater) at constant temperature and huge specific heat capacity, the fact that quality of the water extracted is not necessarily a key factor and the possibility to exploit also natural saline groundwater. Anyway, the most important factor is represented by the higher amount of heat extracted per well compared to closed loop systems, thanks to the forced convection of ground water rather than subsurface conduction.
The main disadvantages are represented by the geology dependency, linked to the presence of a suitable aquifer, the pumping costs to extract groundwater and the risk of fouling and clogging of the heat exchangers.

3.2 Closed loop geothermal systems

Closed loop geothermal systems do not require any water to be abstracted or reinjected at all, as they work using the ground as a big heat exchanger, exploiting the subsurface conduction mechanism to transfer heat.

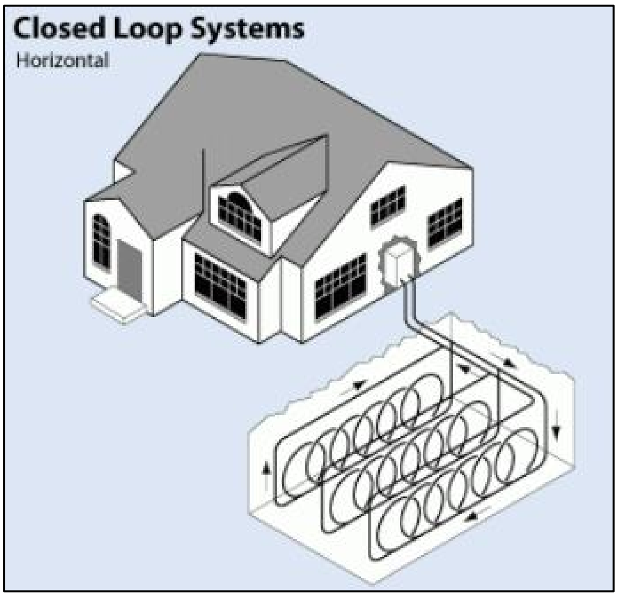

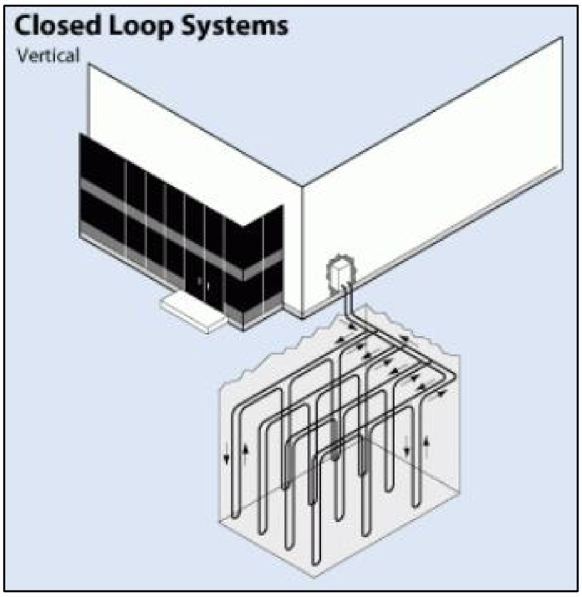

Figure 8: Example of closed loop geothermal scheme, horizontal (left) and vertical (right) from energy.gov

The Fluid flowing within the pipes in the subsurface is typically a water-based antifreeze solution, where the antifreeze may be a solution of ethylene glycol, propylene glycol, ethanol or a salt.

The pipes are usually made of polyethylene (PE), that has a lower thermal conductivity than copper, but is much cheaper, durable and corrosion resistant, while the outer diameter is typically around 26-40 mm.

The different disposition of the tubes in the subsurface determines a subdivision into two macro-categories: horizontal and vertical closed loop systems.

A possible alternative is represented by direct circulation systems, where the pipes are made of metal (typically copper), as the refrigerants are organic solvents. In that case there is only one heat exchanger step, directly from the ground to the refrigerant, but there is also risk of a potential contamination of the subsoil in case of mechanical damage of the copper tube.

3.2.1 Horizontal configuration

This type of installation is generally most cost-effective for residential installations, particularly for new constructions where sufficient land is available. The portion of the soil interested is the shallowest zone of the ground, more subjected to a thermal oscillation, but, differently from the open loop systems, they can work without interesting the aquifer.
The horizontal closed loops installed in a trench are realized using a mechanical excavator to reach a depth around 1,2-2 m, which is enough to provide a sufficient thermal storage to support the heating scheme in winter and isolate the loop from the worst winter frosts.
This depth is shallow enough to allow solar and atmospheric heat to penetrate, replenishing the thermal storage in the summer months.
The easiest configuration for the closed loops in trenches is represented by the disposition of a single tube in a dig, in the shape of a ring, then backfilling the trench once the pipe has been laid out.
Other possibilities are represented for instance by single pipes in parallel trenches (a), or vertically installed double-pipe systems (b).
In case of limited land area, the common practice is to bury not simply a single PE pipe in the trench, but overlapping coils of pipe, realizing the so-called slinky arrangement (c).

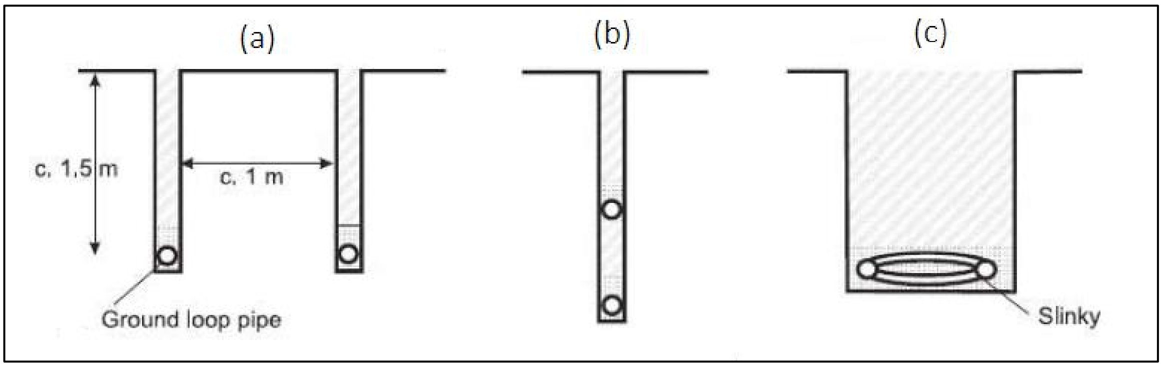

Figure 9: Examples of horizontal closed loop configurations

The main advantages are represented by the widely availability of the installation equipment, an easier removal and reparation procedure and the cost. Among the disadvantages, the most important ones are represented by the larger ground area required, the higher pumping energy requirements with respect to vertical closed loop systems, together with a lower system efficiency.

3.2.2 Vertical configuration

Vertical systems are usually preferred in commercial and institutional buildings, as the land area required for horizontal loops would be prohibitive, also minimizing the disturbance to existing landscaping.
The solution generally employed is that of the borehole heat exchangers (BHE), involving the drilling of a hole with a variable depth between 10-350 m and a diameter of 10-15 cm approximately.

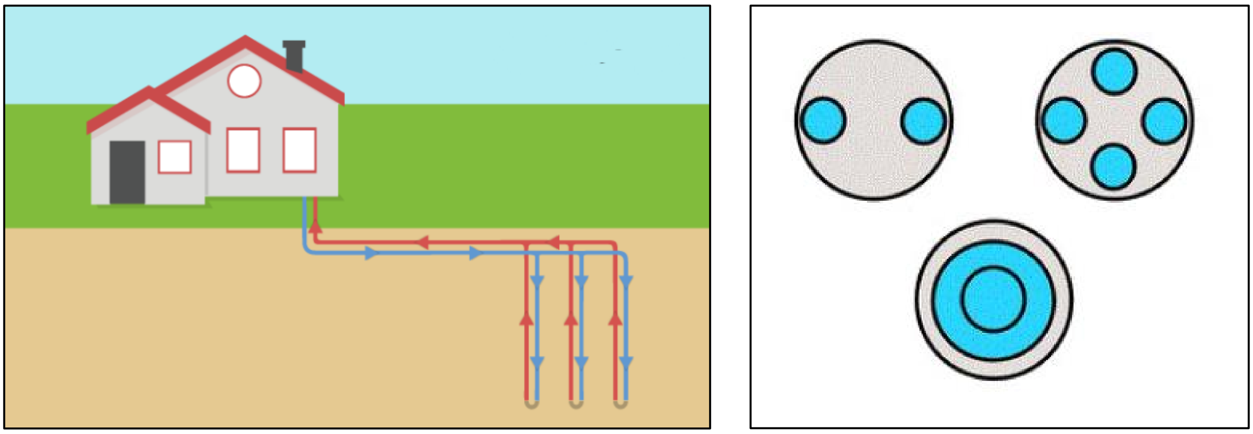

Figure 10 (left): Example of a vertical closed loop geothermal system (three drilled boreholes)
Figure 10 (right): U-tube, double U-tube and Coaxial heat exchanger configurations

For the drilling step, several technologies are available depending on the lithology, as the conventional rotary drilling and the percussion drilling.
Once the drilling of the borehole has been completed, a U-shaped closed loop (U-tube) is usually emplaced down the length of the borehole.
Subsequently, the space between the U-tube and the borehole wall is typically filled with some form of grout, which allows to improve the heat transfer and to avoid possible contamination between different aquifers.
Notably, the ideal grout should generally have a high thermal conductivity and low hydraulic conductivity, representing a good option also from the point of view of the pollution prevention.
The U-tube placed is usually made of high-density polyethylene, with an outer diameter around 32-40 mm, while the spacing between the uphole and downhole tubes (shank spacing) typically ranges between 50-70 mm.
Other geometries of closed loop heat exchanger may be considered for vertical boreholes, aiming at increasing the heat exchange area and improving the overall heat transfer efficiency.

Moving in that direction, it is possible to install a double U-tube, with two downflow pipes and two upflow pipes, plumbed in parallel, or even a triple U-tube.
The negative effects of this implementation are represented for instance by the higher difficulty related to the installation and grouting in a narrow borehole, together with the large fluid flows required to achieve transient-turbulent conditions in double or triple pipes.
Another solution could be represented by the coaxial heat exchange pipes, composed of a narrow-diameter pipe within a larger-diameter one, presenting the advantage to be installed in narrow boreholes.
These vertical loops are connected with horizontal pipes (manifolds), placed in trenches, then connected to the heat pump in the building.
A main advantage of this kind of systems is represented by the fact that they are in contact with soil that varies very little in temperature and thermal properties over the year, together with the fact that they can yield the most efficient closed loop ground-source heat pumps system performance.
On the other hand, the drilling phase involves higher costs compared with horizontal systems, and in case of damage it is almost impossible to remove and repair a pipe.

3.2.3 Energy geostructures

Within the field of the closed circuit geothermal systems are also included innovative solutions belonging to the class of the energy geostructures, which are particular geotechnical structures conveniently instrumented for exchanging heat with the ground.
They are designed to provide a solution to reduce the installation costs of the vertical heat exchangers and the land use, by means of synthesizing both structural and energy requirements in a single building element.
In that way, they could meet the needs of many geotechnical situations, where large buildings require foundations made of drilled reinforced concrete pile structures for instance. Indeed, once it is necessary to drill such holes for structural reasons, the installation of a closed loop system within the pile structure may be evaluated too, with no need for additional excavations and low additional costs compared to those required for the structural elements.
Currently, the main energy geostructures include:

- **Energy piles** (or Geo-piles): deep reinforced concrete foundation works, where the pile's primary function is structural, while the polyethylene pipes equipped inside act as heat exchangers. The dimension of a pile may be over 1 m of diameter, involving depths between 15-40 m, and it usually hosts inside multiple U-tubes with a mixture of water and glycol as refrigerant.

- **Energy walls**: together with the supporting function, they allow to exploit the geothermal energy from the subsoil through heat exchanger tubes buried in the concrete (after being laid and anchored to the reinforcement cage of the wall).

- **Energy tunnels**: they provide a considerable ground contact surface, usually reaching depths which allow the exploitation of high geothermal gradients. The heat exchanged with the surrounding soil can be brought to the surface for heating/cooling purposes.

Specifically, the geothermal system that will be analysed in thit thesis work could be reconnected to the concept of the energy walls, involving heat exchanger pipes anchored to an external wall, directly interfacing with the ground.

4. Heat pumps

In the field of applied physics, both direct and indirect thermodynamic cycles represent a crucial object of study.

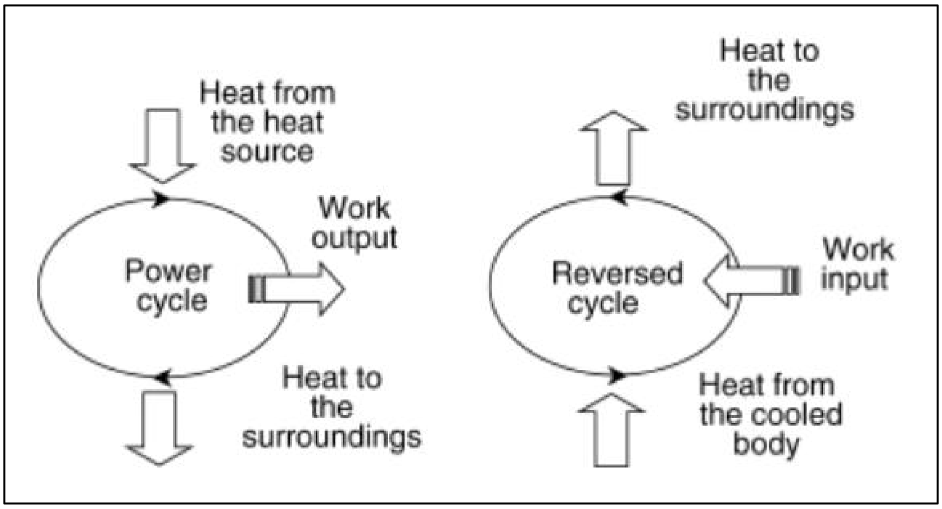

Figure 11: Direct (power) and indirect (reversed) thermodynamic cycles representation

Thermal power plants, combustion engines and reaction engines are examples of direct thermodynamic cycle applications, where the goal is that of producing work by providing heat from a heat source.

Indirect thermodynamic cycle applications are represented by such devices as the heat pumps, where the goal is reversed, aiming at producing or subtracting heat from a certain source by providing work.

In that case the work input to the cycle comes from the external environment, enabling the heat transfer from a lower temperature level to a higher one, in accordance with the second law of thermodynamics.

Within the device, the heat transfer mechanism takes place by means of a circulating refrigerant fluid around a compression-expansion cycle, to be selected accordingly with performance and environmental factors.

The usual applications of this technology are planned to meet space and water heating and cooling needs for residential, commercial and industrial applications.

The heat pumps available on the market differ in performance, on the basis of their technical efficiencies, external operating conditions and system designs.

Basing on the energy source exploited, the main categories that can be identified are represented by:

- **Air to air heat pumps**: transferring the thermal energy between the external air and the internal one for heating or cooling a target environment.
- **Air to water heat pumps**: exploiting the thermal energy contained in the external air, transferred to the water of the heating or cooling system.
- **Water to water heat pumps**: where the thermal energy transferred to the water of the heating or cooling system derives from the groundwater, which could be exploited also as heat transfer medium (compatibly with a previous analysis).
- **Geothermal heat pumps**: where the thermal energy required is taken from the ground and used for heating purposes, together with the possibility of reversing the cycle for cooling applications.

The classification of the heat pumps as a renewable heat technology varies by location, raising in the past discussions about the origin of the energy source exploited. That is what happened during the preparation of the Directive on the promotion of the use of renewable energy sources (2009/28/EC).
The positions on this topic, especially in the European commission, underwent a slow changing process, involving the acknowledging about the real renewable potential from air, water and ground.
The result was that of extending the definition of renewable sources by "aerothermal" and "hydrothermal" sources, used by heat pump technology: the first refers to the energy stored in form of heat in the air, the second one refers to the energy stored in the form of heat in surface water.
In addition to these two, also the geothermal energy belongs to the "energy from renewable sources" classification, defined as the energy stored in the form of heat beneath the surface of solid Earth, together with hydropower, biomass and many other non-fossil sources.
This fact has led to considerable consequences on the treatment of heat pump technology in European and national context, preparing the basis for a strong market growth based on the reliability, affordability and efficiency of these devices.
From the renewable energy sources perspective, the recognition of the heat pump technology resulted in more efficient systems, with a larger countable contribution and fields of application for the energy targets.

That is the case for instance of Japan, where air-source heat pumps have been recognised as renewable energy technologies since 2009, or the European union, where in the same year both the aero-thermal and hydro-thermal energy extracted by heat pumps started to be considered as renewable.
The situation for ground source heat pumps is also good, indeed they are generally defined in national legislation as being renewable, thanks to the fact of relying on a green energy source such as geothermal heat.
In Italy, the recognition of low enthalpy geothermal energy as renewable came with a greater delay, through the legislative decree 28 of May 2021.

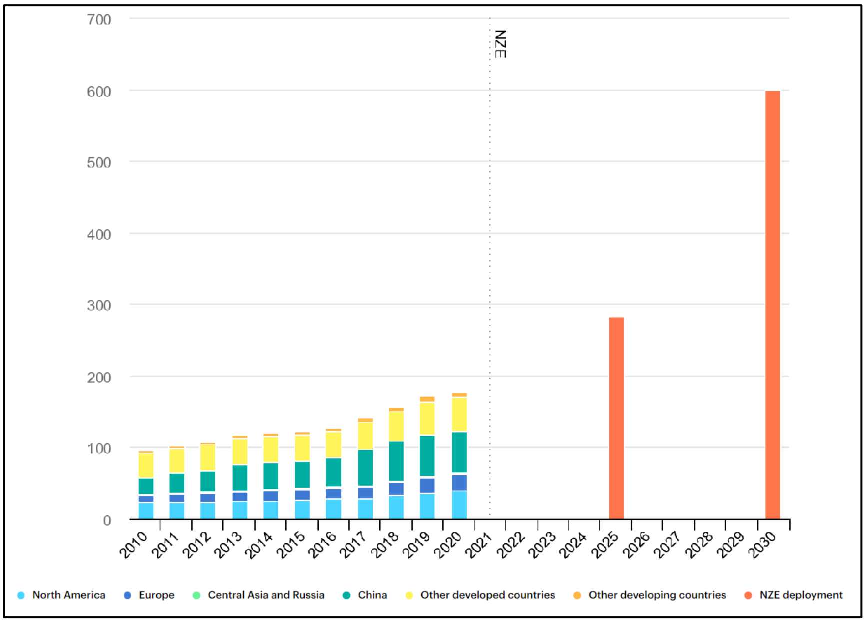

Figure 12: Installed heat pump stock by region and global Net Zero Scenario deployment, 2010-2030, from IEA website

In 2020, heat pumps met only around 7% of the global heating demand in residential buildings, but the trend is changing, making them more common in the new buildings. Indeed, in 2021 more than 20% of heating devices sold in Europe were heat pumps.
Actually, air-source heat pumps continue to dominate the market, with the top markets in China, Japan, Europe and North America. The second place for the largest market share is instead assigned to geothermal-source heat pumps, with a direct geothermal heat use increased to almost 10% in 2021.
Anyway, a problem with the geothermal energy use remains the fact that the global distribution is still uneven and sparse, with more than 75% concentrated among China, Turkey, Iceland and Japan considering the same year.

4.1 Key components

Heat pumps are characterized by a cyclic operation, which is composed of four main thermodynamic transformations, involving a refrigerant fluid, located within a close circuit inside the heat pump.
These transformations are performed by different components of the device, and consist in evaporation, compression, condensation and expansion.

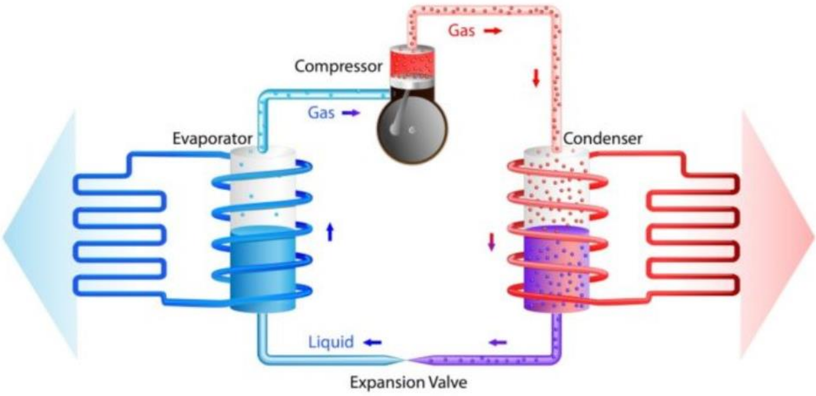

Figure 13: Heat pump refrigerant circuit scheme (Thermal control business update magazine)

In *Figure 13* are reported the four components hosting the main transformation occurring within a heat pump:

- **Evaporator**: the component responsible for the heat subtraction from the external source (mainly air or water), and transfer to the refrigerant fluid.
  This amount of heat warms up the refrigerant, causing a phase transition from liquid to vapour phase, which subsequently enters the compressor.
  The evaporator is a heat exchanger composed by a number of tubes connected in series or in parallel, with the refrigerant flowing inside, and it can be both static or ventilated.
- **Compressor**: the component with the function of aspiring the refrigerant at vapour state and compress it up to the pressure level of the condenser.
  The compression phase requires a certain amount of electrical energy from the external environment to occur, also causing an increment in the fluid temperature and facilitating its fluidification.

Usually, the compressor is of reciprocating type, formed by a cylinder with a piston inside that compress the refrigerant.

- **Condenser**: a heat exchanger component similar to the evaporator, but responsible for the heat subtraction from the refrigerant and transfer to the external source on the other side of the heat pump (usually air of water).
  The condensation transformation allows to bring back the refrigerant at the liquid state.
- **Expansion valve**: located between the condenser outlet and the evaporator inlet, it has the task of regulating the amount of refrigerant that reaches the evaporator.
  The fluid enters the valve and is subjected to an isenthalpic lamination transformation, which decreases both its temperature and pressure, reaching the level at the evaporator inlet.

Another important component to be mentioned, not reported in the figure above, is the **4-way valve** (or reversing valve), which allows to reverse the operating mode of the heat pump, allowing the system to operate both during the summer and winter season.
This valve is necessary as the compressor is a one-way device, so it is mandatory to reverse the thermodynamic cycle without changing the direction of the refrigerant flow within the compressor.

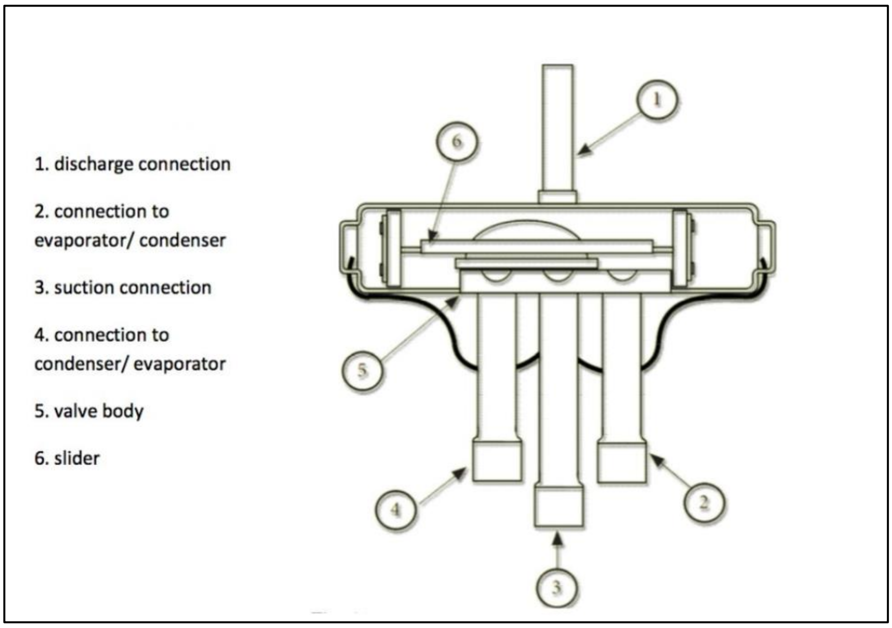

Figure 14: illustrating example of a 4-way valve scheme

In *Figure 14* are reported the main elements composing a 4-way valve, such as the connections to the compressor and to the heat exchangers.
The operation of the component is led by the slider (6), which can move along its guide, choosing to connect for instance the compressor suction with the outdoor unit (evaporator) and the compressor discharge with the indoor unit (condenser) during the heating season. For the cooling season operation, it is the opposite: the slider moves on the other side of the guide, so that the outdoor unit (condenser) is now connected with the compressor discharge and the indoor unit (evaporator) is connected with the compressor suction, but the refrigerant flow direction within the condenser does not change.

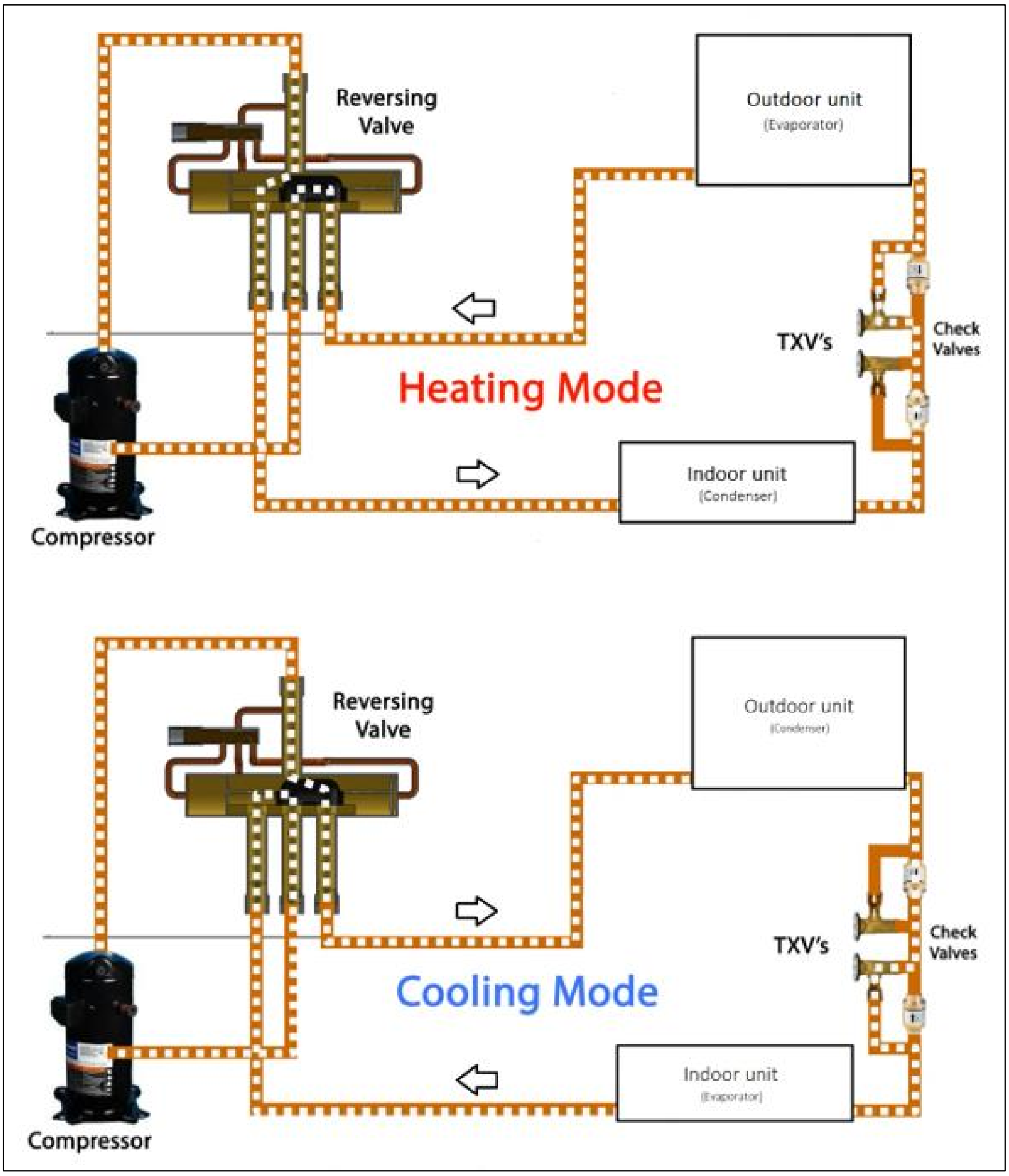

Figure 15: Heating and cooling scheme of a heat pump system with a 4-way valve

4.2 Refrigerant

The operation of a heat pump is based on a small amount of a fluid (pure or mixture) called refrigerant, which flows through the main components reported previously, undergoing a series of transformations in a closed thermodynamic cycle.
This fluid plays the role of heat transfer medium, enabling the transfer of energy through the form of sensible and latent heat.
These substances can be classified according with three main categories:

- **Pure organic fluids**: as water, ammonia, CO2, etc.
- **Hydrocarbons**: as butane, isobutane, propane, propylene, etc.
- **Halogenated hydrocarbons**: as chlorofluorocarbons (CFCs), hydrofluorocarbons (HFCs) and hydrochlorofluorocarbons (HCFCs) and perfluorocarbons (PFCs), etc.

The artificial fluids are generally called Freon and, according to the International Standard notation, the pure synthetic refrigerants are indicated with an acronym formed by the letter R (refrigerant) followed by a series of two or three numbers referring to the chemical composition of the molecule.
The refrigerant selection is related with many criteria, which essentially can be divided into two groups linked with the risk types and the required properties of the fluid.
Within the risk category are mentioned the risk of injuries, fire or property damage in case of leakage. Regarding the required fluid properties are reported instead the chemical, physical and thermodynamic ones which must suit the system and the working conditions at a reasonable cost.
These criteria are then specified more precisely, but unfortunately it is not possible to fulfil all the requirements at the same time.
The most important requirement is the refrigerant stability within the refrigeration system, as it must not decompose or react with other materials inside the device to allow the system operation.
An opposite situation should verify when a refrigerant is emitted in the atmosphere, as it should decompose easily without forming any harmful substance.

From the performance point of view, the thermodynamic and transport properties of the refrigerant are key factors for the system efficiency.
Referring to pressure, the condensing one should be not too high (at the working temperature), while the evaporating pressure should be sufficiently high, above the atmospheric level to avoid unpleasant events such as the air suction from outside to inside the system.
At the same time, the refrigerant should possess such qualities as an elevated density (both at liquid and vapor state), together with an elevated enthalpy of vaporization and thermal capacity.
From the legislation point of view, the European regulation F-Gas on the refrigerant fluids has led to substantial changes about their utilization.

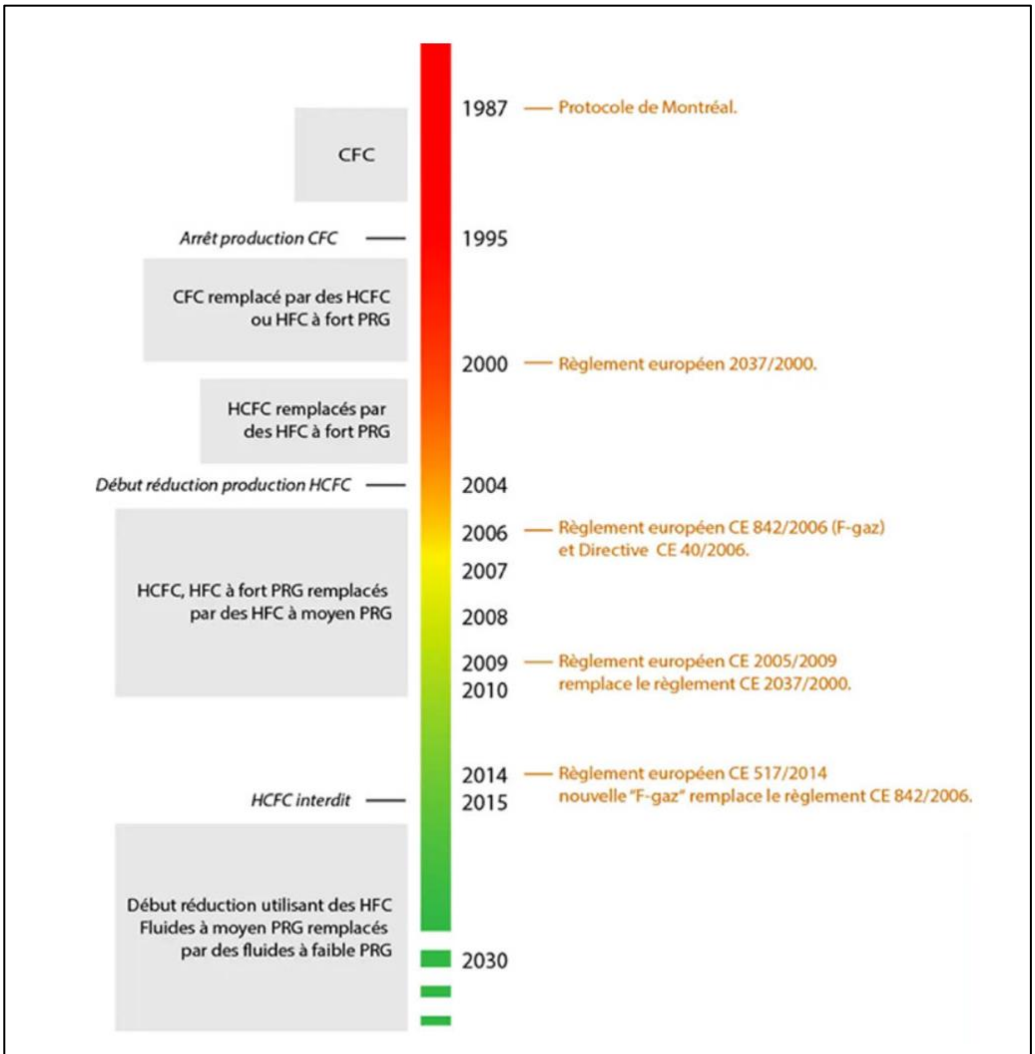

Figura 1- Evoluzione delle norme dal Protocollo di Montréal

Figure 16: Standards evolution from Montréal protocol, from Mecobat website

The regulations formulated by F-Gas regard the recovery, use and distribution of fluorinated gases, imposing a program for the gradual reduction of greenhouse gas emissions by 2030.
This program was set based on the global warming potential (GWP), that is an indicator of the harmfulness of gases in relation to the greenhouse effect and for a given time, considering the CO_2 as the reference fluid (GWP=1).
Further classifications for the refrigerants are based on their flammability and toxicity, as the standard ASHRAE 34 34.
Moving in that direction, the choice of the refrigerant fluid must be done among substances that do not harm the ozone layer, as established by the Montreal Protocol, with a reduced amount of Chlorine and Fluorine, as set by the Kyoto Protocol, avoiding flammability problems too.
For instance, looking at *Figure 16*, from 2015 the use of HCFC refrigerants is forbidden, while the actual situation includes the prohibition of fluids with a GWP>2500, that will be extended to GWP>1500 in 2030.

4.3 Thermodynamic cycle

The thermodynamic cycle is represented by the set of consecutive transformations, that the refrigerant fluid undergoes flowing through its closed loop.

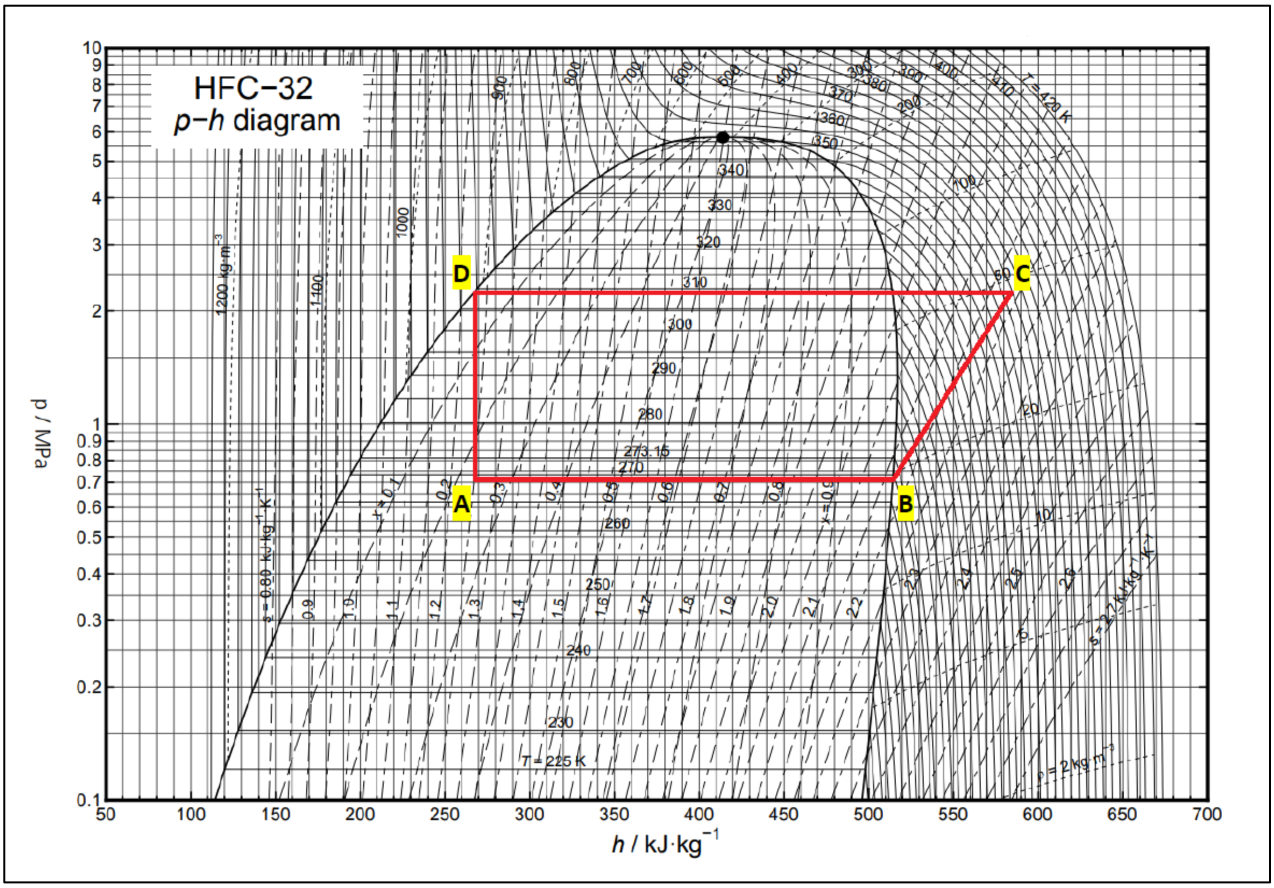

Figure 17: Example of a thermodynamic cycle reported on a p-h diagram, heat pump working with R32 refrigerant

In *Figure 17* is reported, as an example, the pressure-enthalpy diagram of the R32 refrigerant, with the bell-shaped curve dividing the diagram into three main regions. The left part of this curve represents the saturated liquid curve, while the right one represents the saturated vapor curve and they meet in the so-called critical point, where the fluid undergoes a direct transformation from liquid to vapor state.

The four red lines represent thermodynamic transformations incurred by the refrigerant and intersect in four points, indicated by the highlighted letters, which constitute the corners of the thermodynamic cycle.

- **A-B segment**: it represents the evaporation transformation, starting from the thermodynamic conditions at the expansion valve outlet.
  The transformation reported on the diagram above is both isothermal and isobaric, allowing the refrigerant to absorb a huge amount of heat from an external source.
  This fact occurs because the R32 is a pure fluid, while in the case of a mixture (as the R407C) the glide phenomenon occurs. Notably, the formation of azeotropes causes the lack of matching between the dew and bubble point, so the evaporation process is still isobaric, but the temperature of the refrigerant varies.
  The transformation could end on the vapor saturated curve, as in *Figure 17*, or more frequently continue a little beat, so that the refrigerant reaches the superheated vapor state. This occurs because the compressor is usually designed to work with vapor only (as the reciprocating one), to eliminate the remaining water droplets, if any.
  This last step involves the transfer of sensible heat.
- **B-C segment**: it represents the compression transformation, where the gaseous refrigerant at the evaporator outlet is aspired by the compressor and both the pressure and temperature level increase.
  This step requires a certain amount of external energy, which corresponds to the mechanical work of compression.
  At the compressor outlet, the refrigerant is in the superheated vapor state, at the same pressure of the condenser.
- **C-D segment**: it represents the condensation transformation, through which the refrigerant transfers a huge amount of heat to another external source.
  The heat transfer mechanism consists in a first step involving sensible heat, up to the vapor saturated curve, followed by a second step involving the release of latent heat by the refrigerant until the end of the process.
  Similarly to the evaporator case, the condensation process may terminate on the liquid saturated curve or, as more usual, continue a little bit in the liquid region. This subcooling process involves again the transfer of sensible heat, allowing to obtain a greater refrigerating effect.
  If the refrigerant is a mixture of fluids the glide phenomenon is present, as for the evaporation step.

- **D-A segment**: it represents the lamination transformation, so when the refrigerant enters the valve, it undergoes an isenthalpic transformation with a decrease of both pressure and temperature.
  This process is ideally adiabatic, without the exchange of heat, as the compression step.

The thermodynamic quantities coming out from these transformations are used in the determination of some performance parameters:

(1) $$\mathrm{COP} = \frac{Q_{cond}}{L_{compr}} = \frac{Q_{cond}}{Q_{cond} - Q_{ev}}$$

(2) $$\mathrm{EER} = \frac{Q_{ev}}{L_{compr}} = \frac{Q_{ev}}{Q_{cond} - Q_{ev}}$$

The first one represents the efficiency of the heat pump operating in heating mode, when the useful effect is the heat delivered to the external source coupled with the building, while the second one (Energy Efficiency Ratio or again COP) is the efficiency parameter referring to the operation in cooling mode, when the useful effect is the heat subtracted to the external source, like the water flowing through the building heating system.

4.4 Geothermal heat pump system

Talking about the natural temperature gradients (geothermal gradients), proper technologies are required to get the access to the heat stored in the Earth's subsurface, which is a considerable quantity even at normal temperatures and shallow depths.
A solution can be represented by the previously mentioned ground-source heat pump systems, that are characterized by three main components:

- **Heat pump**
- **Earth connection** (the way through which the heat is exchanged)
- **Interior heating or cooling distribution system** (inside the building)

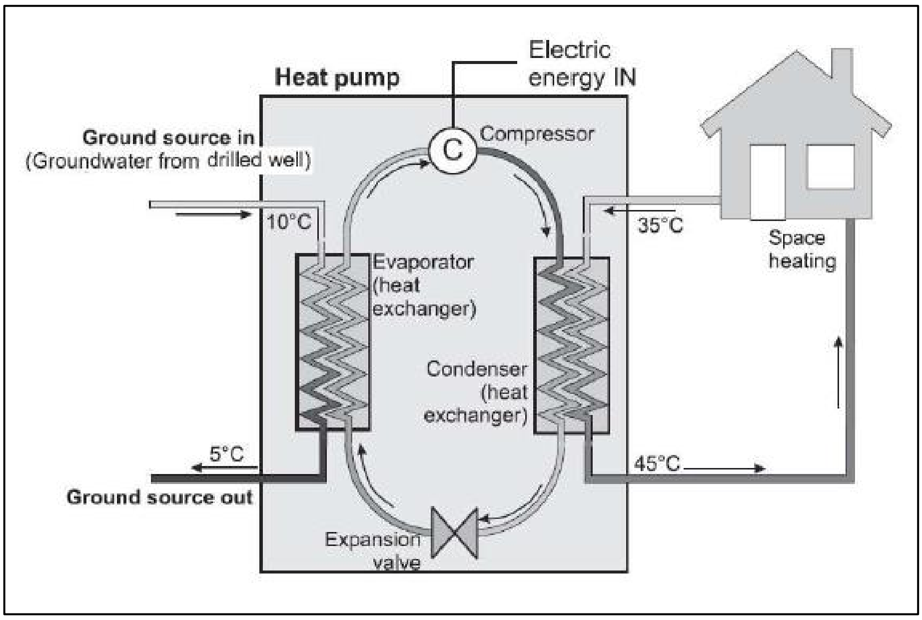

Figure 18: Example of a geothermal heat pump system (water to water case)

Thanks to the fact that at relatively shallow depth (in the order of some meters) the temperature remains almost constant over the year, it is possible to extract heat during the winter season and release it during summer.
This fact is also true for open loop case because the groundwater too has an almost constant temperature over the year, and usually the equilibrium temperature of an unconfined aquifer (the shallow water table) is close to the mean air temperature in the location considered.
The possibility of reversing the operating cycle is so common to many heat pumps, with the outdoor unit and the indoor one that switch their operation from

evaporator to condenser and vice versa, in the same way exposed discussing about the role of the 4-way valve in the key components section.
In these cases, the heat pump operation is analogous to a common system, water to water or water to air depending on the building system working fluid, with the four main components presented in the previous section composing the refrigerant circuit.
On the building side the heat exchange occurs between the refrigerant and the heat transfer medium flowing within the building circuit, commonly through a plate heat exchanger, with the two fluids circulating on either side of a dividing wall. A large contact area for heat transfer, together with a low thermal resistance and the establishment of a turbulent flow motion guarantee an efficient heat transfer mechanism between the fluids.
Even on the ground side, the heat exchanger within the heat pump is commonly a plate one, providing a thermal contact between the refrigerant circuit and the geothermal probes.
Notably, the ground in contact with the probes is a porous medium, composed by a liquid and a solid phase, hence conduction and convection represent the main heat transfer mechanisms established between the heat transfer fluid and the ground surrounding the pipes.
Generally, this pairing at the ground side allows to heat and cool the desired environment with a single system and a high efficiency during the season. For instance, thinking about the summer season, it is far mor efficient for a heat pump to dump the heat to the ground than to the air, as the first one is relatively cool.
The main limitation for this kind of systems is the lower temperature of the fluid circulating through the heating system of the building, with respect to the fossil fuel-based alternatives, so they should be implemented in the case of new buildings designed to work with low temperature fluids.

5. Experimental field description

In the present study, all the efforts were focused on the analysis of the novel geothermal energy system located at the Energy center, in Turin (Italy).
All the tests carried out took place in an experimental field realized in 2019, with the installation of the required equipment in both those that will be defined as the user and the ground side of the field.
The main realization steps, as the excavation works and the installation of the monitoring sensors and all the remaining technical equipment, are described in detail in the doctoral dissertation of Matteo Baralis, consulted also for a better understanding of the data coming from the field.
Concerning more the Energy Center, it is a building with a total gross floor area of about 7000 m^2, established in 2016 with the Energy Center initiative (ECI), launched by the Polytechnic of Turin to undertake a series of actions and projects with the aim of providing support and strategic advice to local authorities, national and transnational bodies, on the policies and energy technologies to be adopted.

Figure 19: Energy Center, Via Paolo Borsellino, 38 int. 16, 10138 Torino TO

In *Figure 19* can be seen the lawn below which the geothermal probes were positioned, specifically on the right side close to the building, anchored to the exterior wall surface. These are part of the energy system prototype, called

GeothermSkin, which represents an example of very shallow geothermal system, conceived to minimize installation costs.
This solution has been designed to be installed during building construction or refurbishment, to provide a full or partial fulfilment of the renewable energy requirements with the advantage of a negligible horizontal area occupancy.
In that way, the earth-contact area of the building is transformed into a heat exchanger, with the system covering as a skin the structural elements in contact with the ground. In the case of the Energy Center, being an existing construction, the realization process required the cleaning of the exterior wall surface, represented by a supporting wall in via Borsellino (Turin).

5.1 Realization of the field

Regarding the realization of the experimental field, taken place in 2019, the full process could be subdivided into four main steps:

- **Excavation and reinforcement realization**: to expose the external surface of the wall, excavation works was performed by removing and then grinding the ground portion involved.
  After an excavation of 80-120 cm, the reinforcement panels were pushed against the ground by the excavator's bucket, and then alternatively pushed down along the uprights.
  Because of the shape of the excavation and the depth reached, the shaft was secured by means of iron trench shores, able to withstand the tensile and compressive stresses generated in such structures.
  The metallic material choice also provides a higher durability in environments where water is present and facilitates the placement with respect to wood.
  The non-cohesive nature of the ground excavated required particular attention, together with the difficulties in handling the metallic elements up to the desired depth.

Figure 20: Early stage of excavation

- **Casting of a horizontal lean concrete layer**: after the insertion of all the panels, the following step consisted in the casting and levelling of a lean concrete layer at a depth of 4,7 m.
  This concrete layer allowed to equalize the bottom of the excavation before pipes installation, facilitating the achievement of the desired configuration.

Figure 21: Bottom of the excavation, equalized before pipes installation

- **Holes drilling with a wet core drilling machine**: to allow the connection of the sensors to the monitoring system, some holes were performed in the wall using a wet core drilling machine.
  Notably, the technology exploited is that of diamond drilling, using a rotary drill with a diamond drill bit (made of industrial diamonds) attached to create precise holes.
  Diamond is used as it is the hardest naturally occurrent material in the word, able even to create openings in a range of materials including concrete, metal and glass.
  A continue water flow was involved too, cooling down the diamond drill bit during the process.

- **Positioning of the geothermal probes**: for the ground insertion of the geothermal probes, the pipes were arranged in three different modules of

energy wall system, then fixed to the external surface of the wall through supporting clamps at almost regular distances.
Each circuit finally presents the heat exchanger coil extending on an area of 2,1 m width and 3 m height, resulting approximately on an effective exchanging area of 6,3 m^2.
After the disposition of the three circuits, the previous holes realized in the wall with the wet core drilling machine were filled with the planned sensors.
Finally, the excavation performed was gradually backfilled with extreme caution, avoiding damaging the pipes

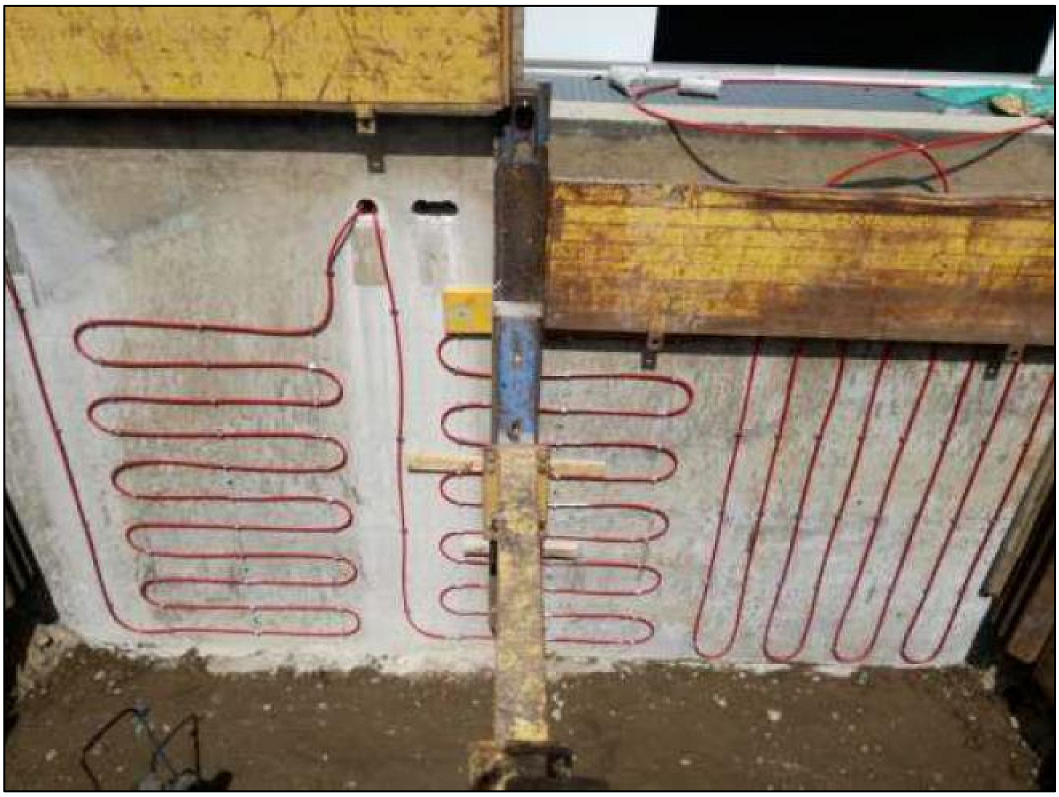

Figure 22: Disposition of the three modules before backfilling

More in detail, the three circuits were realized with crosslinked polyethylene (Pe-Xa) tubes, commercially known as Rautherm S pipes by Rehau, with an internal diameter of 20 mm and 2 mm wall thickness.
The choice of this type of material allows to ensure a sufficiently high resistance to pressures and temperatures, with high thermal conductivity and a good flexibility.
In the case of the last module on the right, the coil is vertically oriented for experimental purposes.

5.2 System configuration

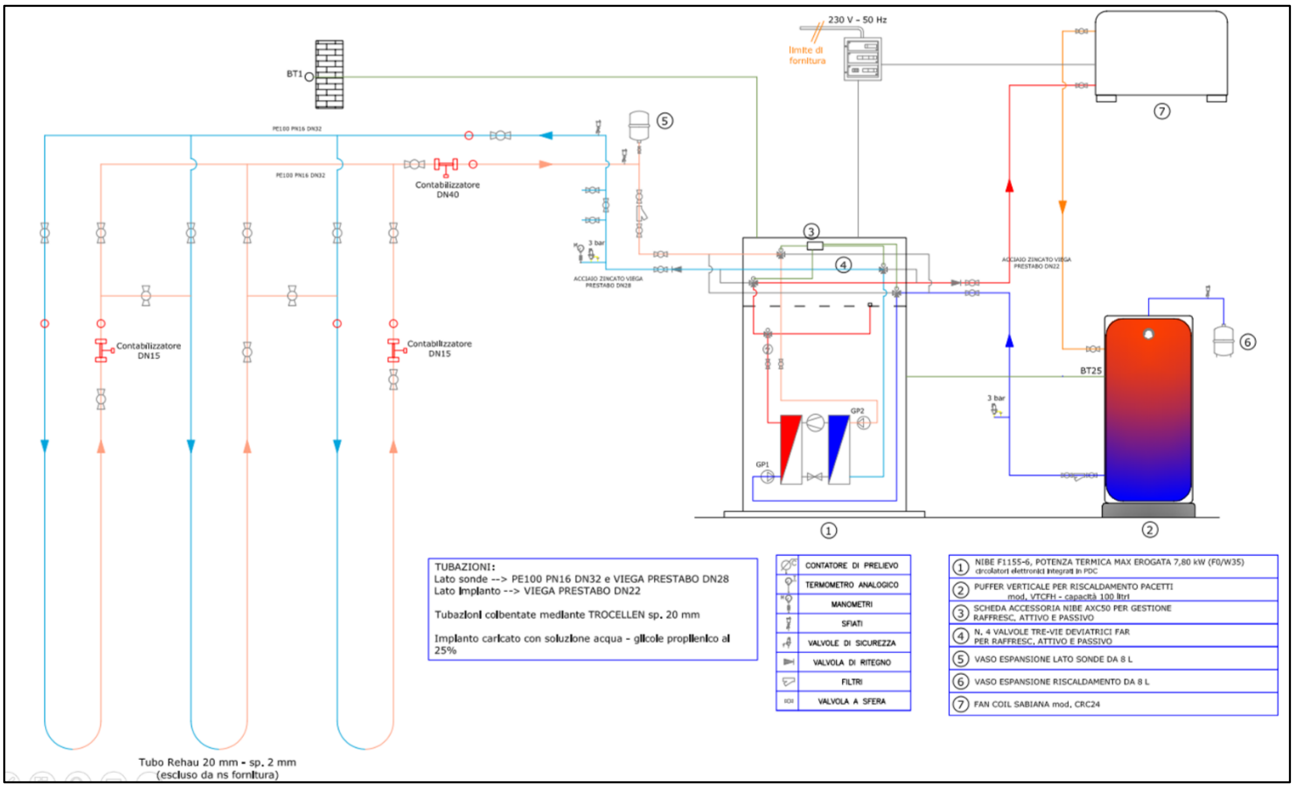

Figure 23: Geothermal heat pump system scheme, GeoNovis-Energia-Geotermica, 2019

In *Figure 23* is reported the scheme of the system coupling the geothermal probes with the NIBE heat pump, that in turn is connected to the final user (the fan coil) represented on the top-right. The plant can then be classified as a ground to air geothermal system.

In winter, the heat source is represented by the ground, thermally connected to the evaporator of the heat pump, with the heat transfer fluid circulating within the geothermal probes that has the task of extracting heat.

In summer the operation is reversed, so the air represents the hot source from which the heat is extracted, to be injected into the ground, with the ground circuit thermally connected to the condenser of the heat pump.

Looking more closely to the geothermal heat pump represented in the figure above, turned on for the first time in September 2019, three main circuits can be noted:

- **Primary circuit** (on the left): the circuit that extends to almost 4 m depth and 7,5 m width within the ground, presented in the section regarding the realization of the field (*Figure 22*).

The heat transfer fluid that flows through the pipes consists in a mixture of 25% propylene glycol and water, while the coil arrangement of the modules allows to exploit as much as possible the ground source for heat transfer.
Thanks to a valve system, the coils forming the three modules can be travelled by the fluid both in parallel or in series, with the flow rate managed by the pump indicated as GP2.

- **Secondary circuit** (on the right): the circuit connected with the final user, represented by the Sabiana CRC24 fan coil, that is connected in series to a Pacetti VTCFH model vessel with a capacity of 100 litres.
  As the primary circuit, it is charged with a mixture of 25% propylene glycol and water, with the flow rate managed by the pump indicated as GP1.
- **Heat pump circuit** (in the middle): the circuit inside the NIBE heat pump, charged with R407C refrigerant.
  On this circuit are installed the four main components presented in section 3.1, used to exploit the energy contained in the refrigerant: the evaporator, the compressor, the condenser and the expansion valve.
  Notably, the two heat exchangers provide a thermal connection to both the primary and secondary circuit, with the condenser connected to the ground one in summer and to the fan coil one in winter, the opposite for the evaporator.

The experimental field is distinguished into two main areas, located in the underground floor of the building, and characterized by a different equipment: the area called "Isola 1" is the location of the heat pump and the final user (the fan coil), while the one called "Isola 2" hosts the vertical heat exchanger modules responsible for the heat transfer from/to the ground.
Together with these main equipments, which characterize each area, other components needed for the system operation are present in both the locations.

Figure 24: Plan of the underground floor, Energy Center

5.2.1 User side

The user side is represented by the area of the experimental field called "Isola 1", located in a technical room on the north-east side of the building, which hosts as main components:

- **Heat pump NIBE F1155** (6kW, 1x230V): characterized by the four main components on the refrigerant circuit, previously mentioned in the heat pump section (3.1), and by additional electrical thermal resistances that help the geothermal system to provide the heat required during winter operation (up to 7 kW), when the energy extracted from the ground is not sufficient. These thermal resistances were deactivated for the experimental analysis.
  Together with the refrigeration components, the heat pump hosts electric components as the interface cards and the inverter, hydraulic components as the service attacks for low-pressure and high-pressure side, HVAC (Heating, Ventilation and Air Conditioning) components such as the two circulation pumps and many sensors.

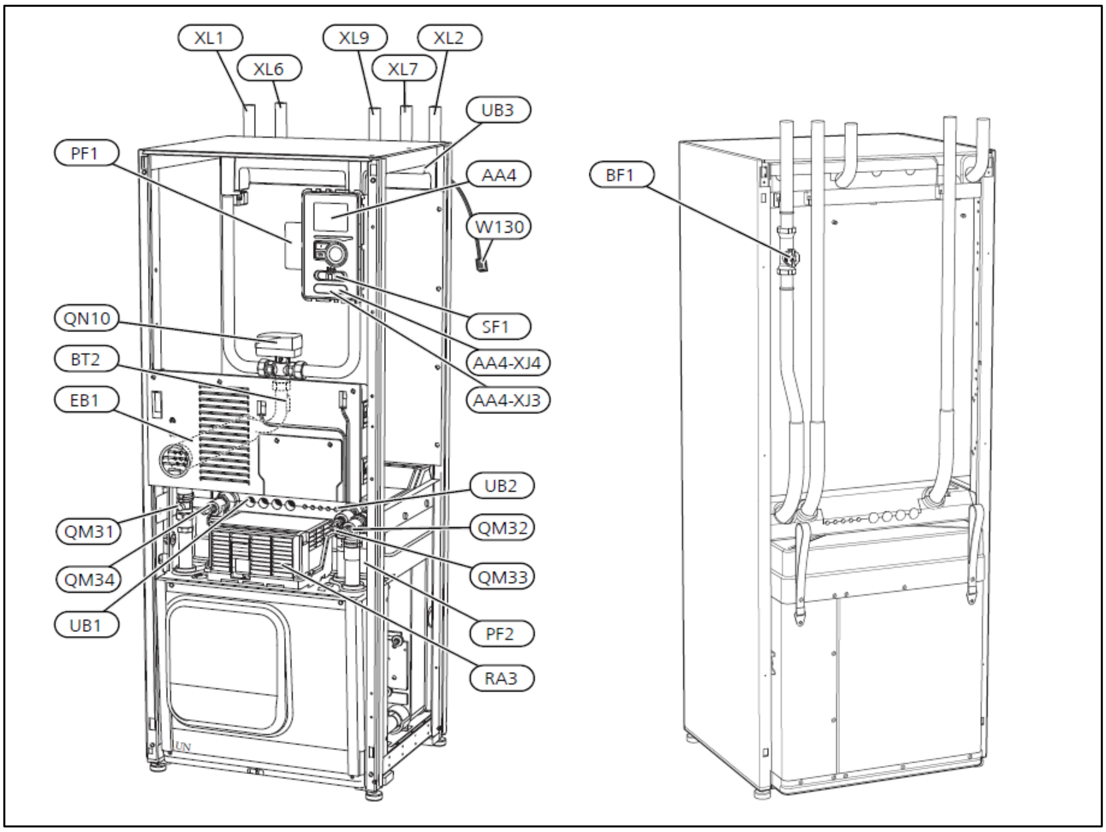

Figure 25: Heat pump structure, general aspects (left) and back view (right)

The components indicated with the acronym "XL" are hydraulic, the sensors are indicated with "BT" and "BF", the HVAC components are indicated with "QM" and "QN", while the remaining ones are electric or various.

The refrigerant contained in the dedicated circuit is the R407C, a mixture of HCFC components (23% R32, 25% R125 and 52% R134A) that allows to provide the fluid at high temperatures, up to 65°C, at the hot side of the cycle.

The R407C is a mixture of zeotropic type, this means that in any condition of liquid-vapor saturation, the dew and bubble point do not coincide, involving the "glide" phenomenon mentioned before. This fact impacts on the evaporation and condensation transformations of the heat pump thermodynamic cycle, which are isobaric, but not also isothermal as for the pure substances.

- **Pacetti VTCFH buffer accumulator tank** (100 litres): installed in series with the heat pump to regulate its operation, to limit the number of compressors switch on/off and so extending the useful life of the thermal machine.

  This tank is insulated by polyurethane foam, being suitable to store fluids with a temperature ranging between -10°C and 90°C.

  The fluid stored is that of the secondary circuit, represented by a mixture of 25% propylene glycol and water, arriving from the fan coil.

Figure 26: Buffer accumulator tank, with an expansion vessel (8 litres) and the fan coil behind it

- **Expansion vessel** (8 litres): installed above the buffer accumulator tank, as reported in *Figure 26*, with the function of containing sudden changes of pressure in the user circuit, that otherwise would have to be absorbed by the system itself.
- **Fan coil Sabiana CRC24**: represents the final user served by the geothermal system, located in the underground floor, close to the heat pump and the buffer bank accumulator.
  The internal heat exchanger can be fed with heat carrier fluid at temperatures in the range of 5°C-85°C, which subsequently is discharged in the 100 litres capacity buffer before returning to the heat pump.
  The secondary circuit pipes are made of galvanized steel with a diameter of 22 mm, and the thermal insulation is the same of the primary one. Also the circulating fluid is the same, since the primary and secondary circuits can be connected in a single loop during free cooling operative phases, so the circulating fluids must have the same characteristics.
  Specifically, in the cooling case, the load can be provided both by active cooling, requiring the operation of the internal compressor, and passive cooling (or free cooling), which is automatically run by the heat pump loading depending on the user thermal demand.
  This last option is made possible by the electrically driven switching of three-way valves, installed at the flow and return ends of primary and secondary circuits.

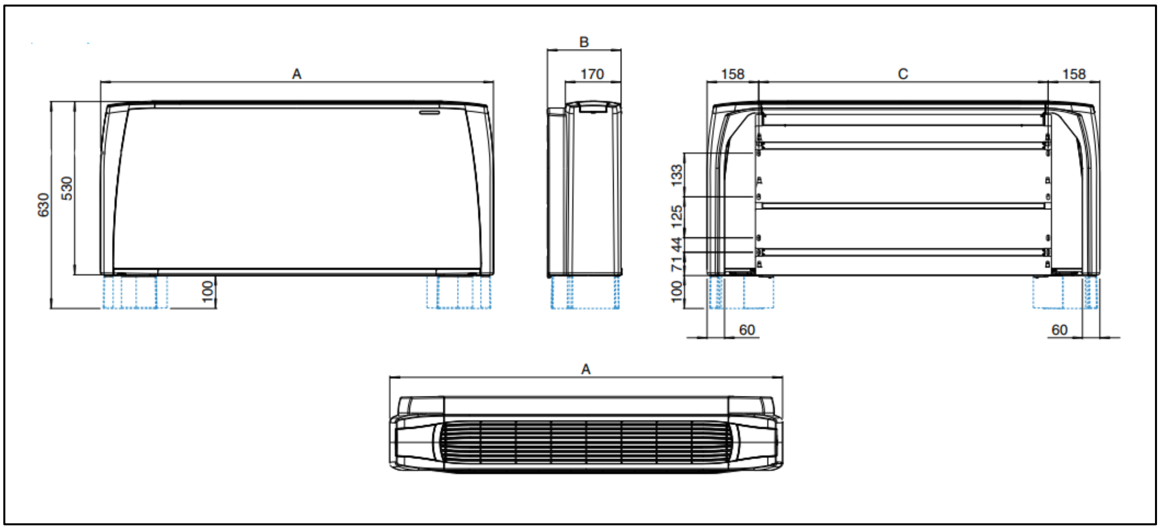

Figure 27: Fain coil Sabiana CRC24 model

- **Electronic circulators** (GP1 and GP2): are embedded in the heat pump, consuming electricity to operate.
  Each circulation pump is conceived to serve separately the user side and the ground side of the experimental field, working at variable speed velocity depending on the head losses.
  The ground side nominal flow is 0,65 $\mathrm{m}^3/$h, while the user side nominal flow is lower, about 0,29 $\mathrm{m}^3/$h, up to a maximum of 340 $\mathrm{m}^3/$h.

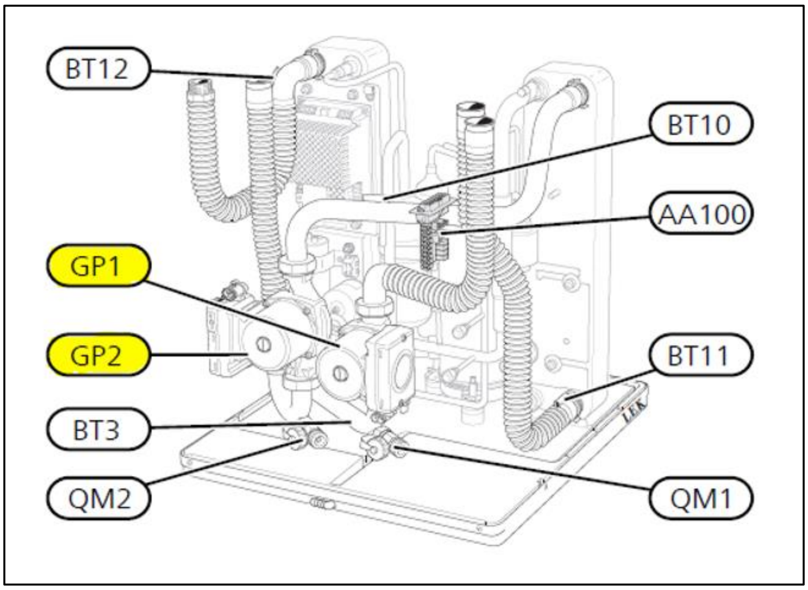

Figure 28: Refrigerant module of the NIBE F1155 (6 kW)

5.2.2 Ground side

The ground side is represented by the area called "Isola 2", hosting the geothermal probes together with some meters and piping systems:

- **Geothermal probes** (primary circuit): the ground pipes material and disposition are the ones presented in the section 4.1.
  The three modules, in a coil arrangement, were anchored to a selected exterior wall surface, located on the most distant corner from the car park, to reduce at the minimum any thermal influence on the ground volume interacting with the geothermal system.

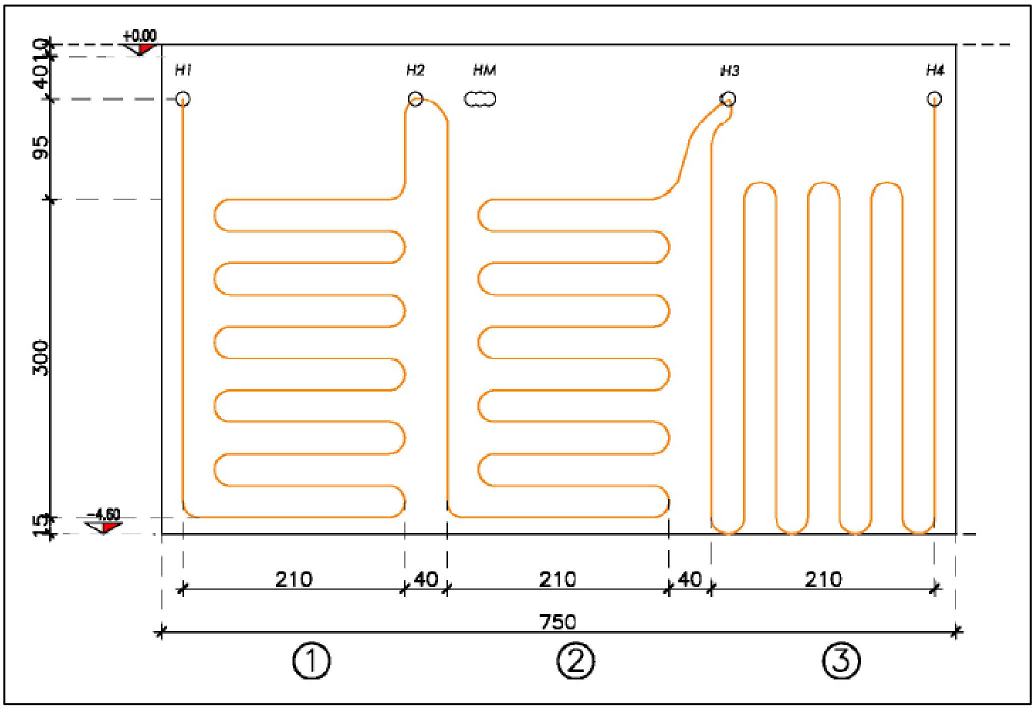

Figure 29: Pipes network inside the ground

In *Figure 29*, H1-H2-H3-H4 indicates the holes drilled for the manifold connection, while HM represents the hole realized for the monitoring sensors wires.

- **Manifold**: equipment added to the hydraulic circuit to connect the pipes from/to the heat pump with the heat exchanger modules, allowing to test different configurations of the last ones.

Notably, the series of valves installed on the manifold allow the singular exclusion of one or more modules from the circulation, together with the possibility to link the modules in parallel or sequentially.

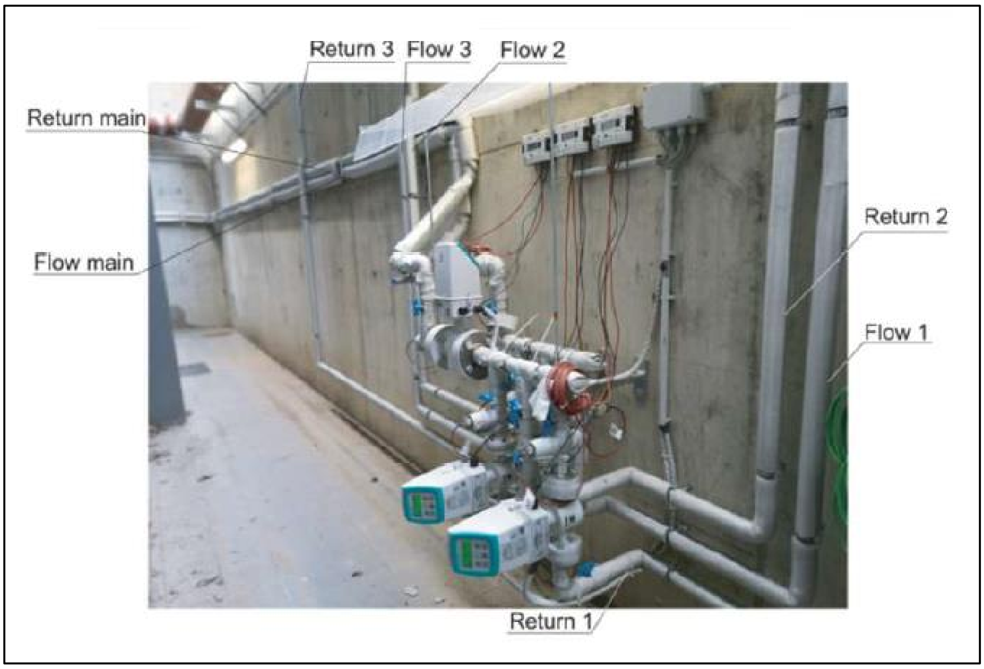

Figure 30: Collector manifold

- **Pipeline connecting the manifold with the heat pump**: with a length of about 65 m and a nominal diameter 32 mm, thus bigger with respect to the ground heat exchangers, this pipeline connects the geothermal probes with the heat pump located in the "Isola 1".
  The line is realized in high density polyethylene PE100, with a closed-cell elastomeric coating (20 mm thick) and a nominal thermal conductivity of about 0,034 W/mK (at 0 °C).
  The hydraulic sealing among the pipe pieces is ensured by electrofusion fittings, and a specific test against leakage was performed before the connection of the manifold system.
  The system is clamped to the wall surface and was pressurized up to 2 bar, while the decrease over time is measured with a manometer.
- **Monitoring system**: an extensive monitoring system was designed to characterize both the heat in the ground media, analysing the thermo-mechanical effects induced on the wall, together with the variation of other proprieties in the ground volume facing the Geothermskin prototype, and the performances of the system.

Regarding the last ones, for instance the heat exchangers functioning is monitored involving the installation of three different energy meters on the collector manifold, the heat carrier flow rate is monitored through an ultrasonic flow meter on the return pipe, while the exchanged energy is measured though the coupling with a double temperature measurement by thermos-resistances.

Figure 31: Examples of monitoring components adopted

- **Expansion vessel** (8 litres): operating in the same way as the one installed in the "Isola 1", and so protecting the ground circuit from sudden changes of pressure.

5.3 Sensors and data collection

Thanks to the sensors the heat pump is equipped with, the temperature levels in different points of the cycle can be measured and registered by an embedded computer.
The heat pump is then provided with an Ethernet and an USB port, so that the data collected can be uploaded on the internet or to an external device, at desired sampling rates.
Additionally, because of the internet connection, the heat pump functioning is remotely accessible, even if the control must be operated on site.
Out of the refrigerant circuit, the data collected regard also the circulation pump speed at primary and secondary side, the inlet and outlet temperatures on both the circuits, together with the temperature of the buffer tank on the secondary circuit and the cavaedium air temperature.

	Name	Location	Function
BT1*	Outside sensor	Outdoor, shaded location on north side of the house.	Set point values for heating and cooling demand calculation. Operating mode change.
BT2	Flow pipe	On flow line after immersion heater (EB1).	Calculation of DM. If BT25 is installed, only view.
BT3	Return pipe	On return line between circulation pump (GP1) and condenser (EP2).	Stopping the compressor at high temperature.
BT6*	Hot water, charging	On water heater lower section.	Stop and start of hot water charging. Also used for display if BT7 is not installed.
BT7*	Hot water, top	At water heater peak.	View.
BT10	Brine in	On incoming brine line before circulation pump (GP2).	View.
BT11	Brine out	On outgoing brine line after evaporator (EP1).	Stopping the compressor at low temperature.
BT12	Condenser flow line	On flow line between condenser (EP2) and immersion heater (EB1).	Stopping the compressor at high temperature.
BT14	Discharge	On hot gas line after compressor (GQ10).	Stopping the compressor at high temperature.
BT15	Fluid pipe	On the liquid line after the condenser (EP2).	View.
BT17	Suction gas	On suction gas line before the compressor (GQ10).	View.
BT25*	External flow line	Externally on the flow line to the heating system.	Calculation of DM. Actual value for additional heat mixing valve.
BT50*	Room sensor	In suitable indoor location.	Correction of the indoor temperature.

Figure 32: Temperature sensors (stays for externally mounted)*

Among the sensors reported in *Figure 32*, those within the blue frame are the most important ones with a view to the heat pump efficiency determination. Unfortunately, considering the temperature sensors mounted on the refrigerant cycle, the recordings coming from the one positioned at the outlet of the condenser (BT15) were not accessible in the periods considered, resulting in the lack of information about the thermodynamic condition in that point.

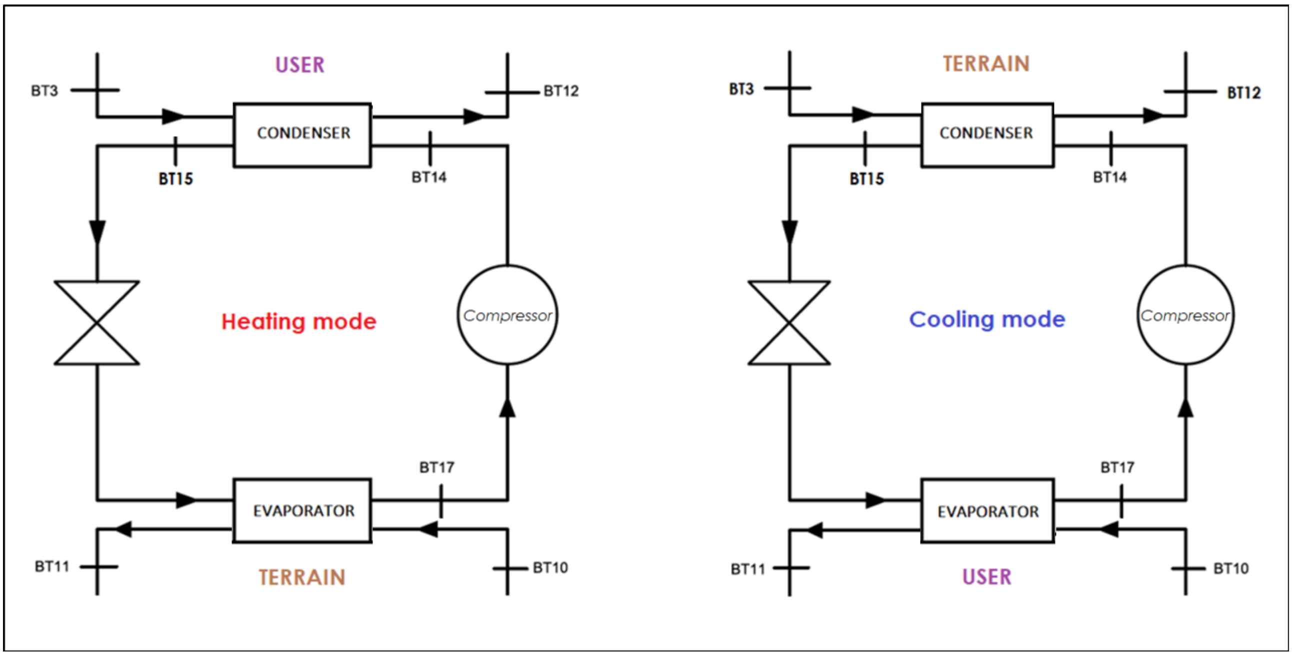

Figure 33: Simplified scheme of the refrigerant circuit with the temperature sensors, reversing valve not represented

However, the main bottleneck in the energy assessment process was represented by the issue of pressure levels, in the high pressure branch after the compressor and in the low pressure one before the compressor.

	Name	Location	Function
BP1	High pressure pressostat	On the liquid line.	Protects the compressor against pressures that are too high.
BP2	Low pressure pressostat	On suction gas line.	Protects the compressor against pressures that are too low.

Figure 34: Pressure sensors

As reported in *Figure 34*, two pressostats are positioned on the high pressure and low pressure branches of the refrigerant circuit, but their function is only that of

protecting the compressor, respectively against too high and too low pressure levels.
No actual pressure measurements are so available from the heat pump system, exacerbated by the fact that not even information about the admissible ranges are reported on the installer and user guide.
As the determination of the thermodynamic quantities useful for the system performance evaluation, like the enthalpy at the inlet/outlet of each component, requires the knowledge of both pressure and temperature at the inlet/outlet of each component, alternative solutions were required.
The first step in that direction consisted in the definition of the preliminary hypothesis, representing the basis from which to proceed with the data elaboration and the calculation of the main thermodynamic quantities characterizing the geothermal system.

6. Preliminary hypotheses

Since the case addressed is a real one, the assumption of some hypothesis was mandatory, making up in most cases for the lack of data from the set of sensors. That is the case, for instance, of the temperature at the condenser outlet, which should be provided by the sensor BT15.
Since the sensor measurements were not available, the assumption made is that the condensation transformation would end on the saturated liquid curve, without involving subcooling phenomenon.
In that way, by knowing the pressure in a way that will be explained later, the temperature was calculated as the saturation temperature at the pressure Phigh (pressure on the branch following the compressor). Indeed, the superheating phenomenon was considered, as the sensor BT17 (compressor inlet) was always operative.
Regarding the pressure levels, the assumptions made and the derived approach will be deeply explained in the section 8.3, analysing both a fix pressures and variable pressures method, with the respective constraints.
The data related to the water/glycol flow rate in the primary circuit were not available too for the cooling period considered (June 2022), so the average value adopted of 0,435 m^3/h derives from those registered in the previous years, in the same period. This value is quite consistent with the values returned by the GP1 and GP2 pumps, involving a fixed speed around 70% of the nominal value, while the nominal flow rate amounts to 0,65 m^3/h.
A similar logic was adopted for the heating period considered, selecting an average water/glycol flow rate of 0,460 m^3/h for the primary circuit.
The refrigerant flow rate was then calculated also starting from those values, for each measurement recorded.
Considering the whole system, the hypothesis of no heat dissipations and no pressure losses were assumed in the heat exchangers, in the compressor and generally in the pipes. Both the compressor and the expansion valve were considered as adiabatic components.
Regarding the primary and secondary circuits, other hypotheses were made regarding thermodynamic quantities such as the density and the specific heat: for both the circuit there are temperature sensors providing the fluid temperature at the inlet/outlet, but no pressostats to get information about the pressure level. As the variability of those values for the water/glycol mixture, observed with

CoolPack software, is not as pronounced, both the density and specific heat were calculated assuming a constant pressure equal to 2 bar.
The specific heat and the density of the R407C, instead, were calculated from the values of temperature recorded by the sensors and the pressure level on the relative branch.

7. Description of the system operation

In the experimental setting, the NIBE F1155 heat pump does not work continuously, but its operation is more like that of a boiler: the compressor is turned on once the delivery temperature to the system reaches a pre-set value, which can be manually imposed as a constant or through the implementation of a climatic curve.
In the case analysed there is not a real final user demand to be met, as the user is represented by the fan coil in the experimental field, so the set value was imposed as a constant (different values for winter and summer operation).
The delivery temperature control is performed through the degree minutes concept (DM), defined as:

$$\mathrm{DM} = \sum_{i=1}^{t_i} (T_a - T_s) \cdot t_i$$

The DM parameter varies over time (t_i represents the elapsed time), as a function of the difference between the temperature T_a (the outlet temperature at the user side, BT3 for heating operation) and T_s (set point temperature manually fixed). Once the cumulative of DM reaches a certain limit, calculated by the control unit, the compressor is turned on.

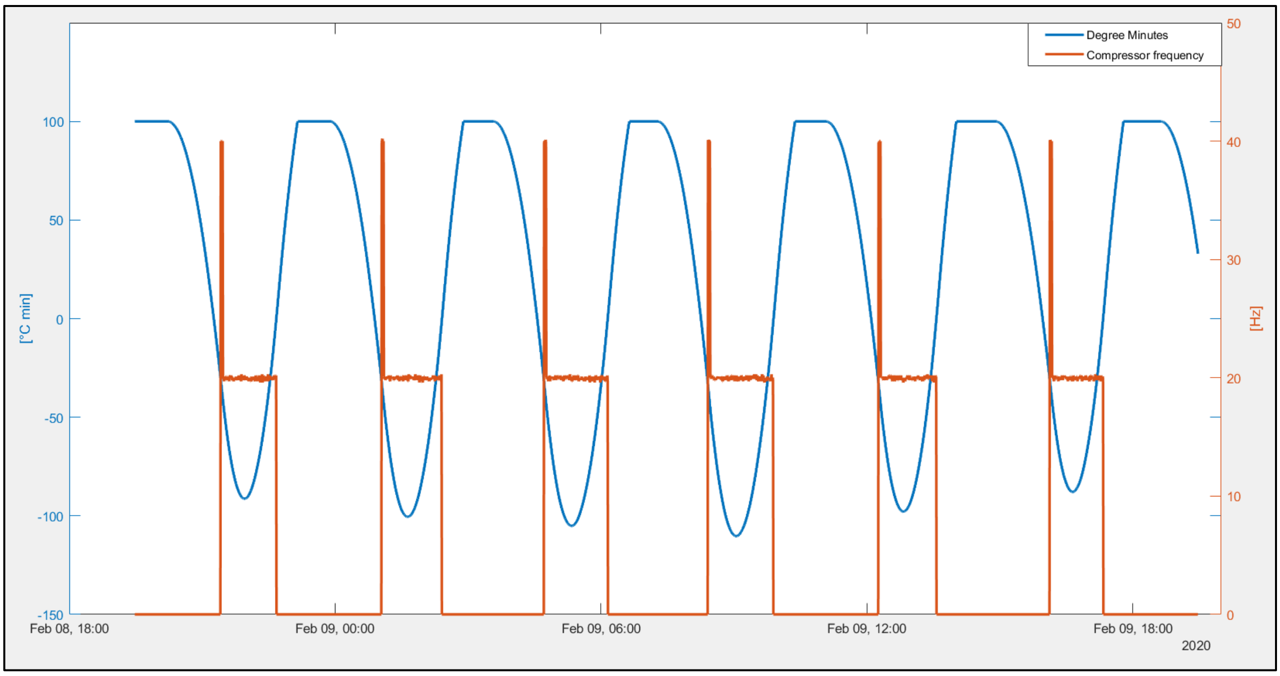

Figure 35: Compressor operation example (MATLAB), heating mode, February 2020

From *Figure 35* the operation of the compressor (represented through its rotating frequency) can be observed with respect to the DM trend during the heating season (February 8-9, 2020): for that experimental campaign the DM threshold value was set to the maximum allowed of -30°Cmin, so once the cumulative of DM reaches that limit the compressor is turned on, taking action to raise the system efficiency through active cooling. In that way the cumulative starts to increase up to the value of 100°Cmin and the compressor is turned off, then after a certain time its decreasing trend starts again until the compressor is turned on, involving a sort of cyclic pattern.

Notably, the choice of this DM threshold was related to the desire for stabilizing the time interval that separates two subsequent compressor starts, but other values could be selected according to the indication in the heat pump user manual.

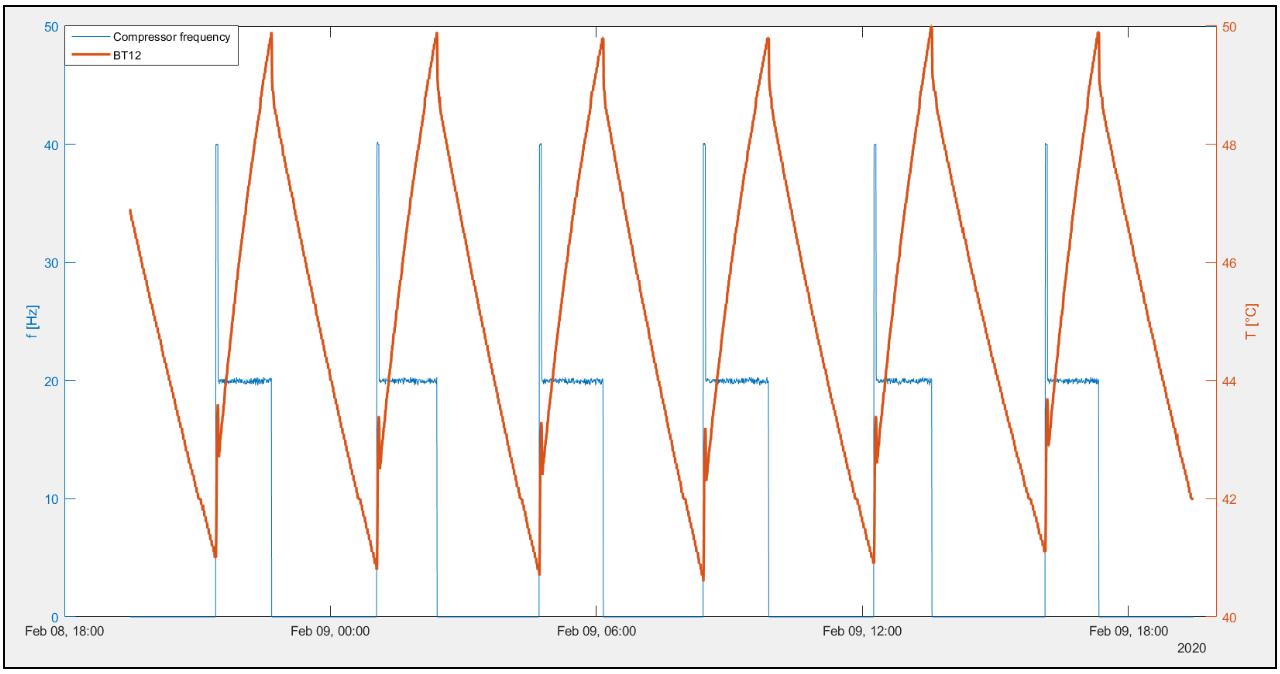

Figure 36: *Delivery temperature trend with respect to compressor operation (MATLAB), heating mode, February 2020*

For the experimental case considered the target value for the delivery temperature was set to 45°C, indeed from *Figure 36* can be noticed that the BT12 curve (sensor for the delivery temperature to the user) oscillates from almost 41°C up to 50°C, with the compressor that is repeatedly turned on and off.

A wider view on the effects caused by this alternating compressor on/off operation can be also obtained by looking at the data from other temperature sensors.

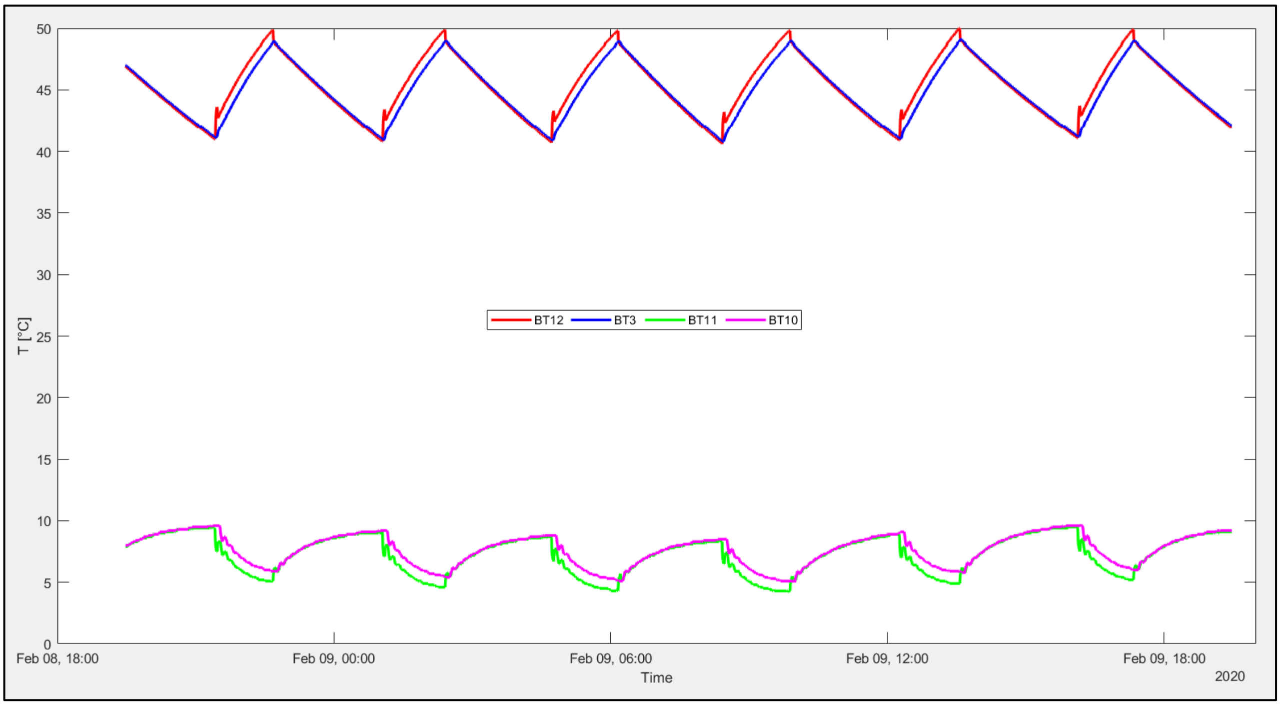

Figure 37: *User-side and Terrain-side temperatures (MATLAB), heating mode, February 2020*

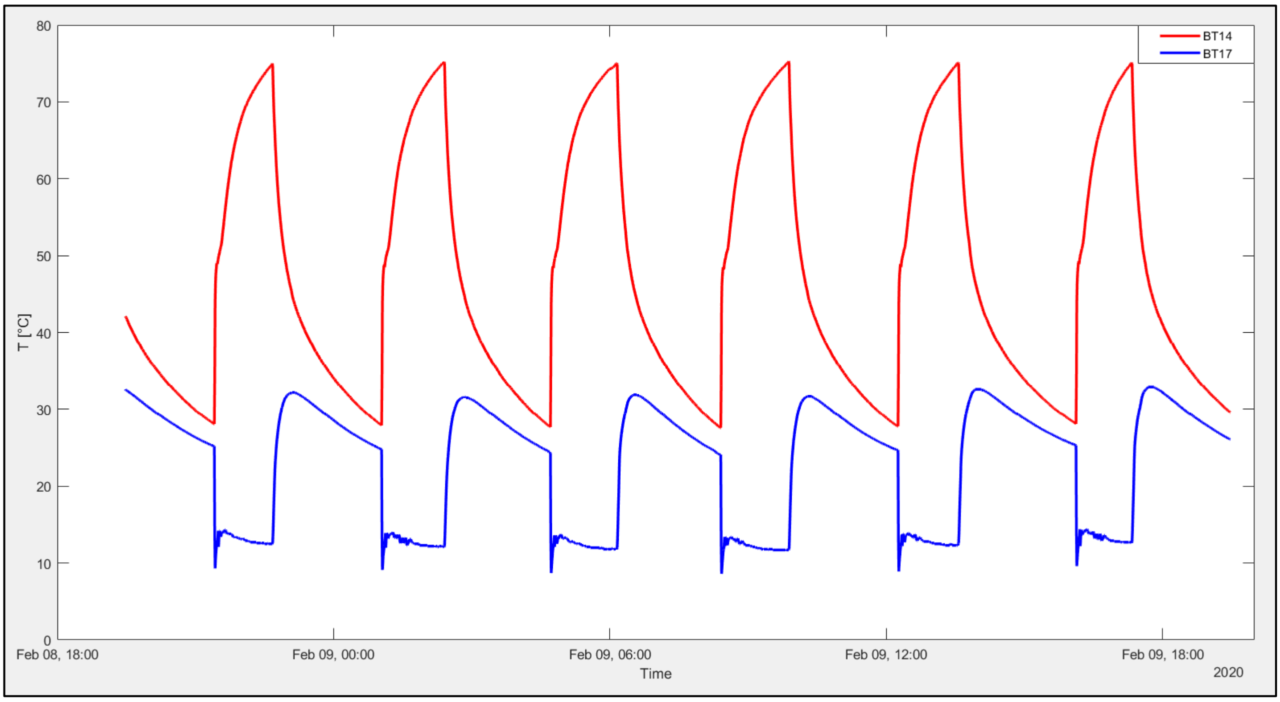

Figure 38: *Temperature difference across the compressor (MATLAB), heating mode, February 2020*

In *Figure 37* are reported the inlet/outlet temperatures trends for both the user and terrain side, and just from the BT12 and BT3 evolution the compressor switching on/off can be noticed, in correspondence of the edges.

Specifically, both the temperatures across the condenser remain almost stackable until the compressor is switched on, when the thermodynamic cycle of R407C starts, involving the heat abstraction from the ground and rejection the secondary circuit (fan coil). Once the compressor is turned off, both BT3 and BT12 decrease and converge towards the same values, because the heat pump is not working.
A similar behaviour can be noticed for BT11 and BT10, with the instauration of a temperature variation across the evaporator when the heat pump is operating.
In *Figure 38* are reported the temperatures across the compressors and, again, an increase of temperature difference caused by the compressor operation can be noticed, whit the return to lower values at the switch-off.
The operation pattern analysed is like that occurred during the cooling season, with a different DM threshold selected, even if the number of switch on/off observed is a bit more smoothed some days, with a reduced number of on/off transients.

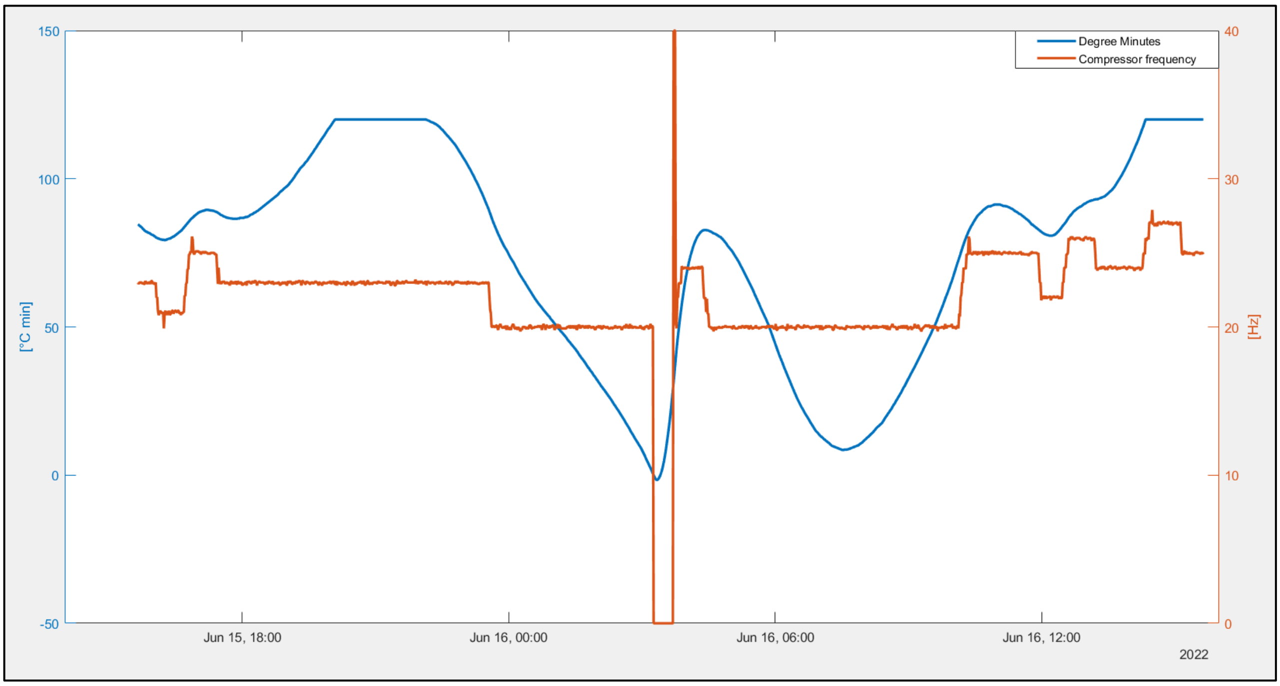

Figure 39: Compressor operation example (MATLAB), cooling mode, June 2022

In *Figure 39* is reported a daily experimental campaign with a target temperature set to 5°C, from which can be noticed only one compressor switch-off, with the cumulative of DM assuming higher values for the rest of time.
As can be noted, the compressor does not simply operate in an "on/off" way, but the frequency can be modulated during the system operation.

8. Databases and tools used for the calculations

The main software adopted in the analysis and calculation process is represented by **MATLAB**, an environment for numerical computation and statistical analysis written in C that allowed to significantly speed up all the calculations.

A dedicated script was written first to automatize the data acquisition from the ".txt" files coming directly from the control unit of the NIBE heat pump, then to process these data, calculating the main properties characterizing the R407C thermodynamic cycle.

The determination of thermodynamic quantities such as specific enthalpy, density and specific heat was performed through the implementation of **CoolProp**, a free C++ library that provides additional features like mixture properties (using high-accuracy Helmholtz energy formulations), correlations of properties of incompressible fluids and brines and the possibility to be interfaced with the databases of NIST REFPROP.

Again, to improve as much as possible the automation in the thermodynamic properties calculation, CoolProp was interfaced to MATLAB, exploiting a Python interpreter through the download of the required installer from python.org.

This Pyhton "wrapper" allowed to implement the CoolProp commands and databases on MATLAB, also exploiting the provided interface with REFPROP, even if the thermodynamic quantities calculated starting from the properties on the respective libraries were very close to each other.

Another software, **CoolPack**, was then used to perform many counterchecks regarding the results obtained with CoolProp, verifying their consistency, especially in the section concerning the pressures determination.

CoolPack is a collection of simulation models for refrigeration systems, developed by the Department of Mechanical Engineering (MEK), Section of Thermal Energy (TES) at the Technical University of Denmark (DTU).

It offers several tools for designing and controlling almost everything that works by means of a fluid refrigerant, among which the exploited ones are: the "Refrigerant calculator" tool, used to calculate single state point properties for refrigerants (enthalpy, entropy, specific heat, …), the "Refrigeration Utilities" tool, that can create tables and plots of refrigerant properties, providing the log(p)-h diagram where to draw the thermodynamic cycles, and the "Secondary fluids for heat transfer" tool, which can be used to calculate transport properties and pressure drop for a range of fluids, as the water/glycol specific heat and density over the operating ranges.

Notably, the "Refrigerant calculator" tool was fundamental to check the thermodynamic properties obtained with CoolProp, such as the enthalpy of the state points composing the cycle, to calculate the desired outputs as the daily average COPs over the experimental campaigns.

Therefore, both CoolProp and CoolPack were considered during the energy assessment process, looking for deviations among the calculated values, as they work probably with a different basis.

These deviations, expressed in percentage terms, were then highly considered and, in the case of pressures determination, represented the basis on which develop a correction factor to enable the convergence of the respective implemented algorithm.

9. Energy assessment for the cooling season

The presentation of the main topics covered by the work done in recent months starts form this chapter, dealing with the data coming from the heat pump monitoring system and the experimental campaign carried out during the thesis period.

As previously mentioned, the energy assessment of the geothermal heat pump in cooling mode represented the main core of this thesis, aiming to provide additional results for the summer season, which has already been investigated a bit in some previous thesis works (as in Filippo Sterrantino's master's thesis), but much less than the winter one.

The study of the cooling operation for this thesis project was allowed by its beginning in late May, when the summer season was sufficiently close. Indeed, while I was dealing with an initial preparatory phase involving the analysis of past measurements, the system was put in operation, collecting data from June 14th 2022 at 15:39:18, up to July 5th at 14:49:24.

After a first look at the data recorded, the time range previously selected was restricted, choosing as last date the 23rd of June 2022 (at 21:31:20). This choice was motivated by the fact that, from that point on, the compressor was definitely switched off for the remaining days of the experimental campaign.

In that way, the data collected concerned the system current year operation, with the three ground heat exchanger modules in series arrangement and thermally coupled with the condenser of the heat pump, while the user side (the fan coil circuit) was connected with the evaporator.

The delivery temperature to the fan coil (the user) oscillated around the target values imposed by the heat pump logic, set to 5°C, with the compressor switch on/off regulated through the degree minutes concept (DM).

Concerning instead the monitoring system, further details regarding the disposition of the temperature sensors inside the heat pump are reported in (section 4.3). All the data measured by these sensors were available with a sampling time of 1 minute, then saved in a series of ".txt" files covering 24 hours of operation.

9.1 COP calculation

In cooling mode, the COP (or EER, "Energy Efficiency Ratio") is defined as:

$$COP = \frac{Q_{ev}}{L_{compr}} = \frac{q_{ev,R407C}}{l_{compr,R407C}}$$

The COP calculation was performed by reasoning in terms of specific quantities rather than in terms of powers, as the refrigerant mass flow rate within the heat pump circuit represented an unknown quantity at the beginning.
Starting from the numerator, the specific heat exchanged at the evaporator was defined as the difference in enthalpy across the evaporator, considering the refrigerant side. The enthalpy at the evaporator outlet was calculated starting from the temperature recorded by the sensor BT17 (compressor inlet) and the pressure in the low pressure branch, while the enthalpy at the evaporator inlet is equal to that at the condenser outlet, as the lamination process is considered isenthalpic.

$$q_{ev,R407C} = h_{compr,in} - h_{sat,liq}$$

The enthalpy at the condenser outlet was obtained on the basis of the hypothesis of no subcooling, so intercepting the isobar corresponding to the high pressure level with the saturated liquid curve.
Considering now the denominator, the specific compression work was calculated as the difference in enthalpy between the compressor outlet and inlet.

$$l_{compr,R407C} = h_{compr,out} - h_{compr,in}$$

These values of enthalpy, such as those at the numerator, were calculated with the support of the MATLAB script and CoolProp databases, starting from the temperature values returned by the sensors BT17 and BT14, and the pressure level in the respective branch of the circuit.
For these calculations, the method adopted for the determination of the pressure levels in the two branches of the heat pump impacts on the results obtained, with some additional considerations to point out regarding the compression transformation.

Considering a fixed pressure levels assumption, a further control step must be performed on the temperatures returned by the sensors BT17 and BT14, as the compressor cannot work with R407C at the liquid state. This means that both the working points at the condenser inlet and outlet must be outside the limit curve reported on the p-h diagram.
This fact is strictly related to the constant pressures approach, indeed for a real case the pressure levels would vary over the experimental campaign, allowing the compressor to work with only gaseous refrigerant.
For the constant pressures case, what can be done is to check for every set of measures recorded by the system that these two conditions are verified:

$$(1) \quad T_{BT17} > T_{sat,LP}$$
$$(2) \quad T_{BT14} > T_{sat,HP}$$

More in detail, the saturation temperature at low pressure level (LP) and at high pressure level (HP) can be determined intercepting the respective isobar with the saturated vapor curve.
This double check allows to perform a first data cleaning regarding the set of measurements with the compressor inlet/outlet falling the in the biphasic region, whose properties would not be calculated by CoolProp (they are not defined inside the limit curve).
In that way only the measurements respecting these two conditions are considered in the calculation of the specific compression work, and so of the COP.
Among the measures discarded, there also those collected with the compressor off, as it would not make sense to calculate the COP of the heat pump when there is no refrigerant flow.
This approach for the constant pressures case involves a different percentage of data removed on the basis of the selected pressures levels, for instance if the low pressure level increases, the number of measures which do not respect the condition (1) increases too. This reflects in the trend of the COP, calculated point by point by the MATLAB script, because some “holes” appear in correspondence of the data removed.
However, this fact can be confined by checking the percentage of data removed mentioned above, and so selecting pressure values that allow to obtain a suitable number of measures accepted to calculate the daily average values later.

9.2 Power calculation

Also in this section are valid the statements discussed in section 8.1, so in the case of a constant pressures approach both the measures collected with the compressor off and the compressor inlet/outlet falling in the biphasic region were discarded.

Once the specific quantities were determined, the following step to talk in terms of compression work and thermal power exchanged at the indoor/outdoor unit is represented by the determination of the R407C flow rate within the heat pump circuit.

The refrigerant flow rate can be determined through the application of the first law of thermodynamics for open systems, considering one of the two heat exchangers. Starting from the hypothesis reported in section 5, the water/glycol average flow rate in the primary circuit was assumed equal to 0,435 m^3/h, then this data was used to apply the first law of thermodynamics to the outdoor unit (the condenser), thermally coupled with the ground.

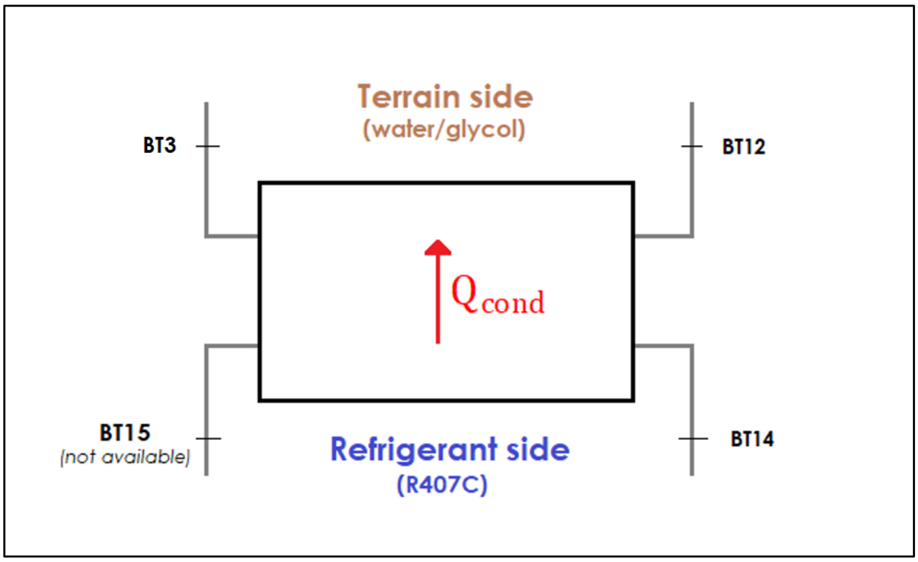

Figure 40: Condenser simplified scheme

In *Figure 40* are reported the primary circuit, at the top, and the heat pump circuit, at the bottom, so the thermal power exchanged at the condenser can be expressed as:

$$Q_{cond} = \dot{m}_{w/g} \cdot c_{p_{w/g}} \cdot (T_{BT12} - T_{BT3}) = \dot{m}_{R407C} \cdot c_{p_{R407C}} \cdot (T_{BT14} - T_{BT15})$$

$$\dot{m}_{R407C} \cdot c_{p_{R407C}} \cdot (T_{BT14} - T_{BT15}) = \dot{m}_{R407C} \cdot q_{cond_{R407C}}$$

$$\dot{m}_{R407C} \cdot q_{cond_{R407C}} = \dot{m}_{R407C} \cdot \left(q_{ev_{R407C}} + l_{compr_{R407C}}\right)$$

$$\dot{m}_{R407C} = \frac{\dot{m}_{w/g} \cdot c_{p_{w/g}} \cdot (T_{BT12} - T_{BT3})}{q_{ev_{R407C}} + l_{compr_{R407C}}}$$

From the last formula, the refrigerant mass flow rate can be determined, even if an additional observation can be highlighted regarding the specific heat of the water/glycol.
As anticipated in the hypothesis section, the specific heat of the fluid in the primary circuit (as the one in the secondary) was calculated point by point with MATLAB, considering a fixed pressure of 2 bar, together with the temperature collected by the sensors displayed in *Figure 40*.
This allowed to determine point by point also the refrigerant mass flow rate, then used to convert the specific quantities calculated previously into extensive ones.

$$Q_{cond} = \dot{m}_{R407C} \cdot q_{cond_{R407C}}$$

$$Q_{ev} = \dot{m}_{R407C} \cdot q_{ev_{R407C}}$$

$$L_{compr} = \dot{m}_{R407C} \cdot l_{compr_{R407C}}$$

Similarly, the first law of thermodynamics can be applied to the evaporator to obtain the water/glycol mass flow rate in the secondary circuit.

$$Q_{ev} = \dot{m}_{R407C} \cdot q_{ev_{R407C}} = \dot{m}_{w/g} \cdot c_{p_{w/g}} \cdot (T_{BT10} - T_{BT11})$$

$$\dot{m}_{w/g\,(sec)} = \frac{Q_{ev}}{c_{p_{w/g}} \cdot (T_{BT10} - T_{BT11})}$$

9.3 The problem with pressure levels

The lack of pressure measurements from the heat pump system is a major issue, because, as mentioned in the previous sections, the calculation of the thermodynamic quantities needed requires the knowledge of both temperature and pressure in each working point.

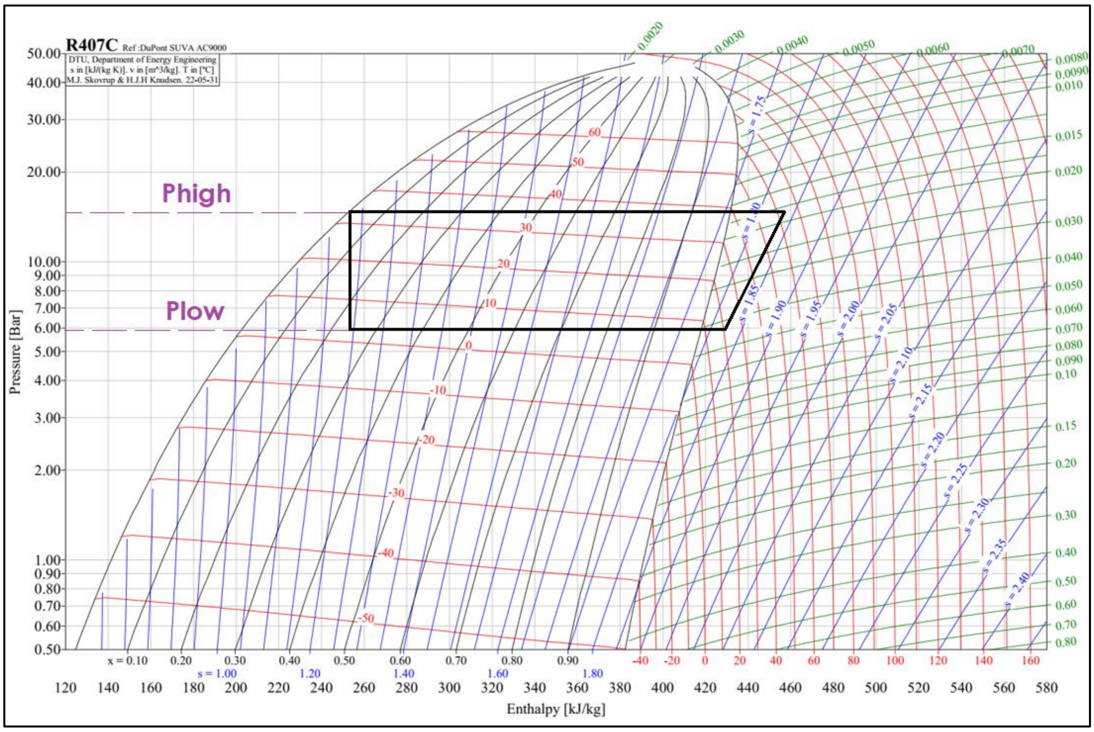

Figure 41: Pressure levels of a heat pump cycle, example with R407C

The two pressure levels to determine, or hypothesized, are those reported in *Figure 41* as Phigh and Plow: they represent respectively the pressure level on the high pressure branch, after the compressor, and the pressure level in the low pressure level, before the compressor.

To solve this pressure problem, two ways were analysed for this thesis:

- **Fixed pressure levels**: in that case Phigh and Plow are considered fixed throughout the experimental campaign, testing various pressure levels to see how the system would behave.
- **Variable pressure levels**: in that case the two pressure levels vary step by step, accordingly with the selected sampling time of one minute. This was made possible by implementing a proper external algorithm to the MATLAB script.

9.4 Fixed pressures approach

In this first step, the pressure levels were considered fixed, involving the problems of liquid compression presented in section 8.1.
A dedicated MATLAB script was realized to acquire the data from the NIBE F1155 and calculate the desired thermodynamic quantities point by point, and finally the COP, implementing a proper section to automatically verify the location of the compressor inlet/outlet with respect to the limit curve on the p-h diagram of the R407C.
This was verified in terms of the conditions on $\mathrm{T}_{\mathrm{BT17}}$ and $\mathrm{T}_{\mathrm{BT14}}$, checking that, for each set of measurements, they are higher than the saturation temperature respectively at low pressure and high pressure (defined through the intersection between the isobar and the saturated vapor curve). In that way, the two working points must lie in the superheated vapor region, or at least on the saturated vapor curve to be accepted.
This control step is not present in the variable pressure script, as once the suitable pressure levels (with the associated uncertainty) are determined for each set of measurements, the compressor works with gaseous refrigerant.
In summary, concerning the cooling analysis, this first approach with fixed pressure levels was essentially used as a preliminary check to roughly determine two suitable ranges for the searching algorithm adopted in the following step, one for Phigh and another one for Plow.
In that way, using the data recorded by the various sensors available, the MATLAB script was run with different values for Phigh and Plow, plotting the trend of COP over time.
The results reported below are referred to the same time interval, to give a first look on the consistency of the collected data with respect to the pressure levels imposed.

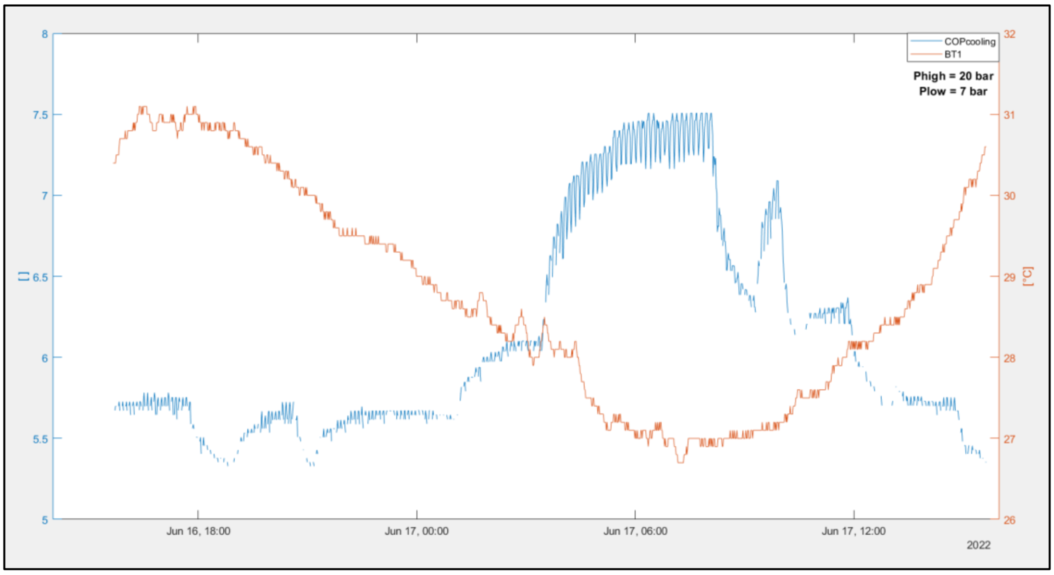

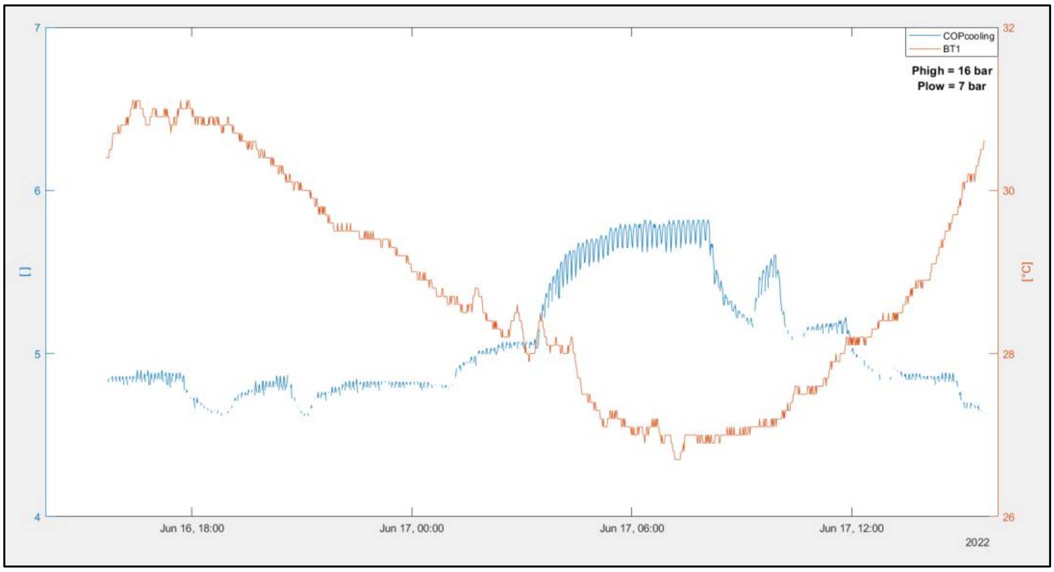

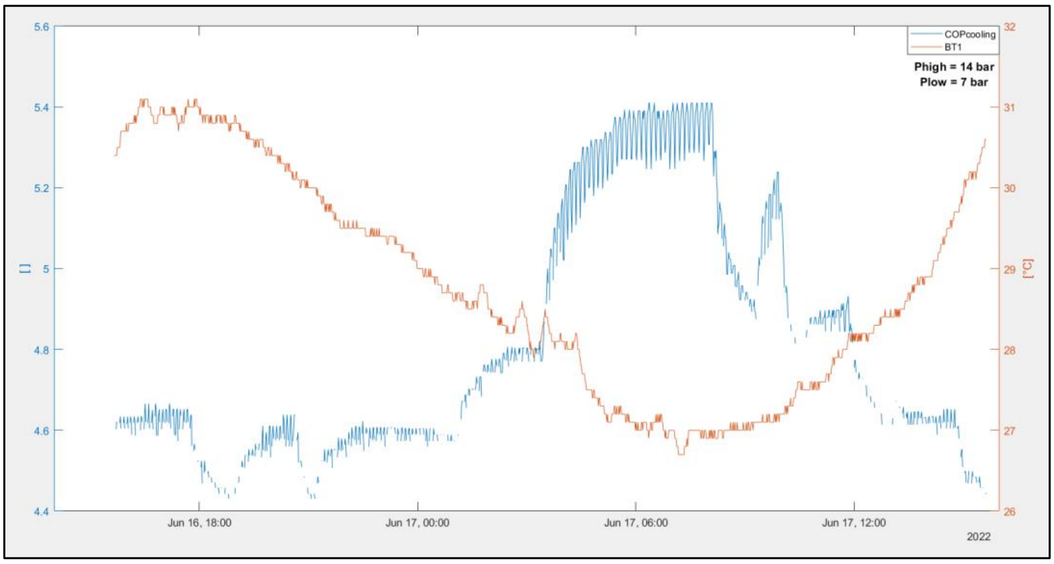

Figure 42: COP vs Time (MATLAB), cooling mode, Phigh=20 bar and Plow=7bar
Figure 43: COP vs Time (MATLAB), cooling mode, Phigh=16 bar and Plow=7bar
Figure 44: COP vs Time (MATLAB), cooling mode, Phigh=14 bar and Plow=7bar

The three figures reported above are the results of a first test series, intended to check the compatibility of the measurements recorded with the pressure levels selected, specifically regarding the high level in a range from 20 to 14 bar.
Starting from a general overview on the two trends, regarding the COP and the outdoor temperature (measured by the sensor BT1), it can be noted that the patterns look quite realistic: the COP and the outdoor temperature follows an almost opposite trend, with the first one increasing during the coldest hours, as in the late evening and at night, while decreasing in the middle of the day.
Even if the COP trend seams realistic, the values assumed for all the three cases reported above are generally too high to be plausible, suggesting that the values selected for Phigh are probably not the right ones.
From the three figures above, it can be also noted that the values assumed by the COP seam to decreases, moving towards more physical ones, with a decreasing Phigh.

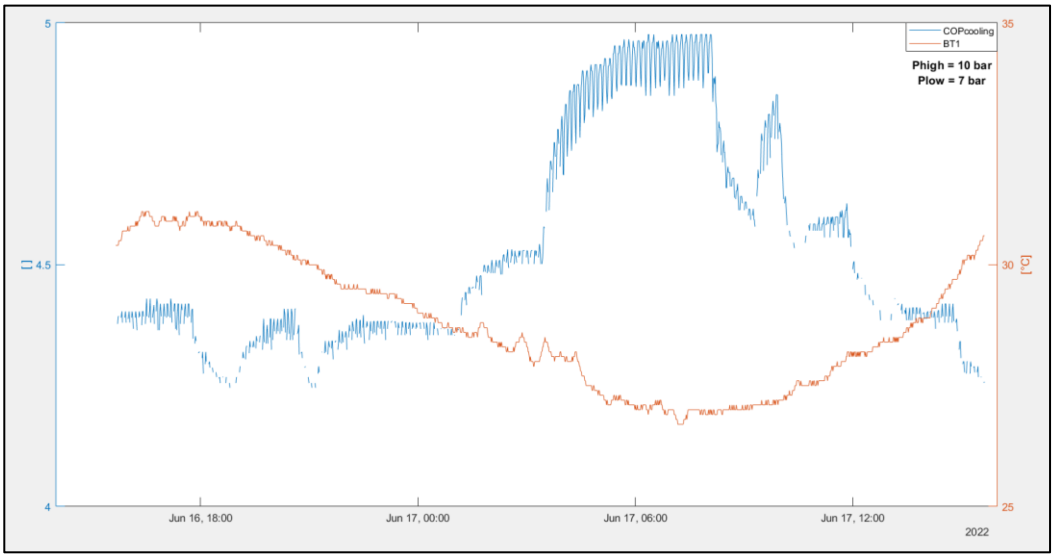

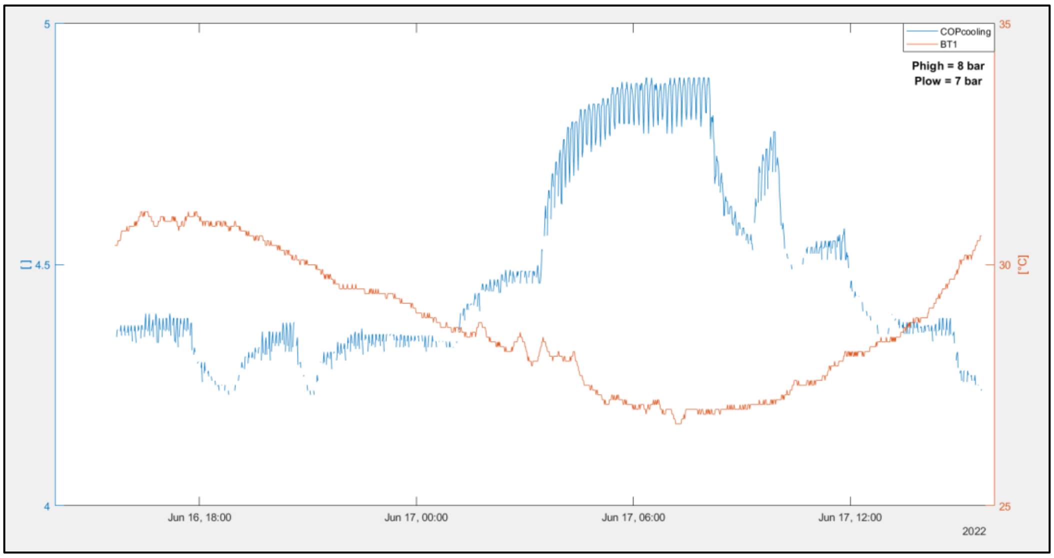

Figure 45: COP vs Time (MATLAB), cooling mode, Phigh=10 bar and Plow=7bar
Figure 46: COP vs Time (MATLAB), cooling mode, Phigh=8 bar and Plow=7bar

Looking at *Figure 45* and *Figure 46*, the value selected for Plow was not changed, while Phigh was set respectively to 10 bar and 8 bar, much closer to the low pressure level.
Although it is a little unusual, compared to what could be expected as working pressure for the high pressure branch, these last attempts seem to provide more suitable values for the COP, comparable with others on the market. Therefore, the range within which the searching algorithm could work, considering the high pressure level, could be set as first assumption in the neighbourhood of 8-10 bar.
Regarding the low pressure level, in the previous tests it was kept fixed to 7 bar, representing the reason why the COP trend is not continuous but presents some holes.
These holes should be filled by the other measurements collected by the heat pump system, but they were discarded by the MATLAB script, because the compressor inlet was situated in the biphasic region.
As the temperatures at the inlet/outlet of the compressor are set quantities, measured by the temperature sensors, the emergence of new holes is strictly related with the pressure level selected, and so reducing Plow, the number of holes will decrease too.

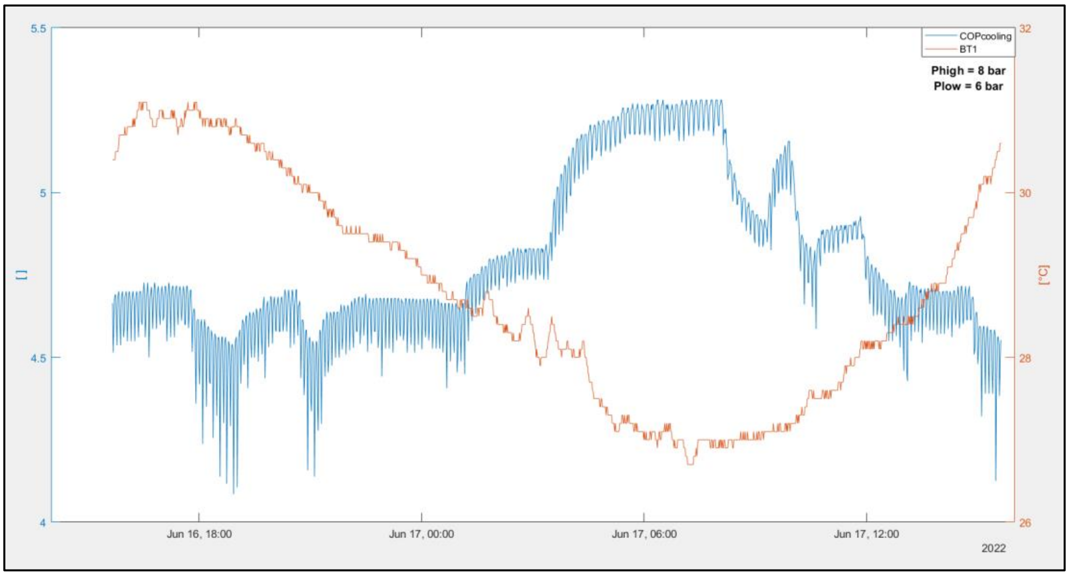

Figure 47: COP vs Time (MATLAB), cooling mode, Phigh=8 bar and Plow=6bar

In *Figure 47* are reported the results of a test run with a Plow of 6 bar, from which can be noted that reducing the low pressure level, with the same values provided by the temperature sensor BT17 (compressor inlet), the trend of COP changes a bit and all the holes are filled.

This fact suggested that, considering the recorded temperatures at the compressor inlet, they are quite close to the saturation temperature at 6-7 bar. Indeed, turning up the pressure above 7 bar, almost all the measurements would be discarded for this experimental campaign.

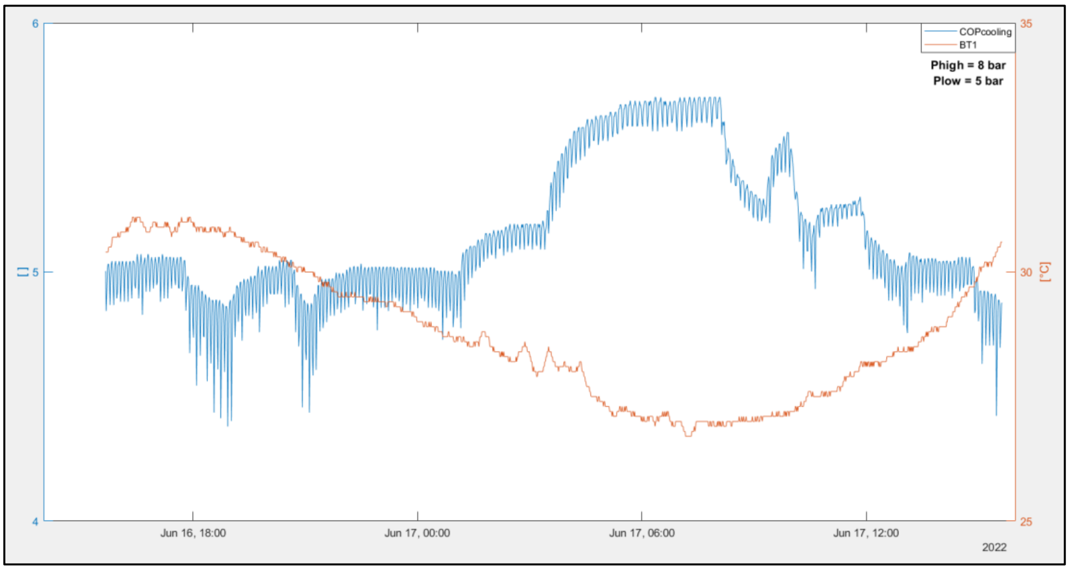

Figure 48: COP vs Time (MATLAB), cooling mode, Phigh=8 bar and Plow=5bar

Trying to figure out a suitable range also for Plow, additional tests were performed considering lower pressure values, as the case of 5 bar reported in *Figure 48*.

Also in that case there are not holes in the COP pattern, but the COP values begin to rise towards higher values, up to 6.

From all that, it was deduced that a suitable range for the low pressure level should range around 6-7 bar.

Focusing again on the Phigh, the reason of the decreasing trend of the COP values selecting lower Phigh values can be better noticed on the R407C p-h diagram, representing heat pump cycles with different pressure levels.

As shown below in *Figure 49*, the particular shape of the limit curve for the R407C, together with the values collected by the sensors BT17 and BT14, lead to a very high slope for the segment representing the compression step in the case of higher Phigh values (as the example at 20 bar on the right).

As both the temperatures at the compressor inlet/outlet are given parameters, once the high pressure level increases, the compressor outlet moves along an isothermal curve in the superheated vapor region, such as occurs for the case reported below with an outlet temperature of 60°C (average value for June 17th 2022).

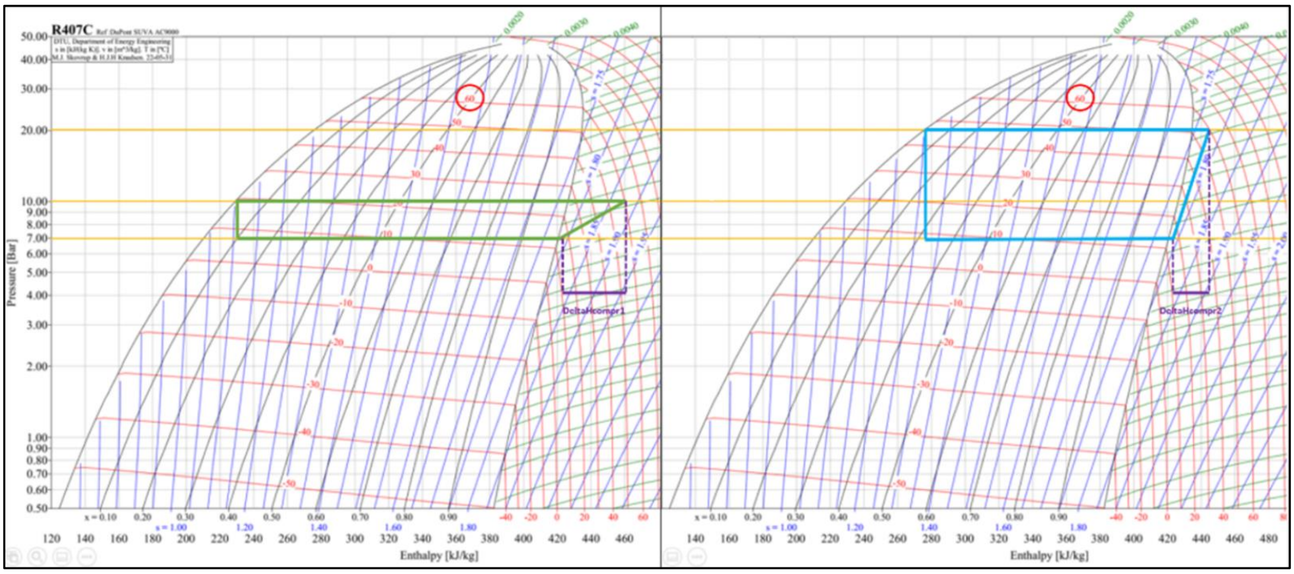

Figure 49: Examples of heat pump cycles with different Phigh

All that leads, in the case of higher Phigh values, to a great reduction of the enthalpy difference associated with the compression work, which is relatively larger compared with the reduction of the enthalpy variation associated to the evaporation step, hence, moving towards higher Phigh, the average COP increases.

The same can be said also considering the results coming from different time ranges, as the pressures ranges that lead to suitable COP are very close to the ones derived previously.

For instance, on the next page are reported three figures showing the results coming from the measurements performed a few days later, on June 21th 2022.

As in the previous case analysed, three different values were selected for Phigh, and also this time the returned COP assumes more suitable values for high pressure levels such as 8-10 bar.

More generally, a similar situation occurred also for the results deriving from the remaining days of June 2022 experimental campaign.

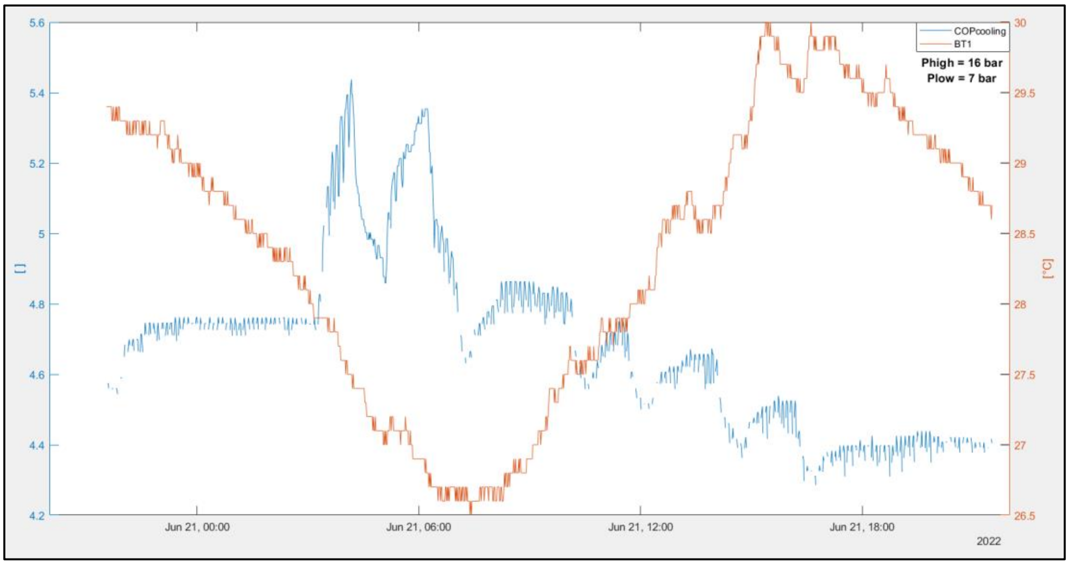

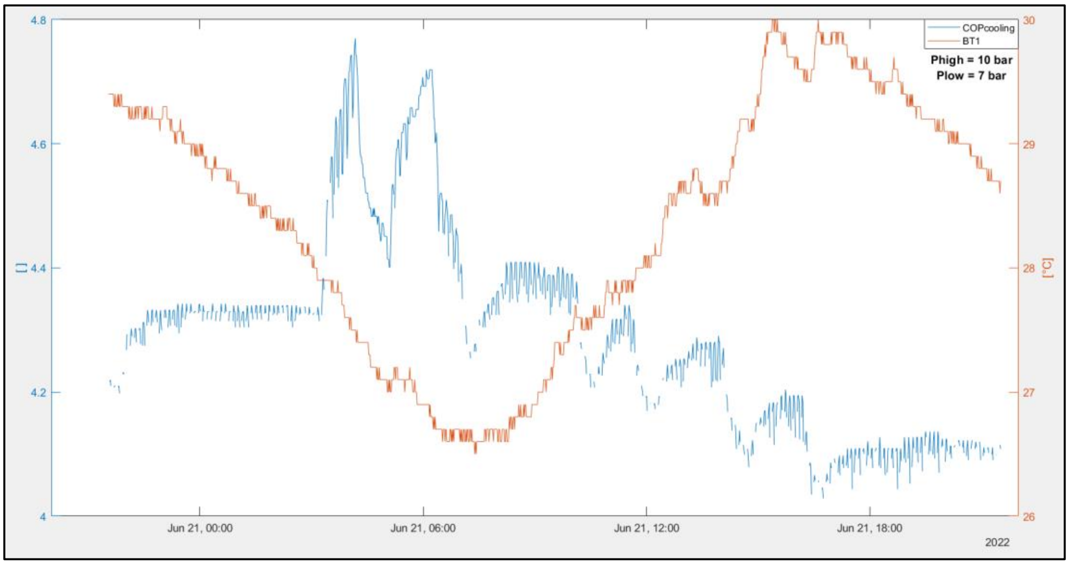

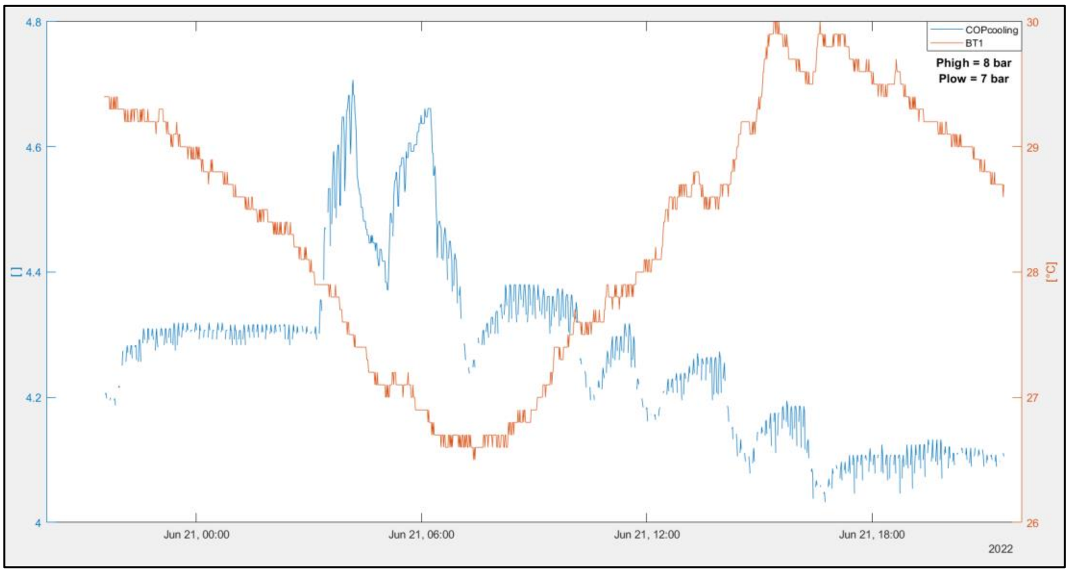

Figure 50: COP vs Time (MATLAB), cooling mode, Phigh=16 bar and Plow=7bar

Figure 51: COP vs Time (MATLAB), cooling mode, Phigh=10 bar and Plow=7bar

Figure 52: COP vs Time (MATLAB), cooling mode, Phigh=8 bar and Plow=7bar

9.5 Variable pressures approach

As mentioned in the previous section, the calculations performed at fixed pressure levels represented essentially a preliminary test to identify suitable pressure ranges for both the branches before and after the compressor.

In this stage, the intervals associated with Phigh and Plow were used as boundaries by the pressure calculation algorithm, which was designed and implemented as an external function called by the main MATLAB script, did on purpose for this section, staring from the one adopted in the fixed pressure case.

The main tools exploited in this step are represented by: MATLAB, still used to automatize the calculations and process the huge amount of data coming from the heat pump with a sampling rate of one minute, Coolprop, providing the databases to calculate all the required thermodynamic quantities and CoolPack, which is now used especially in the pressure calculation algorithm to verify the properties calculated.

Indeed, a significant portion of this section was dedicated to the calculation of the percentage deviation interesting both the single thermodynamic quantities, such as enthalpy and specific heat, and the main results as the thermal power exchanged and the COP.

Different ways to proceed were considered, with the aim of minimizing as much as possible the gap between the calculations performed using CoolProp and CoolPack, considering that only the first one can be implemented in the MATLAB script.

The main results were then plotted and grouped in a daily basis to enable a simpler consultation, involving also some additional considerations regarding for example the treatment of the transients and the main differences with respect to the fixed pressures approach.

9.5.1 Pressure calculation algorithm

The core of this second approach for the determination of the heat pump performances is represented by the pressure calculation algorithm, intended as a further step in view of a more realistic modelling of the system.

The working principle revolves around an iterative process, based on the comparison between two different ways for the calculation of the specific compression work. All the required thermodynamic quantities are calculated on the basis of the temperature measurements recorded by the sensors and the hypothesized values of pressure, coming out from the ranges mentioned before.

These ranges are represented in the form of two different arrays, one for Phigh and another one for Plow, characterized by a constant distance among the elements.

The dimension of these arrays was varied several times, experiencing different results in terms of the pressures returned, even if it was noted that the results differed by a small quantity for a number of elements equal or bigger than forty (involving a difference between an element and its successor below 0,2 bar).

These two arrays are then rearranged in a N x 2 matrix, where N is the number of possible combinations between the elements of the two arrays, in order to check iteratively each couple of pressures Phigh and Plow within the respective range selected.

For each set of measurements collected by the heat pump system (one every minute), the algorithm processes all the pressures couples forming the matrix, then, after calculating the specific compression work in the two ways prescribed, it computes the relative deviation between them and finally select the couple which provides the smallest one.

For each pressures couple from the matrix, there is a preliminary check with the temperatures recorded by the sensors BT17 and BT14 (compressor inlet/outlet), regarding the location of the working points with respect to the R407C limit curve, similarly to what happened for the fixed pressures case, in order to be sure that the compressor works with only gaseous refrigerant.

In case of liquid compression, the pressures couple is discarded, proceeding with the next one.

Additionally, as for the previous case analysed, the measures with the compressor off are discarded, as it has no sense to calculate the COP in that condition.

Once the set of pressures couples is defined and all the controls are carried out, the algorithm proceeds through the calculation of the specific compression work, as anticipated before.
This step is essentially based on the idea of using these pressures to calculate the same quantity in two parallel ways, aiming for results as close as possible.
The first expression selected for the specific compression work is based on the enthalpy variation between the compressor outlet/inlet working points, while the second passes from the calculation of the specific heat, which was both performed considering two separated values or an average one.

$$(1) \qquad l_{compr_A} = h_{compr_{out}} - h_{compr_{in}}$$

$$(2) \qquad l_{compr_{B1}} = c_{p_{average}} \cdot (T_{BT14} - T_{BT17})$$

$$(3) \qquad l_{compr_{B2}} = c_{p_{high}} \cdot T_{BT14} - c_{p_{low}} \cdot T_{BT17}$$

The compression work indicated with the subscript “A” is confronted with one of the other two expressions with the subscript “B”. More in detail this last letter presents two different expressions, because both were analysed to check which of them provided the best match with the “A” one.
In expression (2), the terms “high” and “low” appearing as subscripts for the specific heat, are referred to the property calculation using the pressure recorded as Phigh and that recorder as Plow.
For each set of measurements, the procedure is essentially repeated, calculating the specific works of compression with each pressures couple and updating the registered value if a smaller one occurred.
Additionally, a minimum target for this deviation is set to assure a certain level of convergence, excluding too high deviations which led to inconsistent results.
Once the pressure calculation algorithm finishes its job, the pressures couples (formed by a value for Phigh and Plow) are saved in a n x 2 matrix, where n is the number of the sets of measurements recorded by the heat pump.
This matrix is then returned to the main script, which proceeds with the calculations and the results plotting.
The implications about the use of the compression work in the form (2) or (3), with the associated errors, will be deeply analysed in dedicated sections.

9.5.2 CoolProp vs CoolPack: properties deviation

As previously anticipated, the differences in the thermodynamic quantities calculated with the two software introduced an additional issue in the results testing.
The main idea was that of using CoolPack as countercheck for the results calculated based on CoolProp databases, but the impossibility to automatize the calculations performed by CoolPack imposed to perform many point checks to assess the entity of these deviations, and the main parameters involved.
The calculation procedure of the main power and efficiency parameters, pursued by the MATLAB script, is based on the two working points of the refrigerant cycle for which more information are available: the compressor inlet and outlet.
Starting from these two points, the energy assessment procedure lays its basis on the calculation of the specific enthalpies, so they were the first thermodynamic quantity to be checked.

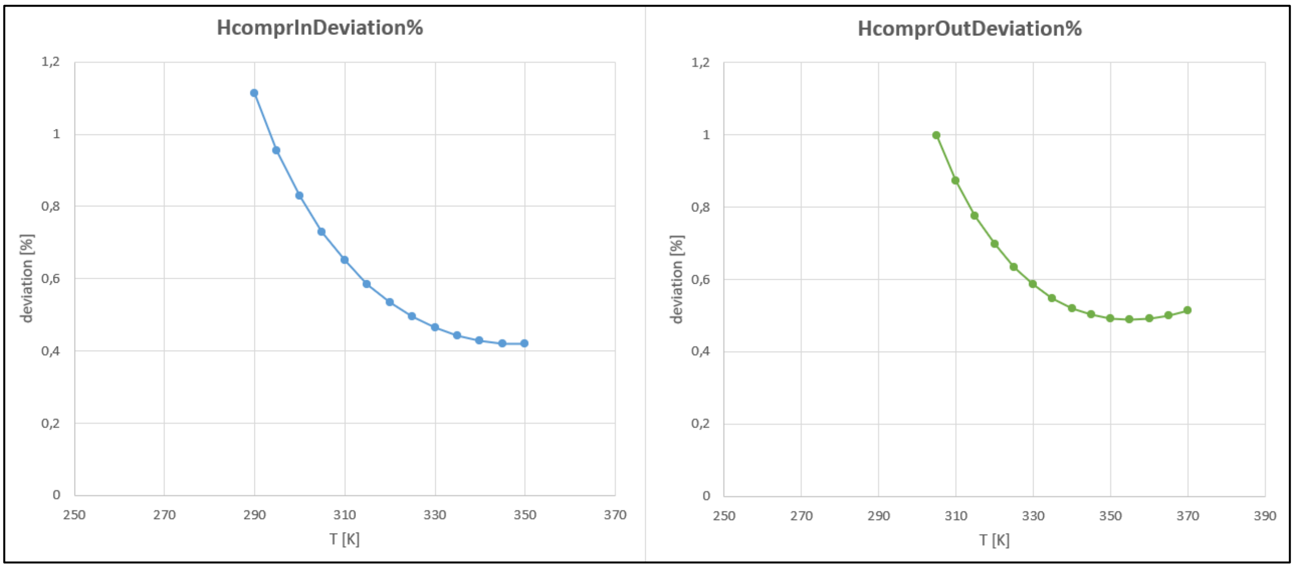

Figure 53: % deviation of the enthalpy at the compressor inlet/outlet vs temperature (Excel)

In *Figure 53* are reported the percentage deviations of the enthalpy, as a function of temperature, while the pressure was fixed to sample values representing Phigh and Plow.
The day selected to test these data was again the June 17th 2022, but the situation for the remaining days of June 2022 experimental campaign is analogous, as the temperatures recorded by the sensors BT17 and BT14 do not change much, and the same occurs for the pressures.

Notably, the plot reported above refers to a pressure of 6,6 bar (in the left) and a pressure of 9 bar (in the right), while a similar temperature interval was selected to better visualize the error trend for different pressure levels.
As can be noted, the deviations in the enthalpies calculation among the two software do not represent a huge problem, as even the worst values reached do not overcome the 1,2%, which was the case of the compressor inlet (the temperatures recorded by BT17 ranges around 285-290 K).
Even considering a lower Phigh, close to 8 bar for instance, the situation involving the enthalpy values remains almost the same, hence, regarding the compressor inlet/outlet, too impacting deviations within the working ranges of temperature and pressure were not expected.
The situation changes for what concerns the specific heat, as many counterchecks reported bigger deviations between the two software, which could not be neglected at all.

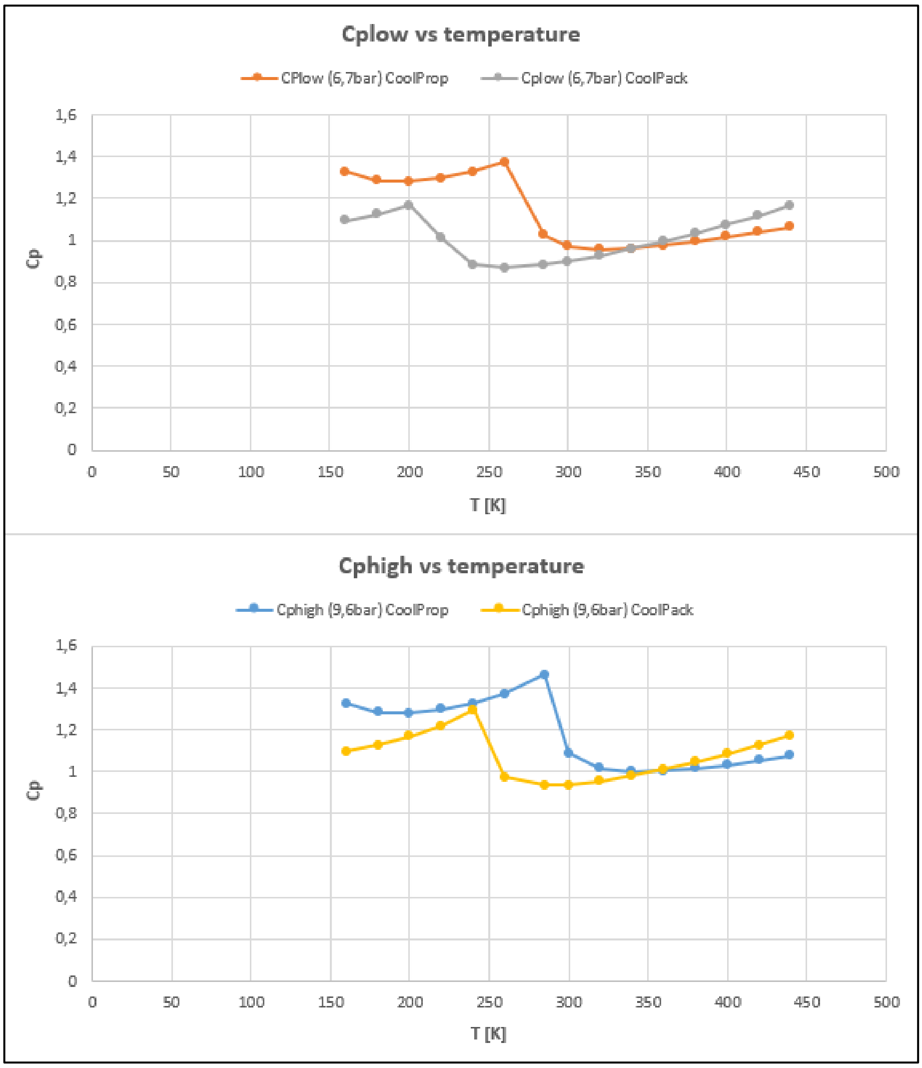

Figure 54: Specific heat vs T trends, temperatures from June 17th 2022, 15:39:37 (Excel)

Looking at *Figure 54*, it is reported a comparison between the specific heat trends calculated both with CoolProp and CoolPack, considering two different pressure levels selected as Plow and Phigh.
Like the enthalpy, also the specific heat is a function of both temperature and pressure, so the trends reported were realized by fixing one of them (always the pressure) and varying the other one (the temperature).
It can be noted that the deviation between the two trends, for both the pressure levels, depends on the area selected, as it tends to decrease towards higher temperatures. That is the case of the compressor outlet working point, where typical temperature values range around 340-350 K.
The situation is more complicated for the compressor inlet working point, for which typical temperature values range around 285-290 K, corresponding to a higher distance between the curves.

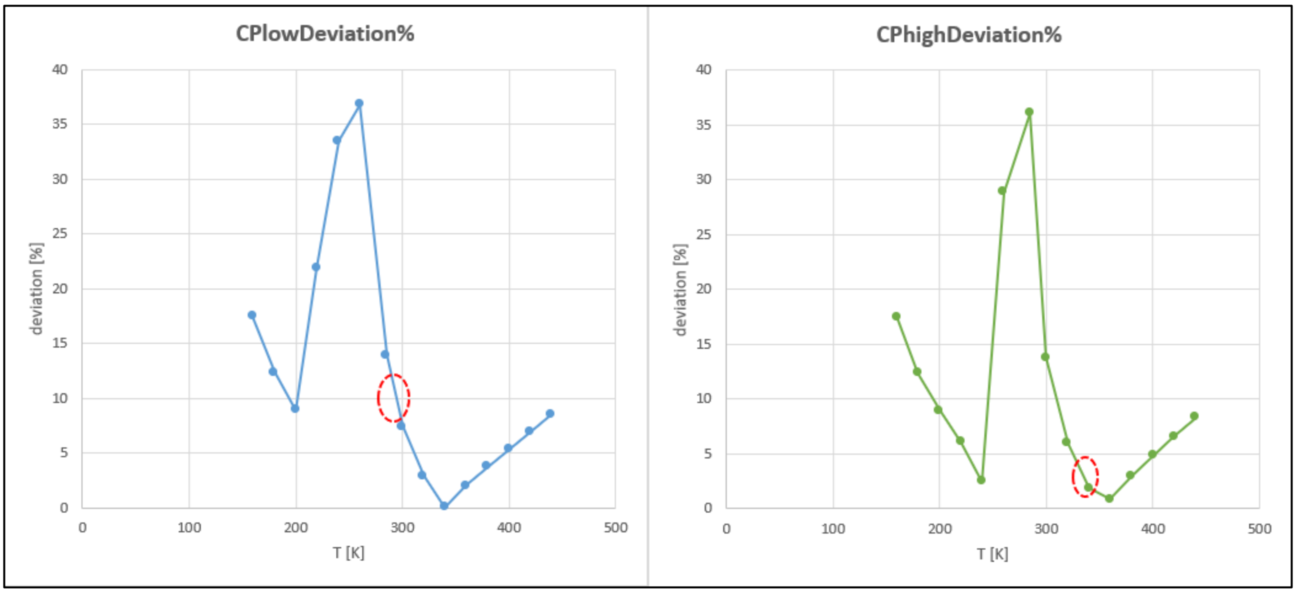

Figure 55: % deviation of the specific heat at the compressor inlet/outlet vs temperature (Excel)

Going more into detail, in *Figure 55* are reported the percentage deviation trends in function of temperature, for both Plow and Phigh sample values (the same as before).
The little areas highlighted in red indicate the average errors associated with the calculation of the specific heat at the compressor inlet (on the left) and outlet (on the right), showing how the situation changes between the two: in the case of the compressor outlet, the higher temperature level leads to an error in the range of 3-5%, which could be still considered acceptable, while in the case of the compressor inlet the percentage deviation grows up to 10%.

This situation is even exacerbated by fact that the specific heat calculation is fundamental for the operation of the pressure calculation algorithm, as it appears in one of the specific compression work formulations.
The result of this deviation is so reflected in the determination of the pressure levels, involving pressures couples that allows a good convergence with the thermodynamic quantities calculated with CoolProp, but a totally different outcome using CoolPack.
At that point the most immediate solution seemed that of adopting a correction factor, thought to be multiplied by the specific heat at low pressure level (at the compressor inlet) calculated by the MATLAB script using CoolProp databases, in order to reach at least the deviation level affecting the specific heat calculated at the compressor outlet.
This solution brought variable results, depending especially on the expression selected for the specific compression work involving the specific heat, and on the pressures range selected for Phigh in the pressure calculation algorithm.

9.5.3 Specific compression work: first couple

$$(1) \qquad l_{compr_A} = h_{compr_{out}} - h_{compr_{in}}$$

$$(2) \qquad l_{compr_{B1}} = c_{p_{average}} \cdot (T_{BT14} - T_{BT17})$$

The two expressions reported above were used to run the pressure calculation algorithm, implementing the average specific heat and representing the first couple analysed.

This parameter was calculated through a mathematical average between the values obtained at the compressor inlet and outlet, checking if it could work ensuring a convergence with a relative error below 10%.

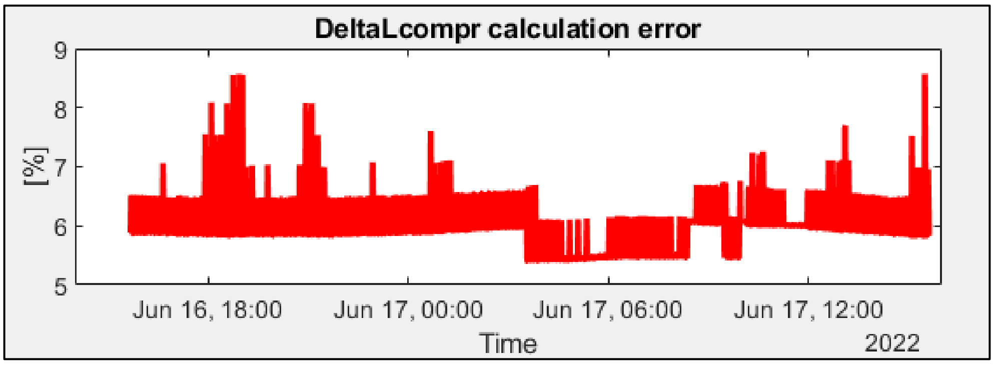

Figure 56: % deviation in the calculation of the lcompr (MATLAB), June 17th 2022

The plot reported in *Figure 56* shows how the percentage deviation ranges in the base case, without the introduction of a correction factor for the specific heat calculated at the compressor inlet.

The initial constraint of an error below 10% is respected, but it was still high to consider the results obtained reliable, especially once compared with the same calculation performed deriving the data from CoolPack.

Indeed, looking at *Figure 57* in the next page, it can be noted that the deviations calculated with the two software are not so close to each other, with the error obtained with CoolPack that in some cases is even the half of that obtained with Coolprop.

This is not acceptable, as the aim was that of reaching a similar precision in the pressures calculation step, to be safer when selecting the values to perform all the further calculations for the energy assessment.

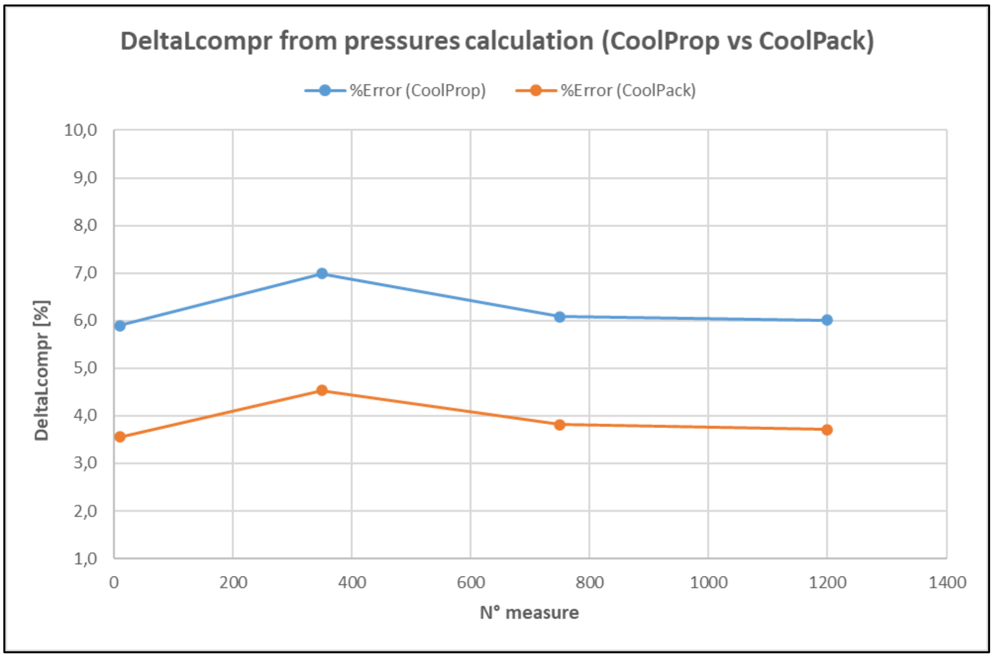

Figure 57: % deviations calculated with CoolProp and CoolPack (Excel), June 17th 2022

To address this situation, the idea was that of introducing a correction factor, as anticipated previously, aiming at obtaining a similar percentage deviation for both the specific heat at the compressor inlet (Cplow) and outlet (Cphigh).
Trying various suitable multiplicative factors, the one providing the better results in terms of convergence of the percentage deviations amounted to 0,95.
Indeed, considering such coefficient, the deviation in the calculation of Cplow passed from around 10% to 5%, much closer to that calculated for Cphigh.

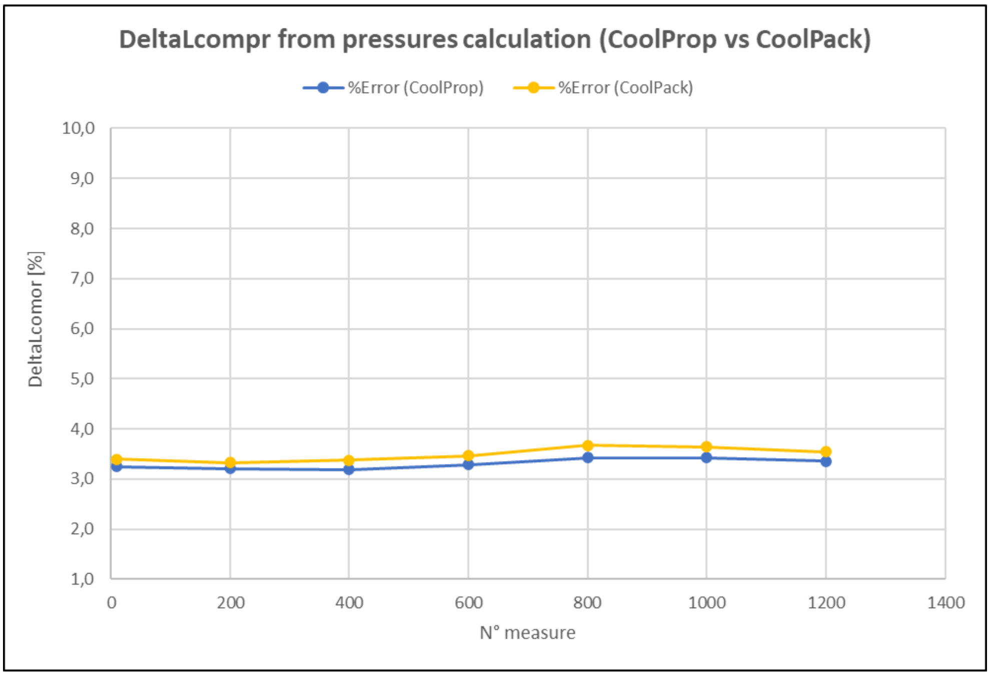

Figure 58: % deviations calculated with a correction factor of 0,95 (Excel), June 17th 2022

In *Figure 58* is reported a plot like that of the previous figure, with a higher number of check points to better verify the closeness of the two trends, calculated from the values of pressure resulting from the adoption of the correction factor (the temperatures were always those recorded by the sensors).
As can be noted, the situation is much better, as the proximity of the two patterns last for many measurements and the deviation generally ranges between 3-4%. Increasing the number of points, the oscillation of the percentage deviation trends could be more appreciated, moving towards a situation like that represented in *Figure 56*.

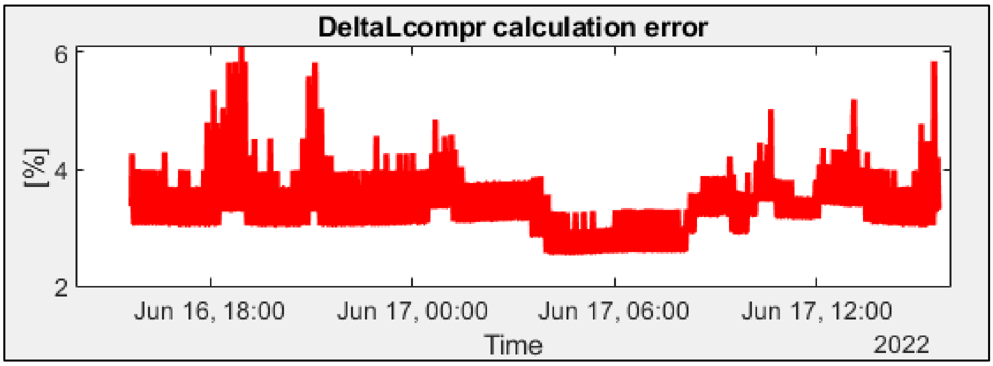

Figure 59: % deviation adopting the correction factor of 0,95 (MATLAB), June 17th 2022

In *Figure 59* is reported the values assumed by the percentage deviation calculated by MATLAB, and so using CoolProp databases, with the application of a correction factor equal to 0,95.
With respect to the pattern reported in *Figure 56*, this time the mean deviation amounts to 3-4%, unlike the 6-7% of the "base case".
This procedure was then applied also to other days of June 2022 experimental campaign, with quite good results too, without reporting cases of percentage deviations above the 6%. Anyway, few exceptions occurred in correspondence of the compressor switching on/off, but close to these events the results are not reliable, so this did not represent a real problem.
Instead, without the introduction of a correction factor, the percentage deviation trends ranged even up the 10% and more, almost the double.
The introduction of a more impacting correction factor was also considered, for instance equal to 0,92 or even less, trying to make the deviation associated with the Cplow reaching zero.
In all that cases, the deviation calculated with CoolProp decreased a little more, but the gap with the same quantity calculated by CoolPack rose again.

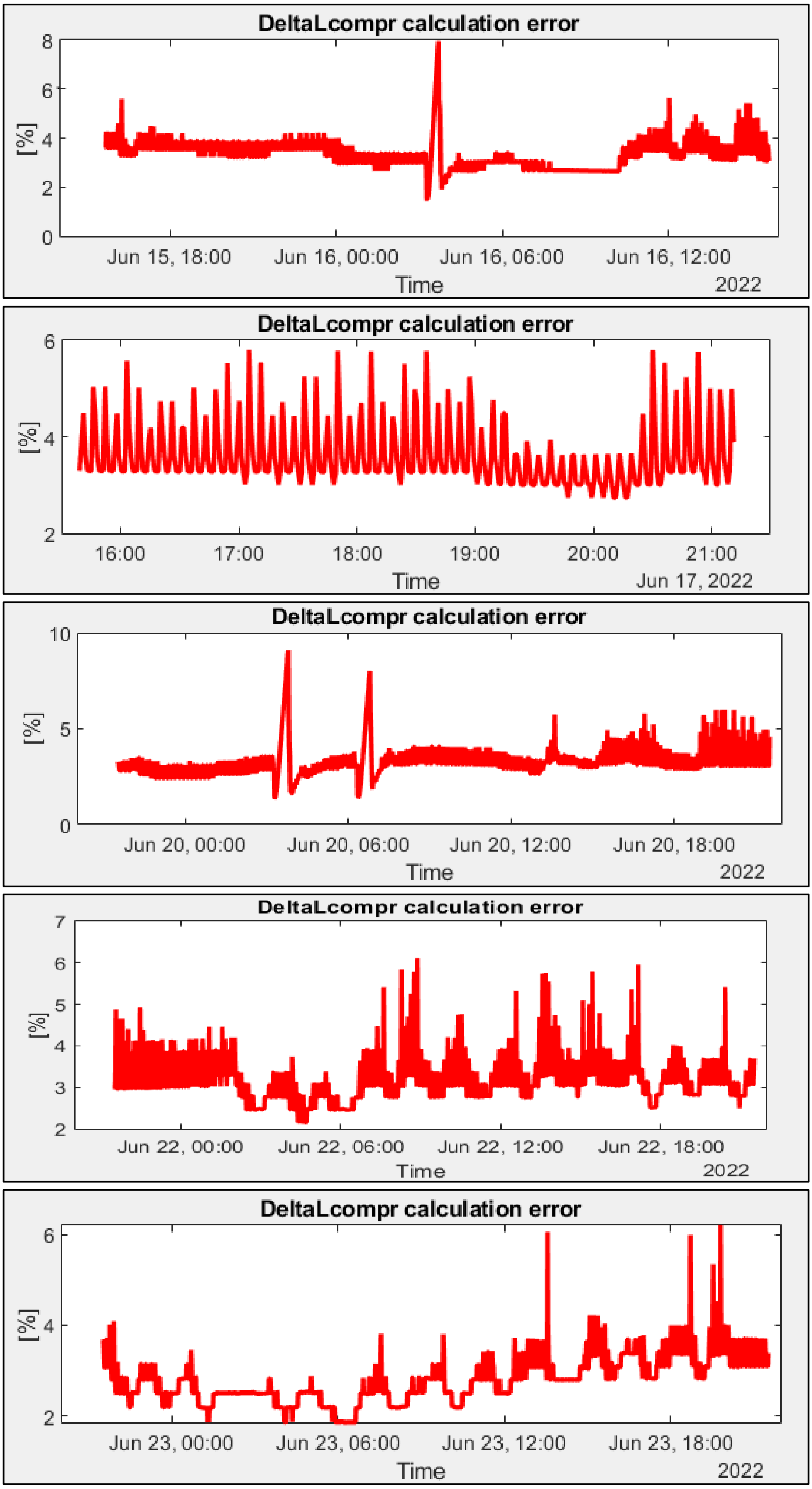

Figure 60: % deviations examples with a correction factor of 0,95 (MATLAB), June 2022

In *Figure 60*, focusing on the first and the third diagram from the top, it can be noted the occurrence of few peaks above 6%, previously mentioned. As just said, they appear in correspondence of a compressor switching on/off, while all the other peaks observed generally remain below that value.

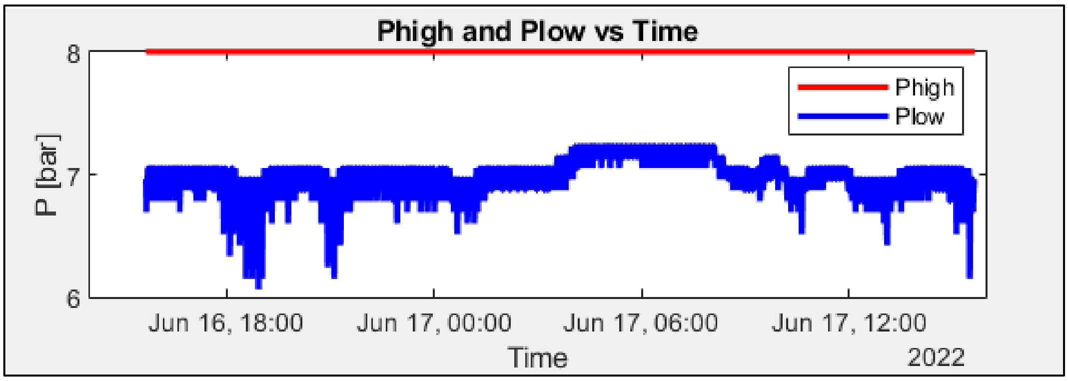

Figure 61: Phigh and Plow trends (MATLAB), June 17th 2022

Unfortunately, the effects of this deviation in the calculation of the specific work of compression affected the pressure levels determination, especially the high pressure level.
As showed in *Figure 61*, while the low pressure level seems to respond quite good to the algorithm, varying throughout the experimental campaign and so assuring the compression of only gaseous refrigerant, the high pressure level is much more static.
From the section related to the fixed pressures approach (8.4), acceptable results in terms of COP were obtained for a wider pressure range, between 8-10 bar and even a little more in some cases, suggesting that those Phigh values could be feasible for the heat pump operation.
A similar oscillation for the values of Phigh was so expectable, such as occurred for Plow, even if, considering the adoption of the pressure calculation algorithm and the relative uncertainty, this trend may be not perceived.
More in detail, the number of pressures that constituted the Phigh array to run the pressure calculation algorithm is not infinite, so additional values providing a lower percentage deviation may have been neglected, replaced by others involving a bigger one, as even a little fraction of 1 bar made the difference.
This fact probably was not the only reason for this phenomenon, as also the implementation of an average specific heat for the compressor inlet/outlet represented an error source too, together with other approximations.

Anyway, the fact suggesting that this phenomenon may be strictly numerical could be found by testing different ranges for the high pressure level.

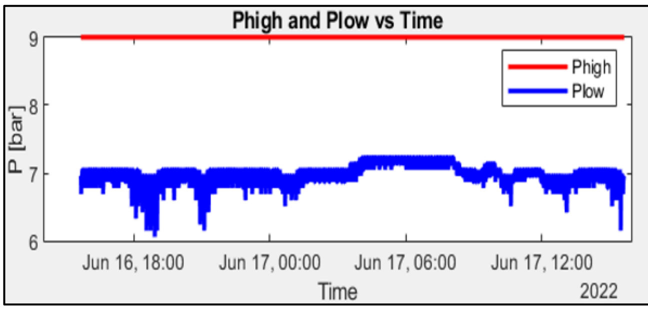

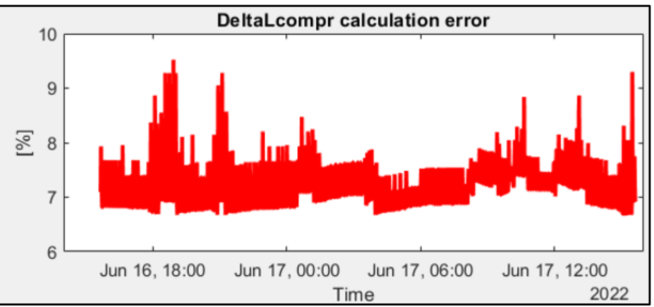

Figure 62 (left): Pressures trends with Phigh lower limit set at 9 bar (MATLAB), June 17th 2022
Figure 63 (right): % deviation, correction factor of 0,95 (MATLAB), June 17th 2022

Increasing the Phigh range and setting the lower limit at 9 bar, the situation did not change: looking at *Figure 62*, it can be noted that the trend is still static (equal to the lower limit imposed), while the percentage deviation increased towards higher values (*Figure 63*).

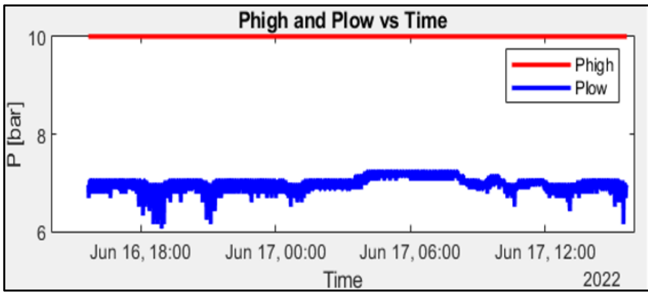

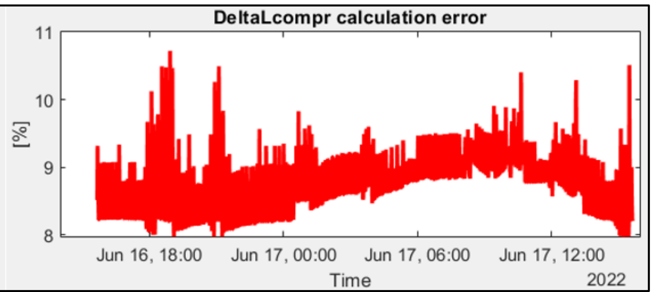

Figure 64 (left): Pressures trends with Phigh lower limit set at 10 bar (MATLAB), June 17th 2022
Figure 65 (right): % deviation, correction factor of 0,95 (MATLAB), June 17th 2022

Also increasing the lower limit of the Phigh range up to 10 bar the situation did not change, again the Phigh trend was static and the deviation values get worse.
Apart from that, the results in terms of COP seemed to be consistent, and the oscillation of the low pressure level allowed also to reach a value of 7 bar and more, without involving the liquid compression phenomena.
On the next page, few COP plots related with some days of the experimental campaign are reported as examples, with values that mostly range between 4 and 5.

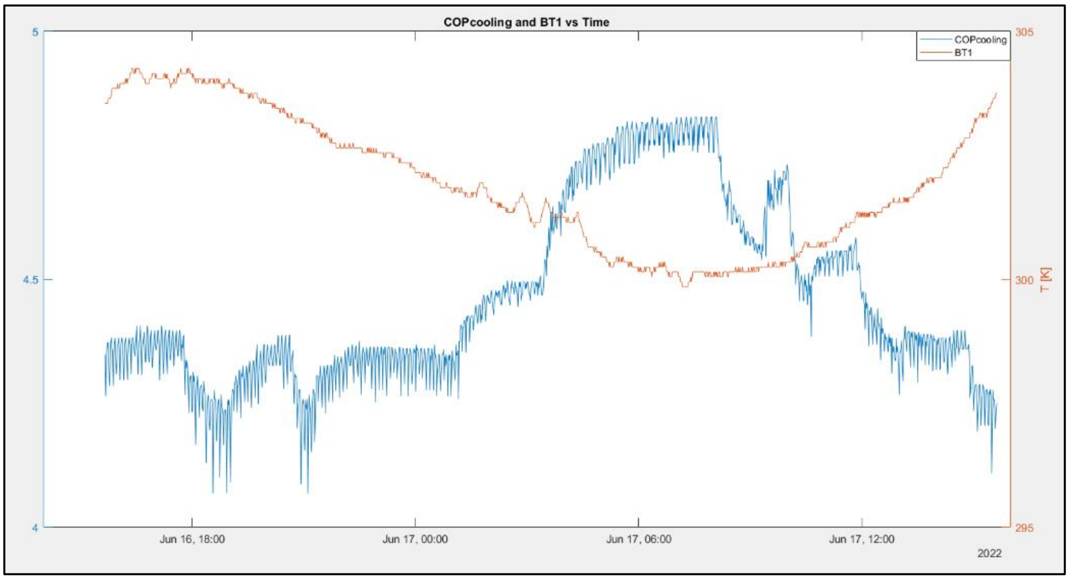

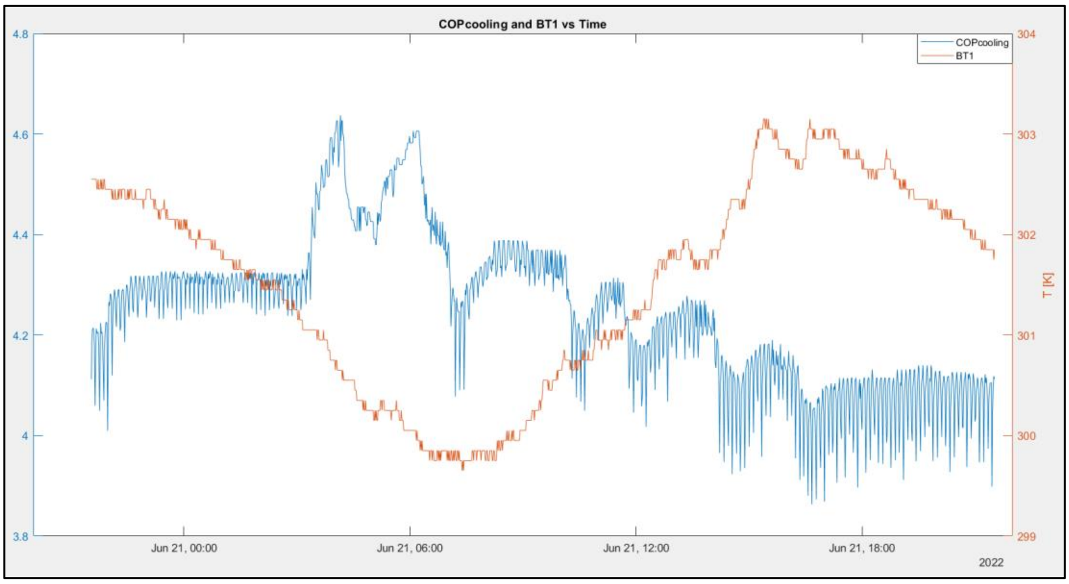

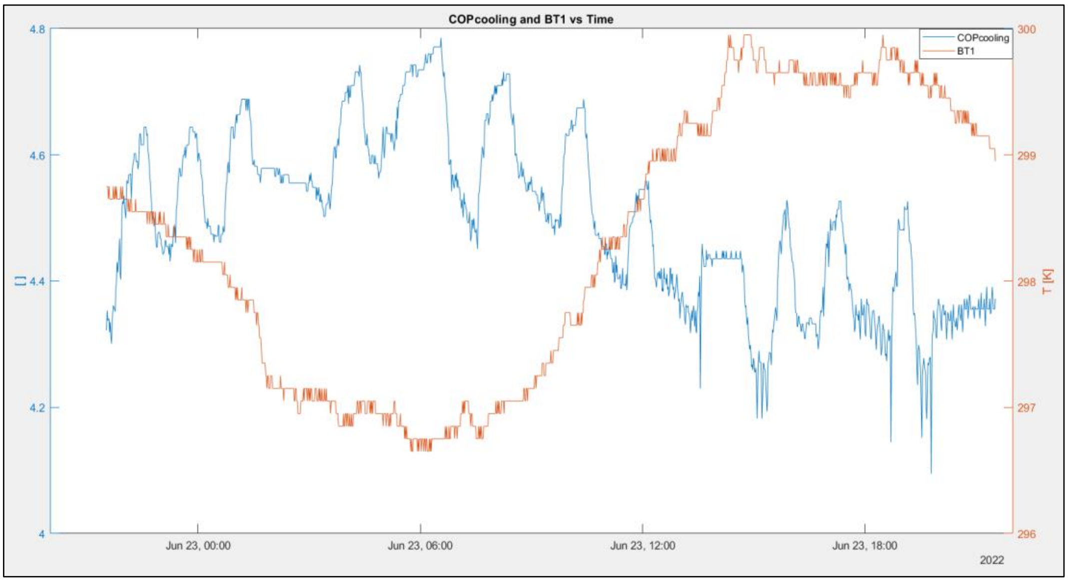

Figure 66: COP vs Time, correction factor of 0,95 (MATLAB), June 17th 2022
Figure 67: COP vs Time, correction factor of 0,95 (MATLAB), June 21st 2022
Figure 68: COP vs Time, correction factor of 0,95 (MATLAB), June 23rd 2022

As additional check for the consistency of these results, further comparisons were performed involving CoolPack: the COP was calculated also on the basis of the thermodynamic properties derived from CoolPack, considering the same temperatures and pressures, for a certain number of sample measurements.

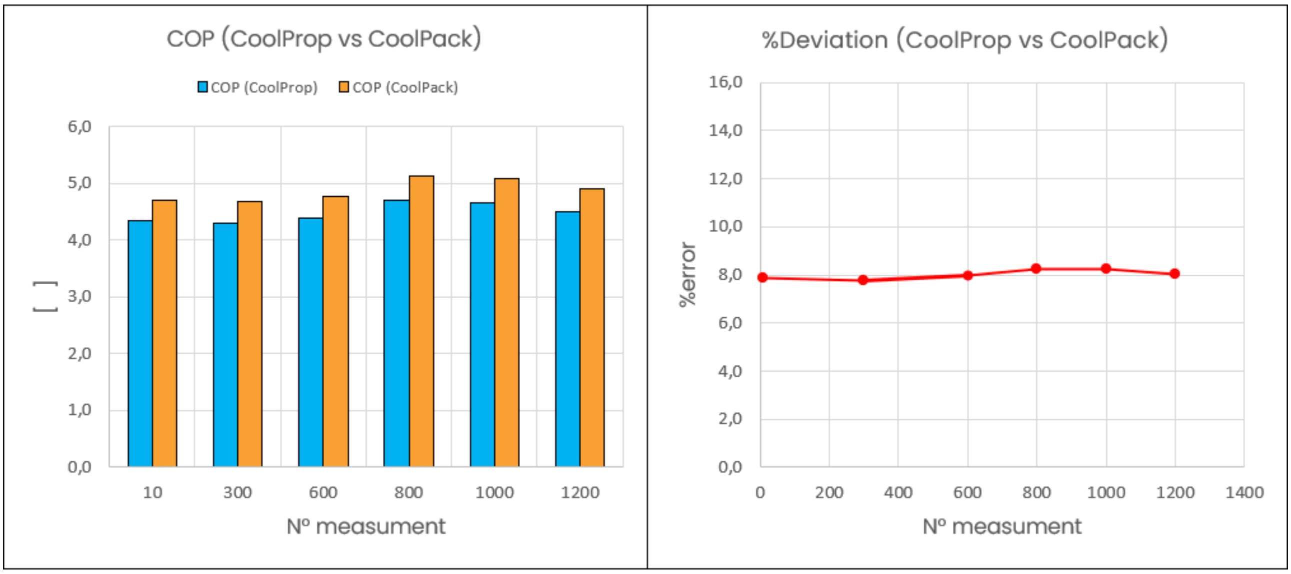

Figure 69: COP and % deviation, CoolProp vs CoolPack (Excel), June 17th 2022

After the preliminary check regarding the single thermodynamic quantities, aimed at "calibrating" the property used to run the pressure calculation algorithm (as the enthalpy and the specific heat), a final check was performed to verify the performance results obtained.

Looking at *Figure 69*, the values assumed by the COP values calculated on the basis of the data coming from the two software are not exactly coincident, but differ by a certain quantity.

Fortunately, from the plot on the right it can be noted that the deviation between the two is roughly the same over the measures selected, and similarly happened for other measurements sets. This could be interpreted as a systematic error, considering the different basis on which the two software probably work, and so it may be easily predicted and fixed through the application of a correction factor.

9.5.4 Specific compression work: second couple

$$(1) \qquad l_{compr_A} = h_{compr_{out}} - h_{compr_{in}}$$

$$(2) \qquad l_{compr_{B2}} = c_{p_{high}} \cdot T_{BT14} - c_{p_{low}} \cdot T_{BT17}$$

Trying to get a solution involving lower percentage deviations, especially concerning the pressure calculation algorithm, an additional expression was considered for the compression work, testing then the couple reported above.
The aim was that of verifying if the Phigh trend would remain static even in that case, considering a less strong approximation for the specific heat, now reported separately for the compressor inlet/outlet.
Starting with the deviation obtained concerning the specific compression work, the results provided by the MATLAB script (using CoolProp) are much better than those obtained using an average specific heat, going towards zero without the implementation of any correction factor.

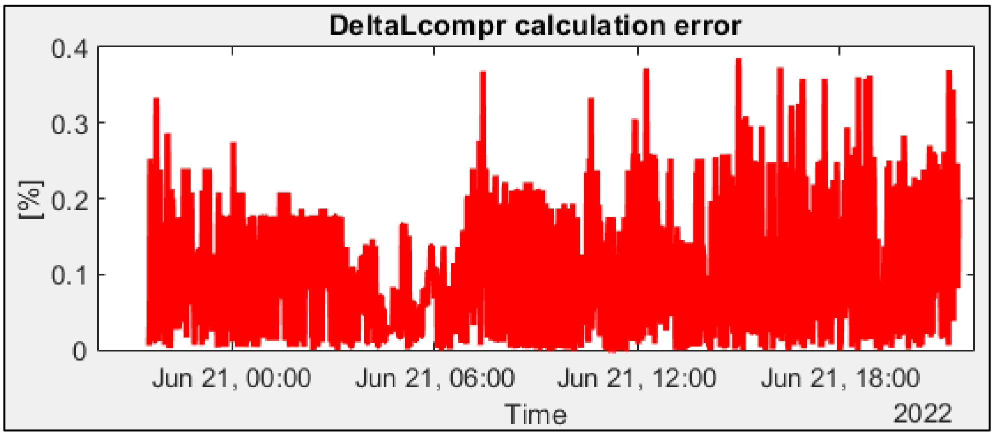

Figure 70: % deviation using Cphigh and Cplow (MATLAB), 21st June 2022

The results reported in Figure *70* seem much better than what was obtained before, but performing a rapid check, by inserting the same values on CoolPack, there was no correspondence between the two.

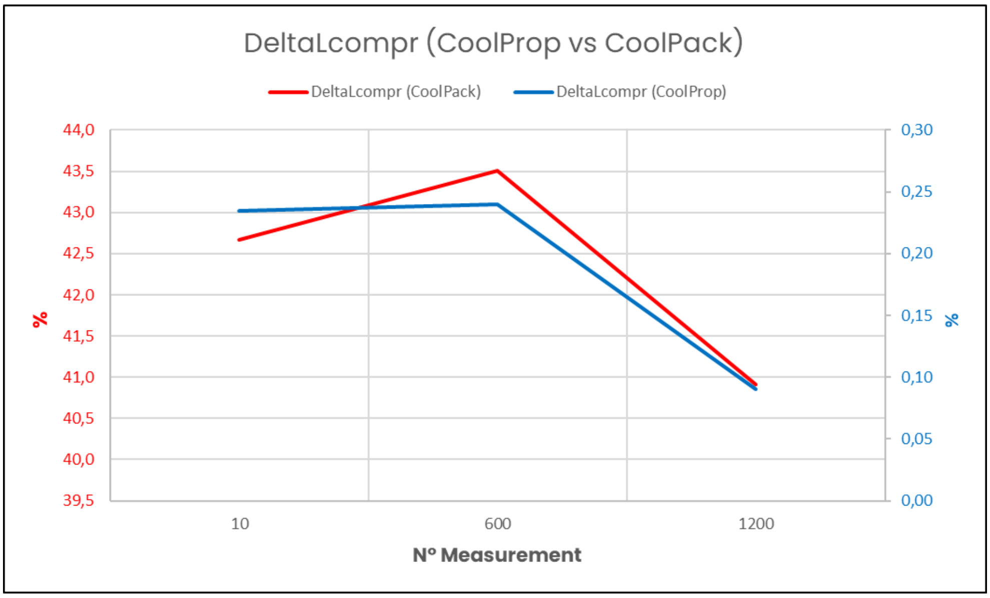

Figure 71: %DeltaLcompr, CoolProp vs CoolPack (Excel), 21st June 2022

Indeed, from the figure above can be noted that this time the deviations calculated by the two software are much different, involving a factor 100.
This probably occurs because of the different values calculated for the specific heat among the two software, which in the case of CoolProp allowed a very good convergence, while using CoolPack the situation is pretty bad.
Regarding the specific heat, especially the Cphigh, the deviation ranges around 10-12%, so even in that case a correction factor was considered, but first it is better to have a deep look at the pressures situation.

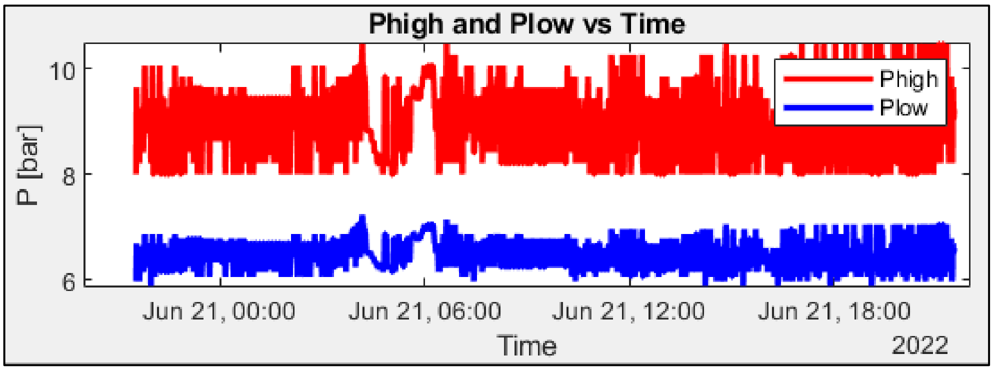

Figure 72: Phigh and Plow (MATLAB), case with Cphigh and Cplow, 21st June 2022

In that case can be finally noted an oscillating trend for the high pressure level too, as occurs for Plow, which in turn assumes also more values close to 6 bar.
The trend of Phigh ranges roughly between 8-10 bar, which are the values already observed in the section of the fixed pressures approach, thus suggesting that this lower Phigh could be consistent.

More in detail, this oscillating trend for Phigh could be associated with a more reliable calculation of the compressor work, obtained by substituting the average Cp with the two values at the compressor inlet/outlet and the associated temperature.
As there is totally mismatching with the results coming from the two software databases, the correction factor mentioned was tough as a solution to verify the results maintaining a low DeltaLcompr deviation.
The value considered was the same adopted before for Cplow (0,95), as again the main deviation is about the specific heat at the compressor inlet.

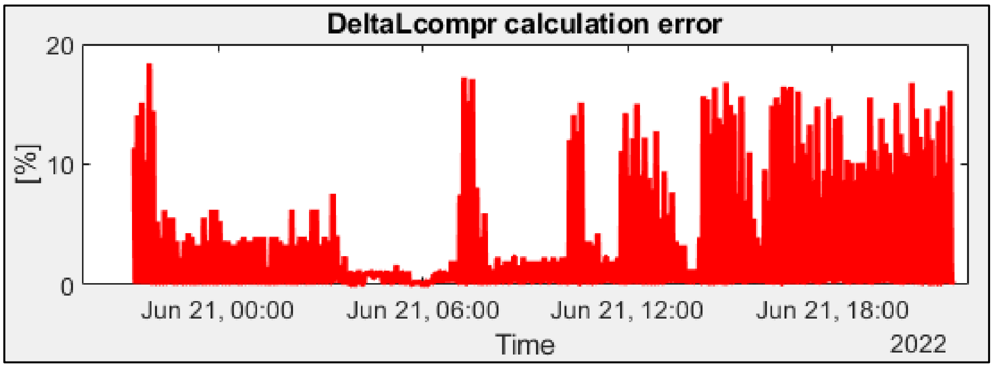

Figure 73: % deviation with a correction factor of 0,95 (MATLAB), 21st June 2022

As reported in *Figure 73*, the results were different from for the previous case (section 8.5.3), as the error trend ranges on a very wide interval of values, almost approaching the 20% with some peaks.
Unfortunately, the introduction of a correction factor led only to worse performances in terms of convergence of the pressure calculation algorithm, without substantial improvements in terms of matching with the results deriving from CoolPack.
Also in that case, different correction factors were proposed, but the situation did not improve, so even if the deviation in the specific work calculation was really good in the "base case", the approach reported in section 8.5.3 was preferred, providing results boasting an acceptable countercheck by CoolPack.
Anyway, a better representation of the Phigh behaviour was probably sacrificed with this choice.
In the next page few COP trends are reported, the first related with the case of CPm adoption, and the other two related with the case of Cphigh and CPlow (with and without the correction factor implementation).

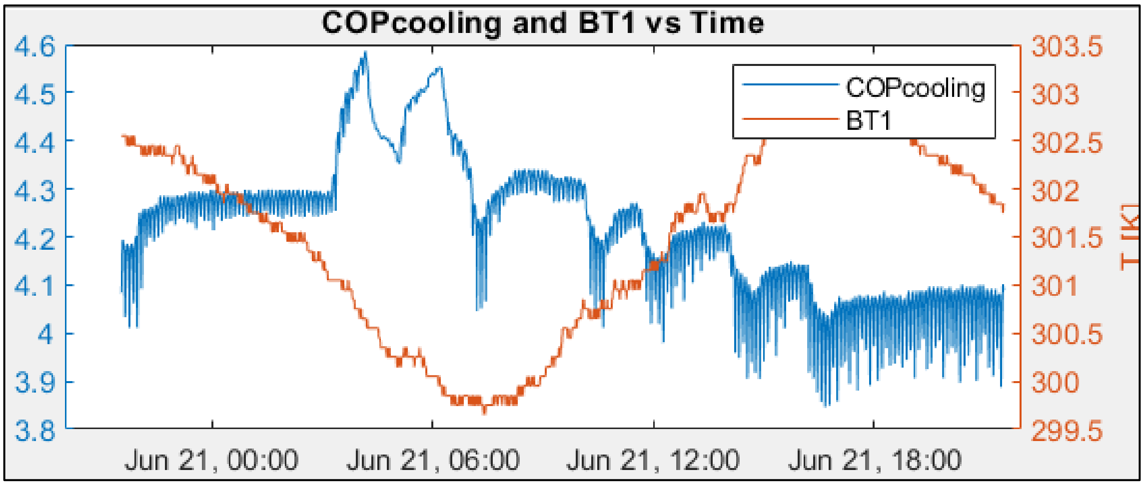

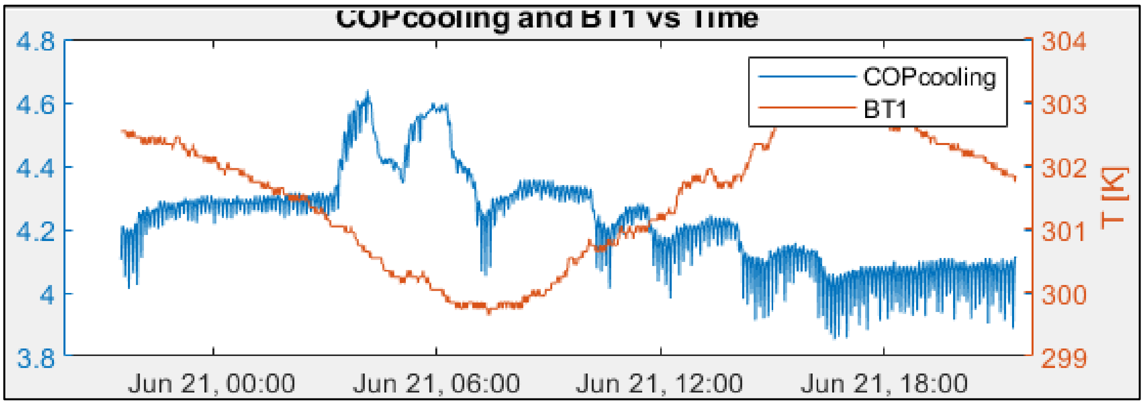

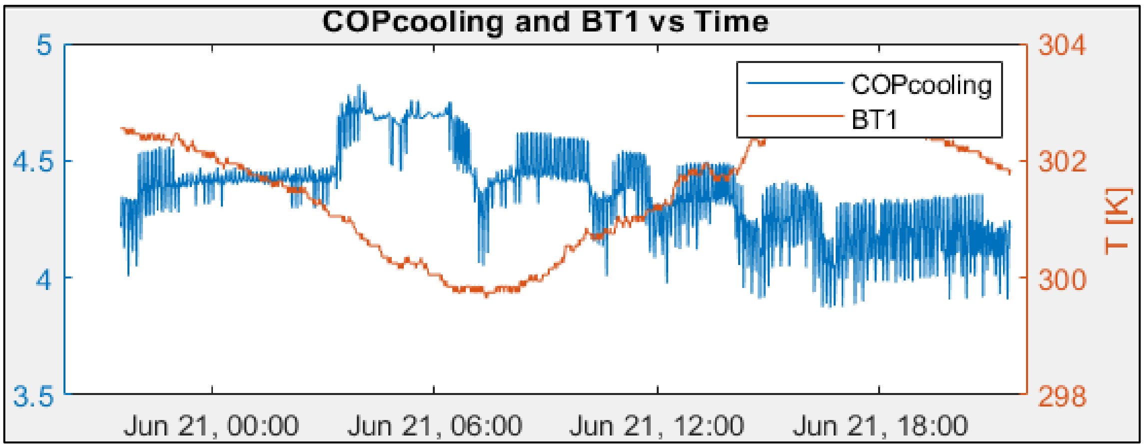

Figure 74: COP vs Time, case with Cpm (MATLAB), June 21st 2022

Figure 75: COP vs Time, case with Cphigh/Cplow and correction factor (MATLAB), June 21st 2022

Figure 76: COP vs Time, case with Cphigh/Cplow (MATLAB), June 21st 2022

An extra attempt was that of improving the formulation of the correction factor, also considering the adoption of additional ones.

These coefficients were conceived as function of pressure, coming out from the polynomial interpolation of the deviation values represented on Excel.

A similar effort was made both for the specific heat and the enthalpy, even if the last one did not involve significant deviation problems as the Cp.

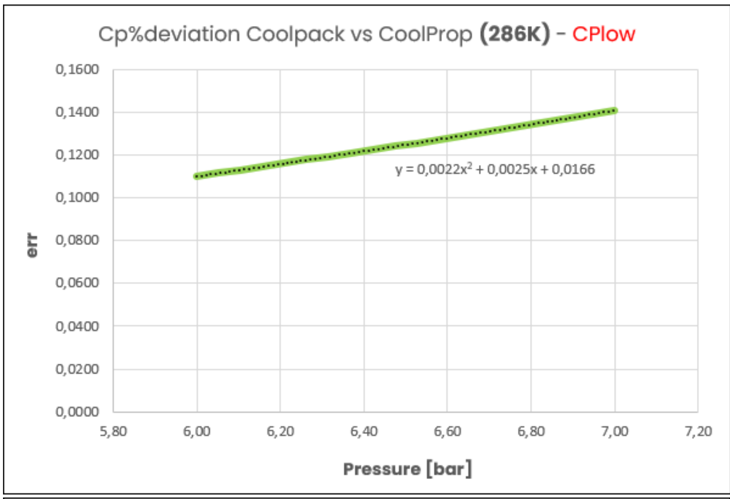

$$K_{high} = 1 - 0,0003P^2 - 0,023P + 0,0112$$

(CPcoolprop*K = CPcoolpack)

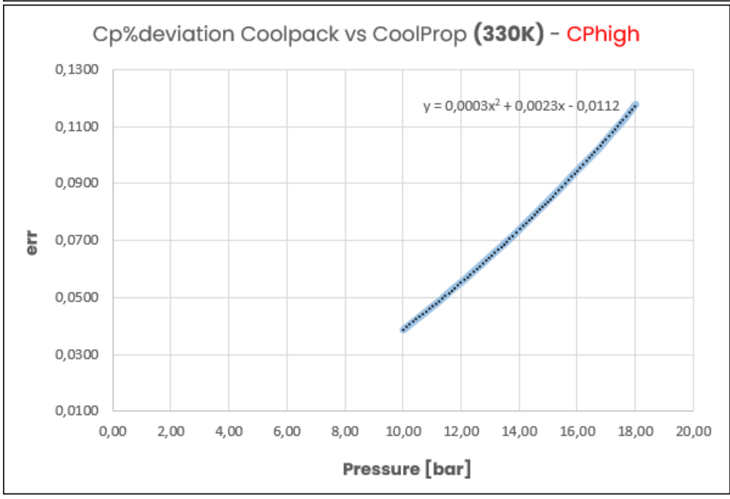

$$K_{low} = 1 - 0,0022P^2 - 0,0025P - 0,0166$$

(CPcoolprop*K = CPcoolpack)

Figure 77: Deviation curves parametrization (Excel), based on June 21st 2022 measurements

In *Figure 77*, the second-degree polynomial curves (the black dotted ones) fit the points (arranged on the coloured curves) representing the deviation between the specific heat calculated by CoolProp and CoolPack, as a function of pressure.
The temperature was fixed, because looking at many samples recorded by BT14 and BT17 sensors (compressor inlet/outlet), these values did not vary too much (they are all inside a range of 4-5 K around the average). Hence, the temperature values selected were precisely the average ones for the day considered.
These pressure dependent coefficients were then implemented in the pressure calculation algorithm, correcting Cphigh and Cplow for the actual pressures considered, but the results were not as good as those provided by the constant case previously analysed.
Probably, even considering slightly different coefficients based on the day selected, the assumption of constant temperature was too strong.
At the end, the solution reported in section 8.5.3 was the adopted one.

9.6 Fixed vs variable pressures method

Once exposed the methods evaluated for the modelling of the heat pump system, few additional considerations can be made, such us about the impact of the variable pressure levels choice on the COP trend, with respect to constant ones.

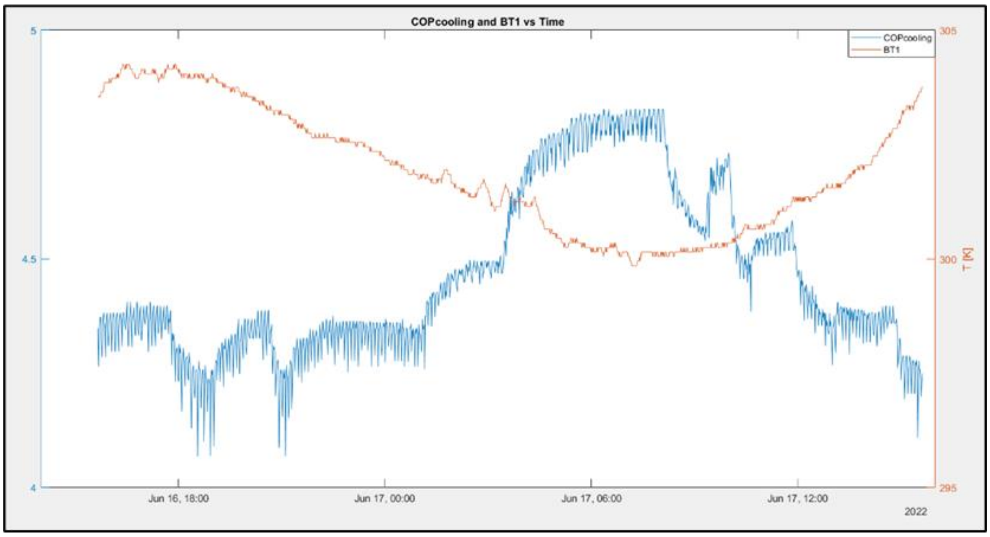

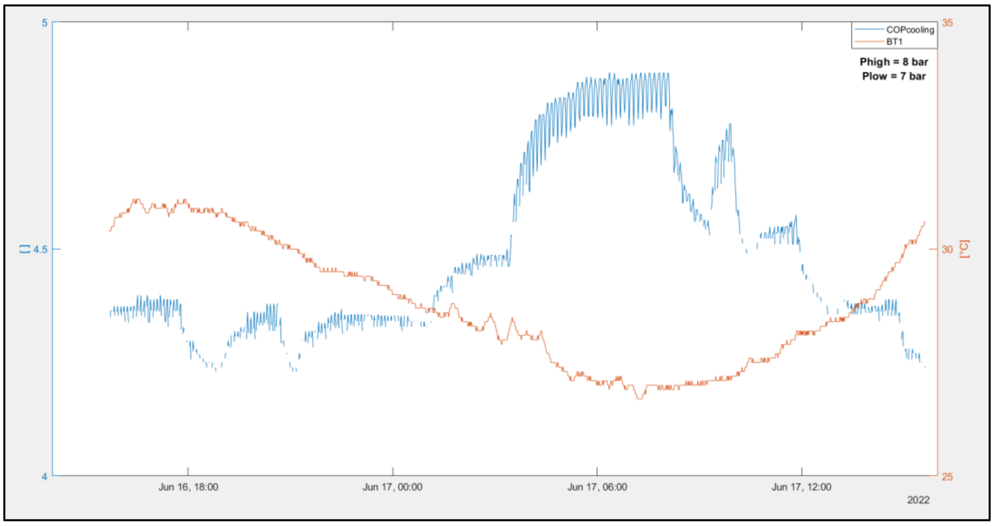

Figure 78: COP vs Time, variable pressure levels (MATLAB), June 17th 2022
Figure 79: COP vs Time, fixed pressure levels 7-8 bar (MATLAB), June 17th 2022

From the figures above can immediately noted that the trends are quite similar, as the pressures selected for the second plot are close to the ones derived by the algorithm in the first one, but there are visible differences in terms of the curves continuity.

Looking at *Figure 79*, it can be immediately noted the high number of holes that interrupt the pattern, which, as said in the previous sections, are due to the

problem of liquid compression. This issue is not present in *Figure 78*, as during the searching step, performed by the pressure calculation algorithm, the pressures couples which would cause that kind of problem were immediately discarded.
In that way the number of measurements considered as “acceptable” is much bigger than in the fixed pressures case.
In the case with fixed pressures, especially the Plow level must be chosen with more attention, checking for the percentage of measurements discarded to obtain reliable average values.
However, the method with variable pressures presented some issues too with the occurrence of compressor switching on/off, as the pressure ranges selected to run the algorithm cannot intersect to allow a proper working condition.
This fact could create some problems, for instance considering the switch on transients, when the pressure levels should gradually increase towards the working ones. Indeed, the ranges selected were thought to allow the pressure levels determination for the heat pump operating in “default” working conditions, so they were purposely limited in their size to allow the convergence with the lowest DeltaLcompr deviation possible.
This fact caused the occurrence of few interruptions in the COP trend, in correspondence of the switch on/off, also requiring the introduction of additional interventions to smooth the strong variation of the COP close to these events.

9.7 The problem with ON/OFF transients

The measurements in correspondence of an on/off transient represented a problem for both the method analysed, creating strong variations in the COP and, in the case of the variable pressure method, also a huge increase in the DeltaLcompr deviation (which was almost duplicated in most cases).
In correspondence of these events, the pressures provided by the pressure calculation algorithm could not be considered reliable, as the error ranged around the 10% or even more, so a solution was designed to preserve the calculation of the average COP from these events.
More in detail, a dedicated section was implemented in the main script, searching for the compressor switch on events and thus neglecting the COP values deriving from the following 45 measurements in the calculation of the average daily COP. The number 45 was arbitrary, set after consulting the evolution of the COP trend following a switch on of the compressor, and checking for how many measurements it remained visually affected by this phenomenon.

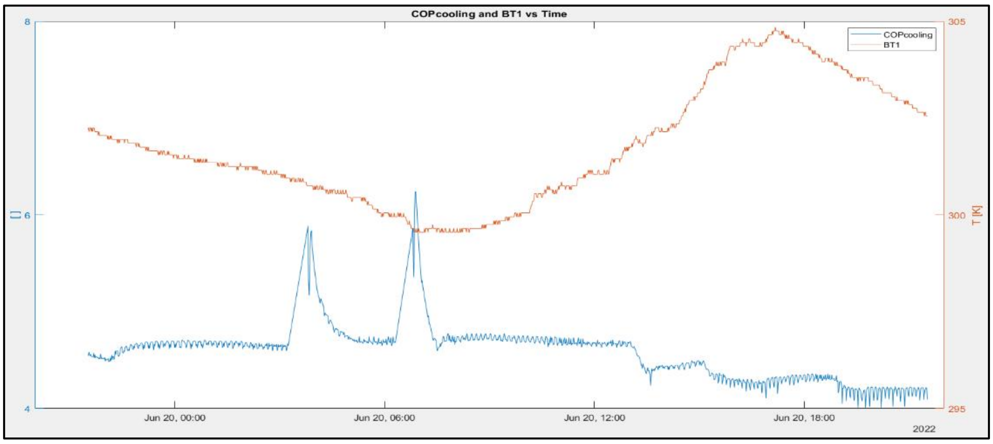

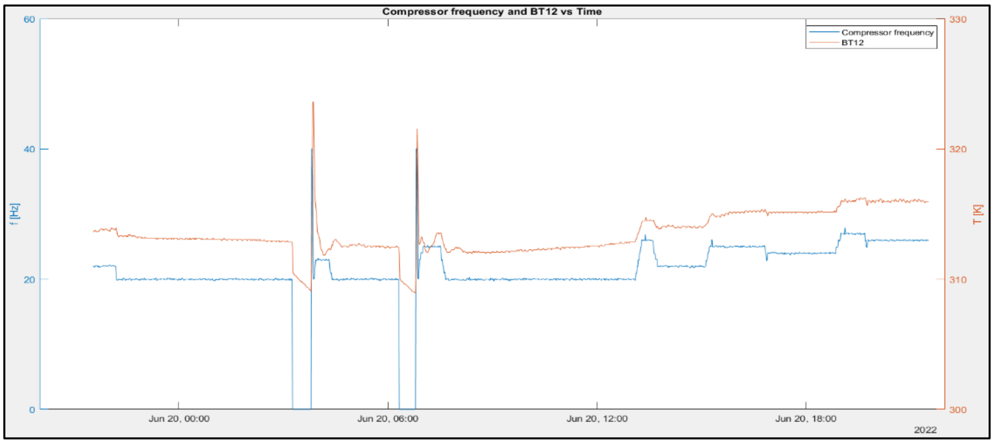

Figure 80: COP and BT1 vs Time, variable pressure levels (MATLAB), June 20th 2022
Figure 81: Compressor frequency vs Time (MATLAB), June 20th 2022

The data collected, and the further results achieved by these, for the day of June 20th 2022, presented two on/off transients, which can be noted from the figures above. In correspondence of these two events, the compressor frequency (*Figure 81*) reaches zero, then increasing again rapidly after a short time, with many implications in the calculation of the other parameters.
First the COP, reported in *Figure 80*, whose trend presents two peaks as results of the compressor switch off/on: when the compressor is turned off, the heat pump is not working, so both the heat exchanged and the work of compression decrease. In that situation, the delivery temperature to the user (BT11) progressively increases, while the delivery temperature to the terrain (BT12) decreases. Once the system is turned on again, it causes the instauration of a temperature difference across the compressor, with an increasing temperature at the compressor outlet. In that case the temperature variation across the condenser, on the refrigerant side, rapidly increases so that a great amount of heat can be immediately injected into the ground. Consequently, the amount of heat extracted at the evaporator increases too, causing a peak in the COP which will be progressively smoothed, stabilizing to usual values.

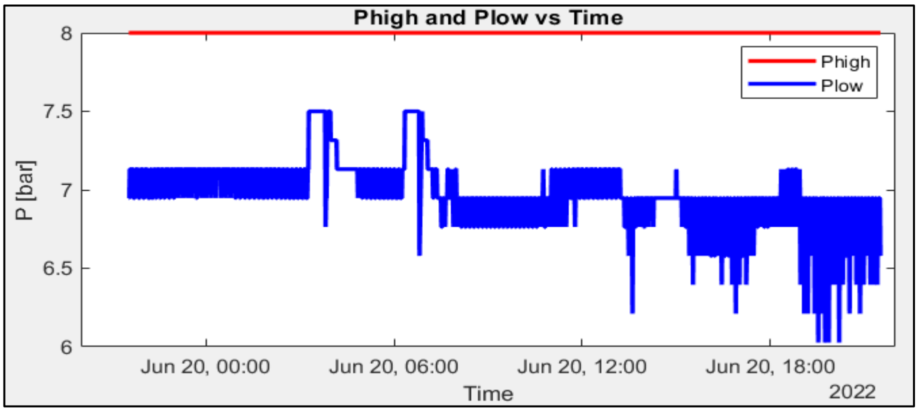

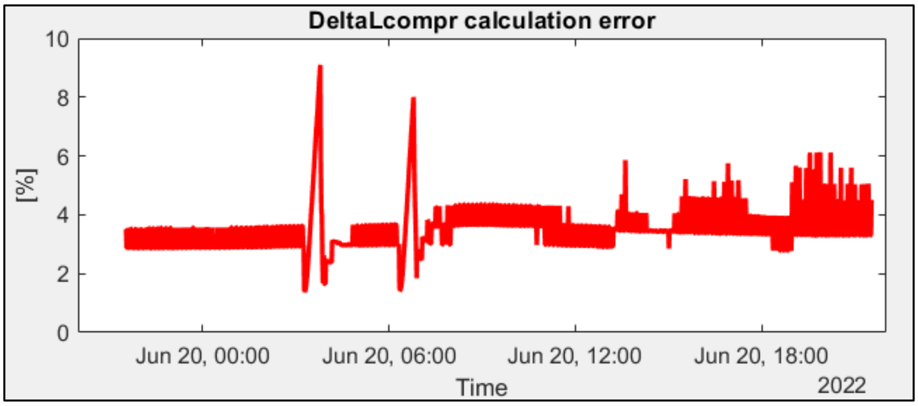

Figure 82: Phigh and Plow trend, variable pressure levels (MATLAB), June 20th 2022
Figure 83: % deviation trend (MATLAB), June 20th 2022

From the pressures point of view, the on/off switching involve huge peaks in the DeltaLcompr deviation. These peaks emerging in *Figure 83*, are reflected too in *Figure 82*, where the Plow trend reports an unusual oscillation in correspondence of these phenomena.
The Phigh trend seams again to not be affected by such events, but the cause could be again considered as numerical, because of the method adopted previously.
However, the effects of the on/off transients on the heat pump operation seam to involve generally few rapid fluctuations in the properties evaluation, which then come back to the usual values.
As the uncertainty in the calculations, with reference to the DeltaLcompr for instance, seamed to be quite relevant, the data registered nearby these events were not considered for the computation of the desired results, also treating of quite sporadic events in the period considered.

9.8 Discussion of the results

To obtain a better overview of the system performance, the results coming from the elaboration of the single sets of measurements recorded by the sensors were further rearranged on daily basis.

The results of this step consisted so in the mathematical averages of the measures collected minute by minute by the heat pump over the total duration of almost 24 hours, for each day of the experimental campaign. The data collected over the 24 hours and reported in the form of a ".txt" file formed the "set of measurements" mentioned above.

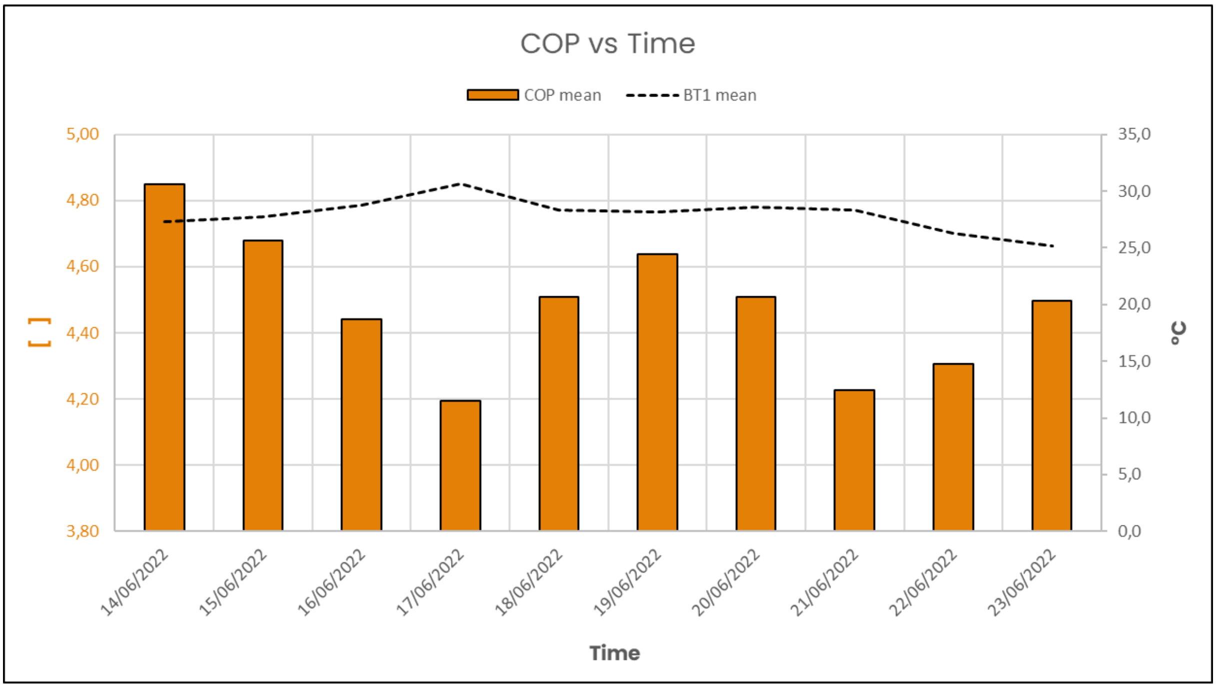

Figure 84: COP vs Time (Excel), daily basis, from June 14th to June 23rd 2022

In *Figure 84* are summarized the main achievements in terms of COP, considering the cooling experimental campaign carried out in the current year.

The black dotted line, representing the daily average of the BT1 sensor recordings, was added to better visualize the COP evolution as a function of the outdoor temperature.

As can be noted, the COP presented generally an opposite trend with respect to the outdoor temperature, as it initially decreased reaching minimum values in correspondence of June 17th. In the following days the average temperature started to decrease, while the COP increased up to the peak on June 19th.

The trend presents only a little deviation, from which could be considered as its expected behaviour, in correspondence of the period spacing between the 20th and 21st of June: in that interval, the outdoor temperature slightly decreased and the COP decreased too. The situation than stabilized to the expected trend in the following days.

This curious phenomenon may be related to a difference involving the days before and after this time span. More in detail, the set of measurements deriving from the days before the 20th of June included at least one on/off switching of the compressor, which could have affected, even in a little dimension, the average COP calculated (few elevated COP, due to the switch on of the compressor, could not be removed for instance).

A second hypothesis, the most probable after checking deeply the operation of the pump in those days, could be related with little problems related with the compressor, incurred in the period from June 21st to 23rd.

Nothing serious anyway, probably linked with small fouling phenomena, as the experimental field has not been used in the period preceding this thesis work.

However, a good confirm of the verisimilitude of the COP is represented by the fact that the smallest value occurred in correspondence of the highest outdoor temperature, precisely on June 17th.

Together with the COP, also the thermal power exchanged at the evaporator/condenser, the work required by the compressor and the refrigerant mass flow rate were calculated and finally arranged on daily basis.

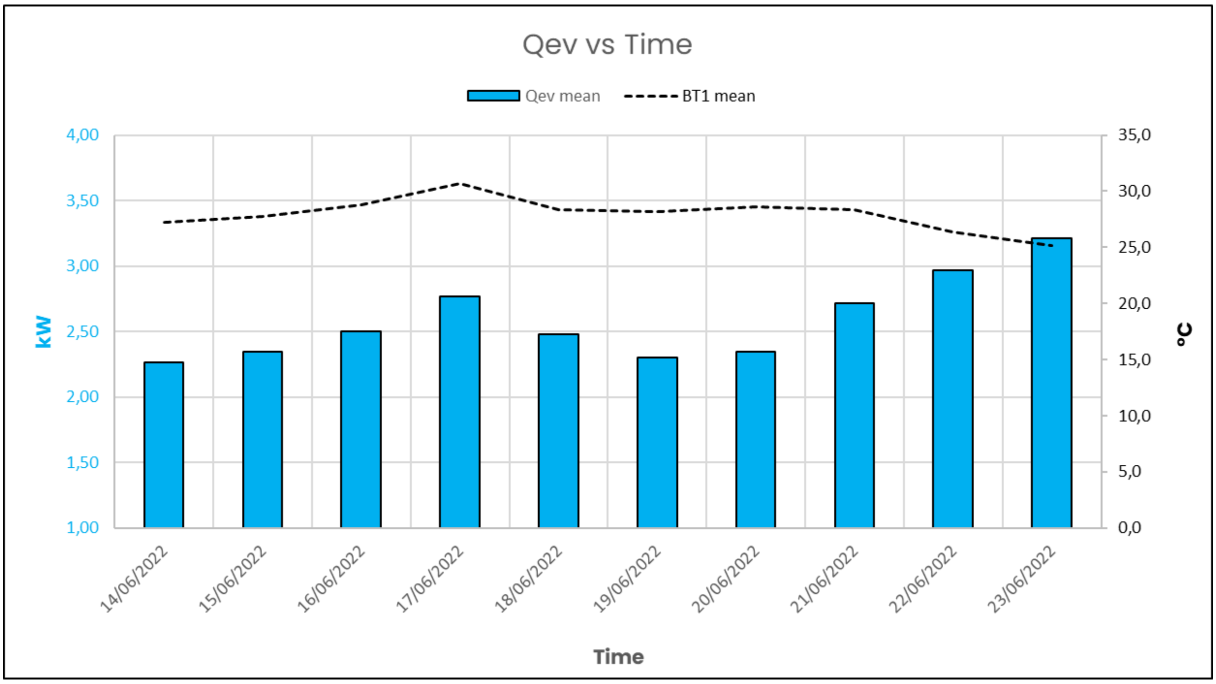

Figure 85: Qev vs Time (Excel), daily basis, from June 14th to June 23rd 2022

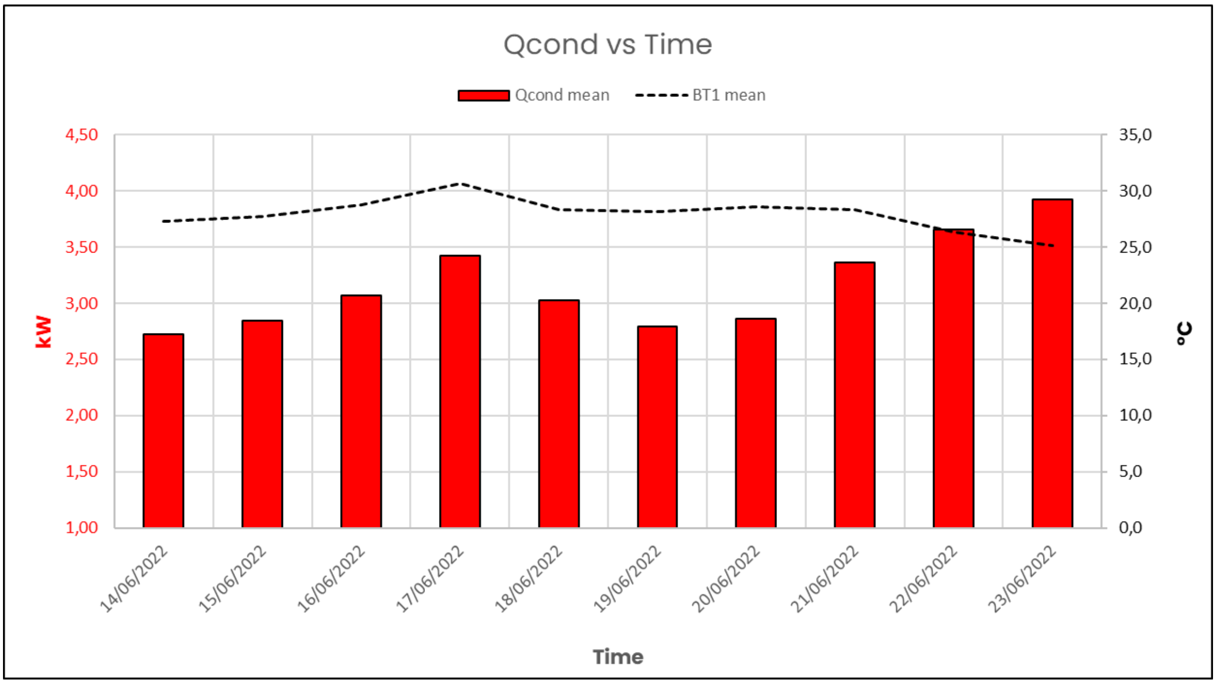

Figure 86: Qcond vs Time (Excel), daily basis, from June 14th to June 23rd 2022

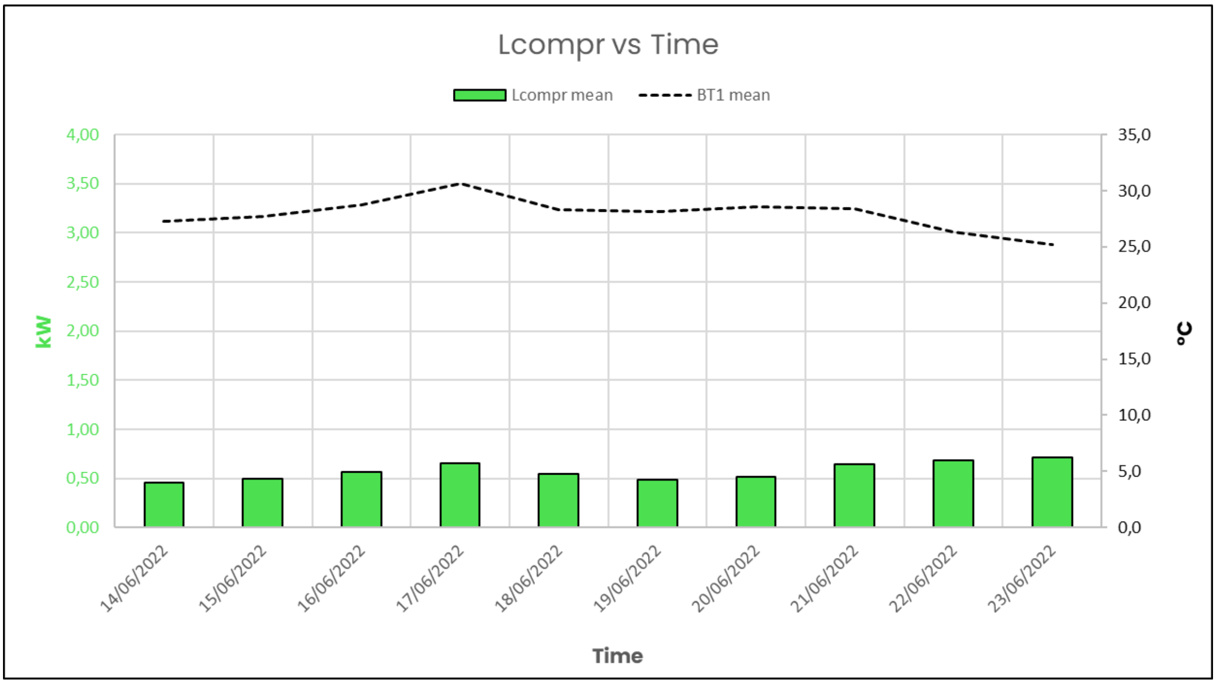

Figure 87: Lcompr vs Time (Excel), daily basis, from June 14th to June 23rd 2022

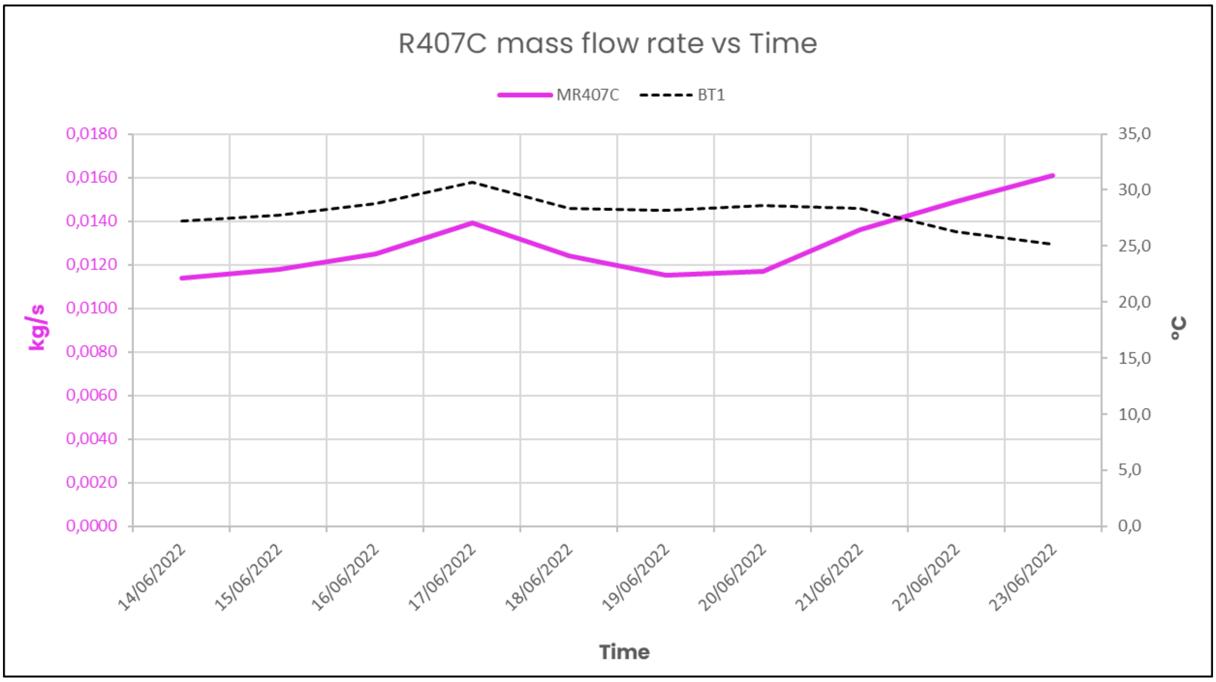

Figure 88: *MR407C vs Time (Excel), daily basis, from June 14th to June 23rd 2022*

Starting from the thermal power exchanged at the evaporator (*Figure 85*) and at the condenser (*Figure 86*), together with the power required by the compressor (*Figure 87*), they present a similar trend with respect to the outdoor temperature. This is because, when the outdoor temperature was increasing, the heat pump had to "boost" its operation to provide the target delivery temperature set for the user (5°C for this experimental campaign). Indeed, as the amount of heat to be removed from the user circuit (secondary circuit) increased, the compression work required increased too.

A higher amount of thermal power removed from the user resulted then in a higher amount of heat to be rejected into the ground.

While the water/glycol mass flow rate in the primary circuit was considered as a constant (assumed equal to 0,435 m3/h), a higher refrigerant mass flow rate was required to exchange the additional amount of heat (as show in *Figure 88*).

When the outdoor temperature was decreasing, the situation was exactly the opposite involving Qev, Qcond, Lcompr and MR407C.

For these four quantities, a largest deviation from the expected trend can be noted in correspondence of the last three days of the experimental campaign: in the case of COP, the trend was the expected one with only a little deviation, while in that case all the three quantities continue to increase with the outdoor

temperature decreasing. Anyway, the reason for that behaviour could be reconnected again to the problems encountered with the compressor.
From a more temperature-related point of view, additional considerations may regard the measured values at the evaporator outlet on the user side (BT11) and at the condenser outlet on the ground side (BT12).

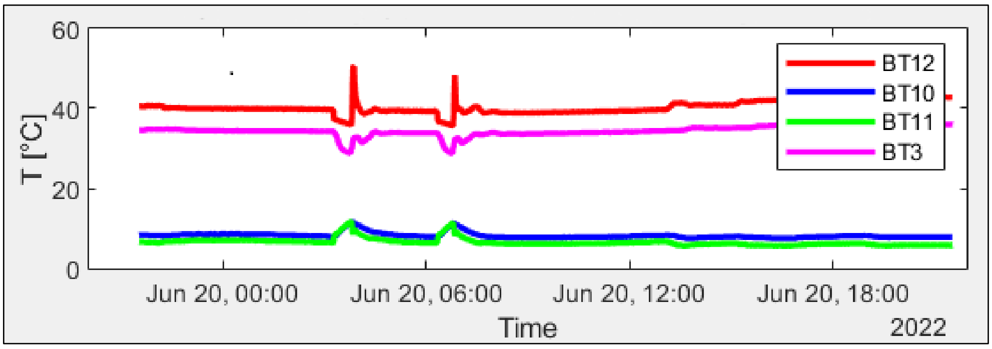

Figure 89: Delivery/return temperatures trends on ground and user side (MATLAB)

In *Figure 89* are reported the delivery/return temperature trends on the user side (BT11/BT10) and on the ground side (BT12/BT3), for the 20th of June, which is a day belonging to the experimental campaign analysed.
All the four temperature trends present an oscillation in correspondence with the switch off/on of the compressor, occurred between 00:00 and 06:00 a.m.
Looking at BT11, the delivery temperature to the user (the fan coil), it presents a sudden increase in correspondence to the compressor switch off, departing from the previous value which oscillates around 5°C (the target imposed by the heat pump logic). This value is then reached again once the compressor is switched on, maintaining a fairly steady trend until the next switch off. This trend for the delivery temperature to the user is quite close to that experienced in the other days monitored, as the regulation of the heat pump system is based on the DM concept.
Regarding the delivery temperature to the ground (BT12), it assumes values ranging around 40°C, presenting an opposite trend with respect to BT11 for the switch off/on of the compressor: once the compressor is switched off the temperature decreases, as the heat pump system stops to reject heat (Q_{cond}) into the ground, increasing again once the compressor is switched on again.
Generally talking about the delivery/return temperature differences, the values recorded across the condenser (on ground side) ranges between 5-10°C (with peaks up to 15-20°C in correspondence with the compressor switch on), while those across the evaporator (user side) ranges between 1,5-3°C.

10. Coolable volume and system sizing

Once obtained the main results in terms of thermal power exchanged and mechanical power required by the compressor, these represented the basis for a first rough estimation of the volume that the geothermal heat pump system can actually cool. However, the aim of this thesis project was not that of providing an accurate representation of the thermophysical properties of the building, so all the results reported below were considered only in view of a preliminary evaluation of the system sizing.

Starting from these measures, the first step involved the thermal power exchanged at the evaporator (removed from the user internal environment) for the estimation of the coolable volume and, consequently, the coolable area.

In that way, the thermal power removed from the internal environment was linked with the coolable volume by means of a coefficient (size in W/m^3), suggested by many energy sector websites for a first evaluation.

Generally speaking, the Viessmann's website, according to that of Enea for instance, reports values for this kind of coefficient ranging between 25-30 W/m^3 for cooling and 35-40 W/m^3 for heating. These values are then subjected to variations related to the ambient under analysis, as the presence of a loft or poorly insulated walls, thus only the technical inspection of an experienced installer may determine accurately the cooling/heating demand.

Since each environment needs its "cold emission point", just as in the case of radiators for heating, the evaluation was performed considering a single environment, as the system prototype presents only one fan coil (representing the user).

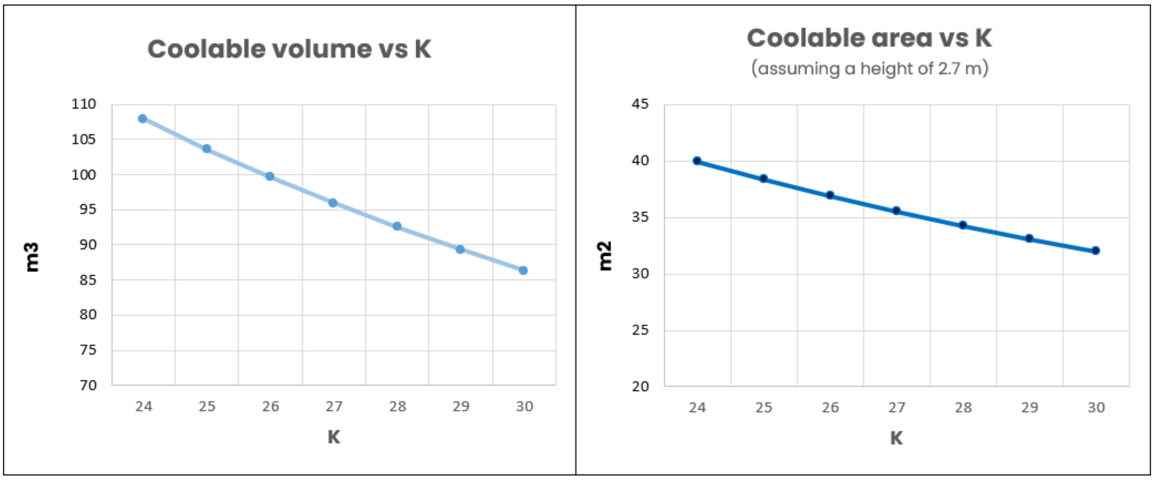

Figure 90: Coolable volume and Coolable area vs K (Excel)

From *Figure 90* it can be noted that, with the obtained amount of thermal power removed from the user environment, the area that can be effectively cooled ranges around 35-40 m^2 (considering K around 24-27 W/m^3).
As previously said, this is only an indicative value, and the K coefficient may assume higher values in the case of a poor insulation, involving results like those reported in the previous figure.

The second step differed from the previous one concerning the starting point, as it was represented by the environment to be cooled, rather than the thermal power to be removed from such ambient. In that way, the object was that of performing a sort of rough verification of the system sizing, checking if the thermal power removed from the "type" environment assumed was enough to ensure the target internal temperature, set to 27°C as example.
The environment considered to simplify the calculations was a little reference apartment with a rectangular plan, confining with two other apartments and a corridor assumed at the same set temperature, while the remaining side confined with the external environment. No partition walls were considered, so it actually consisted of an open space of about 40 m^2, with two windows located on the wall separating the indoor environment from the outside.
To verify if the size of the geothermal system analysed is sufficient to keep the indoor temperature at 27°C, it was necessary to calculate the energy needs of the environment selected, deriving the hypothetical thermal load for the cooling period considered.

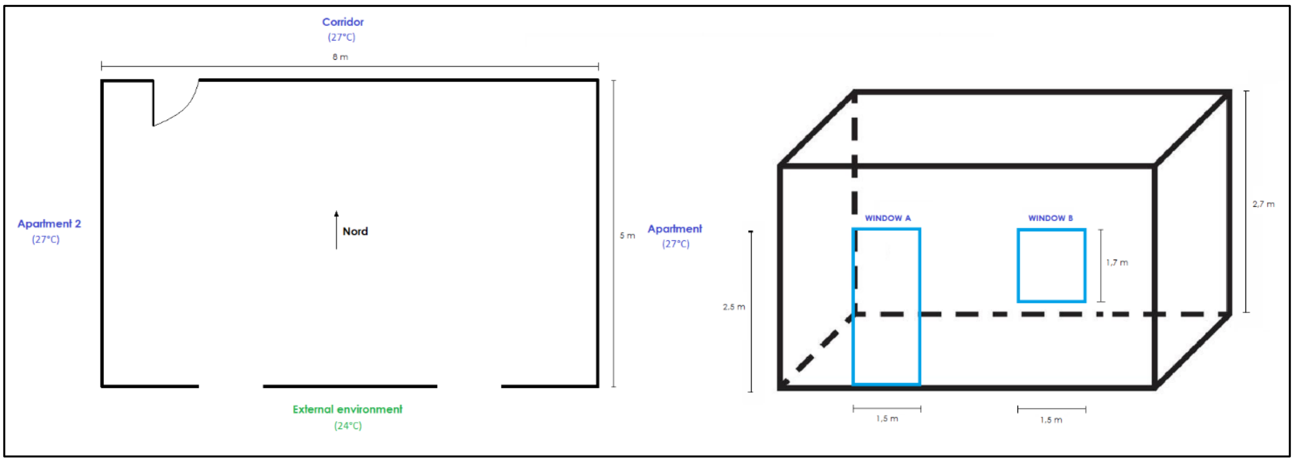

Figure 91: Reference apartment plan

The apartment reported in *Figure 91* was imaginarily located in Turin (climatic zone E), while the outdoor temperature considered was not the average value derived from the recordings of the experimental campaign section (formed of only ten days), but the average one reported for the month of July in Turin, around 24°C.
Among all the six surfaces, those considered as involving heat transfer mechanisms were the South-exposed one (confining with the external environment) and the top horizontal one. The others were considered as bordering environments at the same temperature (heat transfer neglected).

Dispersant surfaces	Exposition	Area [m^2]
Opaque vertical wall	South	15,3
Top roof	(horizontal)	40
Transparent surfaces (window A)	South	3,75
Transparent surfaces (window B)	South	2,55
Total dispersant surfaces [m^2]		61,6
Total cooled volume [m^3]		40

Figure 92: Dispersant surfaces measurements

Concerning the stratigraphy of the components of the transparent and opaque envelope, the climatic zone considered determines different requirements, concurring both to the thermal and sound insulation.
Referring to the Implementing Decree "Requisiti minimi" of D.Lgs. 192/2005, in the section referred to the climatic zone E, the limit value for the thermal transmittance (U) was set to 0,30 W/ m^2K for vertical opaque walls, to 0,26 W/ m^3K for horizontal or inclined opaque roofs and to 1,90 W/m^2K for transparent technical closures.
Hence, the stratigraphy selected for the components reported in *Figure 92* was derived from few reference ones reported on the material of the course "Energetica dell'edificio" (Prof. Capozzoli), in order to respect these limits.
The overall transmittances obtained for the vertical wall and the top roof were calculated as the inverse of the sum of the thermal resistances of the layers involved, which in turn was calculated as the ratio between the thickness of the layer and the thermal conductivity of the material of which it is composed of (with the hypothesis of homogeneous layers). Among the layers, were considered also the contributions of the internal/external air, as they involve heat transfer

mechanisms (convection and radiation) with the surface of the vertical wall and that of the top roof.

Regarding the transparent surfaces, it was considered a softwood frame with a thickness of 70 mm, while the useful properties were derived from ACG Yourglass website.

The transmittance of the glass surfaces was then calculated as the weighted average among that of the frame, the glass one and an additional contribution represented by the linear thermal transmittance (Ψg).

$$Uw = \frac{AgUg + AfUf + lg\Psi g}{Ag + Af}$$

Where Uw is the overall transmittance of the window, Ug is only related with the glass, Uf is referred to the frame and lg is the perimeter length of the glass.

<table>
<tr><th>Opaque vertical wall</th><th>Top roof</th><th>Window A</th><th>Window B</th></tr>
<tr><td>Aria interna</td><td>Aria interna</td><td rowspan="2">Planibel Clear</td><td rowspan="2">Planibel Low-e</td></tr>
<tr><td>Malte di gesso per intonachi o in pannelli senza inerti</td><td>Intonaco di calce e gesso</td></tr>
<tr><td>Isolante termico in poliuretano espanso in situ per interni</td><td>Blocco da solaio (Codice elemento: 2.1.07i)</td><td rowspan="3">Intercapedine d'aria</td><td rowspan="3">Intercapedine d'aria</td></tr>
<tr><td>Doppio strato di mattone semipieno (250x120x120) ISO10355</td><td>Bitume</td></tr>
<tr><td>Malta di calce o di calce e cemento all'esterno</td><td>polistirene espanso sinterizzato in lastre interne</td></tr>
<tr><td rowspan="2">Aria esterna</td><td>Ghiaia grossa senza argilla</td><td rowspan="2">Planibel Clear</td><td rowspan="2">Planibel Low-e</td></tr>
<tr><td>Aria esterna</td></tr>
<tr><td>U = 0,297 W/m3K</td><td>U = 0,258 W/ m²K</td><td>U = 2,65 W/ m²K</td><td>U = 1,57 W/ m²K</td></tr>
</table>

Figure 93: Dispersant surfaces' layers and overall thermal transmittances

The values obtained for the four elements, reported in *Figure 93,* were then used to calculate the various contributions to derive the cooling power required.

As can be noted, the value of the thermal transmittance obtained for the window A did not respect the limit imposed by the legislative decree mentioned above, anyway it was considered for the calculations.

Proceeding with the main terms considered for the thermal balance of the control volume, represented by the indoor environment to keep at the set point temperature, they were mainly five:

- $\mathrm{Q_{imp}}$ (thermal power to be removed by the geothermal system)
- $\mathrm{Q_{sol}}$ (solar contributions)
- $\mathrm{Q_{int}}$ (internal contributions)
- $\mathrm{Q_{ve}}$ (dispersions by ventilation)
- $\mathrm{Q_{tr}}$ (dispersions by transmission)

Considering the summer season, the thermal balance assumed such expression:

$$Q_{imp} + Q_{tr} + Q_{ve} = Q_{sol} + Q_{int}$$

Then a further coefficient, the utilization factor ($\eta_{C,ls}$), was introduced to take into account also the dynamic properties of the building envelope. Specifically, considering summer operation, it was multiplied by the dispersions ($Q_{sol} + Q_{int}$). Starting with the dispersions by transmission, both the contributions related with the opaque and transparent components were calculated:

$$H_{tr,OP} = \sum_{j=1}^{n} U_{tr,OP,j} \cdot A_{tr,OP,j} = 15{,}3 \cdot 0{,}297 + 40 \cdot 0{,}258 = 14{,}86\ W/K$$

$$Q_{tr,OP} = H_{tr,OP} \cdot (T_{ai} - T_{ae}) = 14{,}86 \cdot (27 - 24) = 44{,}58\ W$$

$$H_{tr,W} = \sum_{j=1}^{n} U_{tr,W,j} \cdot A_{tr,W,j} = (1{,}7 \cdot 1{,}5) \cdot 1{,}57 + (2{,}5 \cdot 1{,}5) \cdot 2{,}65 = 13{,}941\ W/K$$

$$Q_{tr,W} = H_{tr,W} \cdot (T_{ai} - T_{ae}) = 13{,}941 \cdot (27 - 24) = 41{,}823\ W$$

An additional contribution considered was that of the heat flux dispersed through the thermal bridges, located in correspondence of the two edges of the South-facing vertical wall (interface with the vertical wall of the confining apartments), the vertical wall/roof interface and the frame/wall interface for the two windows:

$$H_{tr,PT} = \sum_{j=1}^{n} \Psi_{i,j} \cdot L_j = (0{,}025 \cdot 2{,}7) \cdot 2 + (0{,}05 \cdot 2{,}7) + (0{,}55 \cdot 8) + (0{,}1 \cdot 14{,}4) = 6{,}11\ W$$

$$Q_{tr,PT} = H_{tr,PT} \cdot (T_{ai} - T_{ae}) = 6{,}11 \cdot (27 - 24) = 18{,}33\ W$$

Summing all the contributions, the overall dispersion by transmission amounted to:

$$\boldsymbol{Q_{tr,TOT}} = Q_{tr,OP} + Q_{tr,W} + Q_{tr,PT} = 104{,}733\ W$$

The term calculated subsequently was that related to solar contributions, starting with the opaque building envelope:

$$T_{sa,sud} = T_{ae} + \frac{a_s \cdot I_{v,sud}}{h_e} = 24 + \frac{0{,}45 \cdot 690}{25} = 36{,}42°C$$

$$Q_{OP,sol,wall} = U_{op,h} \cdot \left(T_{ai} - T_{sa,sud}\right) \cdot A_S = 0{,}297 \cdot (27 - 36{,}42) \cdot 15{,}3 = -42{,}80\ W$$

In the two equations reported above, T_{sa} is the "sole-aria" temperature, while $I_{v,sud}$ is the average solar radiation incident on the vertical surface (South-exposed). The remaining terms a_s and h_e represent respectively the solar absorption coefficient and the liminal thermal exchange coefficient on the external wall.

$$T_{sa,horizontal} = T_{ae} + \frac{a_s \cdot I_h}{h_e} = 24 + \frac{0{,}45 \cdot 271}{25} = 28{,}878°C$$

$$Q_{OP,sol,roof} = U_{op,h} \cdot \left(T_{ai} - T_{sa,horizontal}\right) \cdot A_S = 0{,}258 \cdot (27 - 28{,}878) \cdot 40 = -\ 19{,}38\ W$$

The minus sign of the results related with the solar contributions reported above refers to the fact that the heat flux is directed towards the indoor environment.
Regarding the transparent building envelope, the procedure adopted was the following:

$$Q_{sol,w} = \left(A_{g,A} \cdot g_A + A_{g,B} \cdot g_B\right) \cdot I_{v,sud} = (2{,}12 \cdot 0{,}39 + 3{,}4 \cdot 0{,}77) \cdot 690 = 2376{,}912\ W$$

Where g is the solar factor, derived from the data sheets of the window types selected, and the areas reported are those referred only to the glass.
The last formula adopted, related with the transparent building envelope, is a simplified one, introduced under the hypothesis of negligible shading and shielding phenomena (in that way the solar contribution to be removed for the cooling season increased).

The overall solar contribution, summing all the terms calculated before, amounted to:

$$\boldsymbol{Q_{sol,TOT}} = Q_{OP,sol,wall} + Q_{OP,sol,roof} + Q_{sol,w} = 2439{,}092\ W$$

Considering then the dispersions by ventilation, the first step consisted in the determination of the current airflow, successively multiplied by the specific heat of the air (c_a) to calculate the ventilation global heat exchange coefficient (H_{ve}).

$$\dot{m}_a = \rho_a \cdot \dot{V}_a = \frac{\rho_a \cdot n \cdot V}{3600} = \frac{1{,}2 \cdot 0{,}5 \cdot 99{,}5}{3600} = 0{,}0166\ \frac{kg}{s}$$

More in detail, the terms n refers to the hourly air circulation, while the net volume (V) was calculated approximately considering the thickness of the walls.

$$H_{ve} = c_a \cdot \dot{m}_a = 1000 \cdot 0{,}0166 = 16{,}6\ \frac{W}{K}$$

$$\boldsymbol{Q_{ve}} = H_{ve} \cdot (T_{ai} - T_{ae}) = \ 16{,}6 \cdot (27 - 24) = 49{,}8\ W$$

The final term to be calculated was that related with the internal contributions, which could be sensible or latent. Specifically, it was calculated with reference to the intended purpose, as suggested by the relative legislation. In that way, talking about a floor area below 120 m2, this term was calculated as:

$$\boldsymbol{Q_{int}} = 7{,}987 \cdot A_f - 0{,}0353 \cdot A^2 = 7{,}987 \cdot 36{,}86 - 0{,}0353 \cdot 36{,}86 = 246{,}44\ W$$

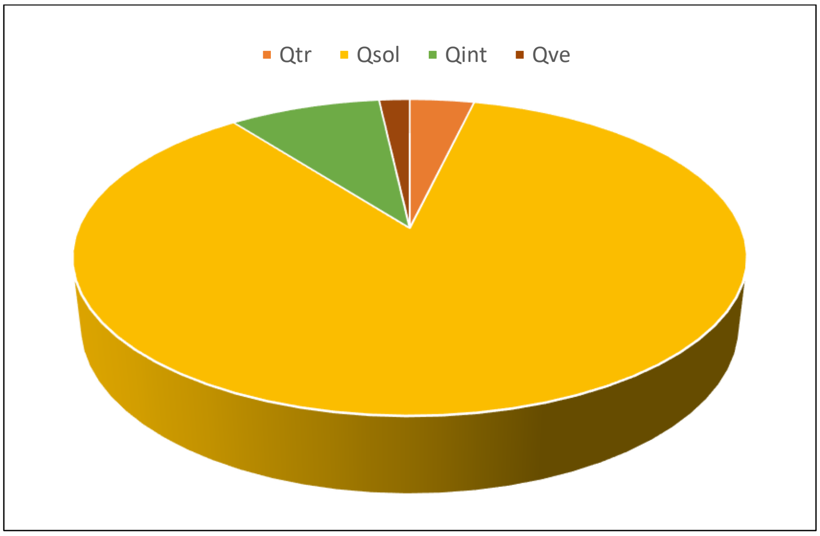

Figure 94: Repartition of the total heat flux among the various terms (Excel)

Finally, all the terms previously calculated were used for a preliminary estimation of the thermal power that should be removed from the indoor environment, by the heat pump system (Q_{imp}).

$$Q_{imp} = Q_{int} + Q_{sol} - \eta_{C,ls} \cdot (Q_{tr} + Q_{ve})$$

Concerning the utilization factor, it lies between 0 and 1 and for the summer season it multiplies the dispersions. Generally, its value goes towards 1 considering more massive building envelopes, because the dispersions could be better exploited. For that particular case it was assumed equal to 0,70.

$$\boldsymbol{Q_{imp}} = 246{,}44 + 2439{,}092 - 0{,}70 \cdot (104{,}733 + 49{,}8) = 2577{,}36\ W \cong 2{,}58\ kW$$

The value obtained was then compared with the thermal power exchanged at the evaporator of the heat pump, always considering that the calculations performed were the results of many assumptions, representing so a general indication.

For the period ranging between the 14th and the 26th of June 2022, the average value for the heat exchanged at the evaporator amounted to 2,59 kW, considering all the ten days (also the last ones reporting the compressor problem previously mentioned), or to 2,43 kW, neglecting the values obtained for the last three days.

Comparing the average of the results obtained during the June 2022 experimental campaign with the required thermal power coming out from the previous calculations, for the “type” apartment selected, it can be noted that they are quite close to each other. This fact suggests that, for similar cases, the approximative calculation of the coolable volume adopted as first step gave a range of results not too far from the reality.

Even if further calculations with proper software must be performed, an important fact is that the geothermal system analysed sems to be able to satisfy the cooling needs of a small volume, as the one which hosts the fan coil (considering in this case the different components of the building envelope and the confining environments).

10.1 Ground heat exchangers and land use

Always considering the summer operation of the geothermal system, few final considerations involved the surface of the geothermal probes, and specifically its connection to the thermal power removed at the evaporator (the useful effect).

In the configuration considered (reported in section 4.2.2), the three panels provided an overall effective heat exchange area of approximately 18,9 m^2, which allowed to inject into the ground a thermal power ranging around 3 kW (averaged on daily basis) in the period considered. This amount of heat was then removed from the refrigerant of the heat pump circuit, allowing to extract from the secondary circuit around 2,5 kW (again on daily basis). However, before going any further, it is necessary to underline again that all the results obtained for the June 2022 experimental campaign are related with many factors, as the site hosting the experimental field (ground composition and depth), the period considered and the meteorological conditions.

A variation of one or more of these conditions, together with the arrangement of the heat exchange panels in a different configuration (the investigated one was that in series) or the implementation of different shapes for the probes, would cause a modification of the thermodynamic quantities calculated too, that should be assessed through additional tests.

In that case, to reason in terms of scalability of the geothermal probes area, and so meeting different thermal loads, all the factors reported above were assumed as unaltered. This means that the configuration considered was always that involving all the three circuits connected in series.

The starting point in that direction was that of assessing the amount of thermal power exchanged at the evaporator per m^2 of the geothermal probes, employing the results arranged on daily basis. In that way, the procedure was simplified by considering a direct relationship between the two, explored in the form of:

$$Q_{ev} = S_{tot,GHEs} \cdot Y$$

Where Y is a coefficient with the dimension of kW/m² and $S_{tot,GHEs}$ is the total effective area of the ground heat exchangers.

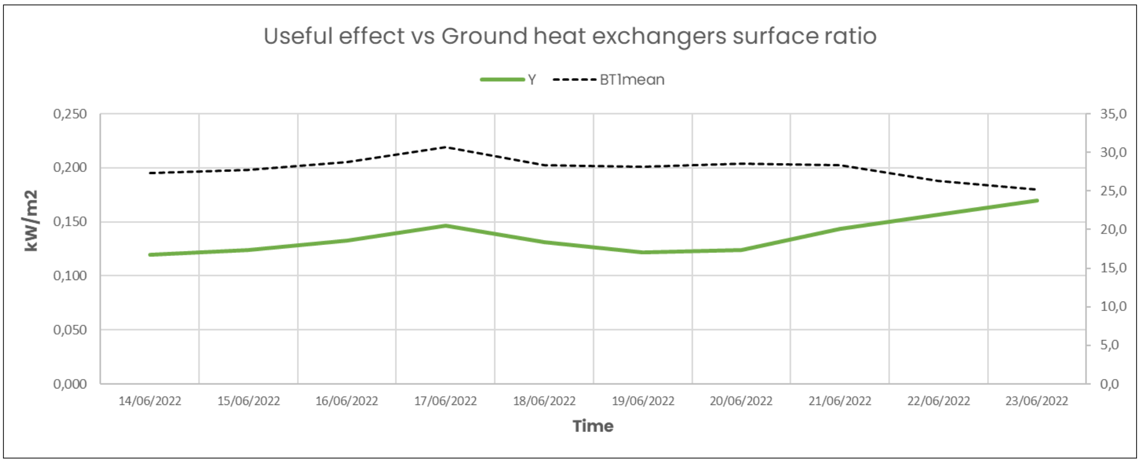

Figure 95: Useful effect vs Ground heat exchangers surface ratio (Excel)

Computing the ratio starting both from the data reported on daily basis and the actual ones provided by the heat pump monitoring system, the results obtained always ranged approximately between 0,10 kW/m² and 0,15 kW/m².

As the effective heat transfer surface with the ground, the one represented by the geothermal probes, was not modified over the experimental campaign of June 2022 (involving all the three circuits in series connection), this ratio depended on the variation of the thermal power exchanged at the evaporator. Indeed, in *Figure 95*, it can be noted how the ratio follows the trend of the outdoor temperature (BT1), similarly as it occurred for $\mathrm{Q_{ev}}$ (with the same deviation involving the last three days because of the compressor-related operating problems). Anyway, it appears quite constant (without large oscillations), assuming an average value which ranges around 0,129 kW/m², representing the amount of thermal power extracted from the indoor environment per m² of geothermal probes surface (neglecting the thermal losses of the fan coil circuit).

Considering that the average Y calculated was based on the results obtained from a sampling time of just ten days, further experimental campaigns should be analysed in the future, to improve its accuracy by considering also different periods and operation modes.

In that way, the values of Y obtained could be analysed, looking for an average one that may be used by the manufacturer for the preliminary assessment of a new system (to estimate the heat exchange surface needed on the ground side). Alternatively, another approach could consist in the direct exploitation of these results coming from different experimental campaigns to define a range for Y, with the aim of building a table from which the value for a specific case could be derived with more accuracy though interpolation.

This topic could be also extended considering the approach presented in section 9 for the approximative estimation of the coolable volume/area, deriving a relationship between this last one and the heat transfer surface required for the geothermal probes. Indeed, the preliminary formulation presented as first step showed a sufficiently good correspondence with the results of the second one, based on the definition of a "type" environment.

Thinking of scaling the probes surface with reference to a specific target volume to be cooled, a preliminary formulation could assume such kind of form:

$$S_{tot,GHEs} = \frac{K \cdot h}{Y} \cdot A_{cooled} = \frac{K}{Y} \cdot V_{cooled}$$

Where $\mathrm{V_{cooled}}$ and $\mathrm{A_{cooled}}$ are respectively the volume and the area to be cooled, while K is the coefficient introduced in section 9 (assumed around 25 W/ m^3 for cooling, depending on the insulation level).

In that way, the geometry of the geothermal probes analysed in the previous sections could be increased/reduced in size on the basis of the target volume, always under the same assumptions considered for the starting case.

11. General overview for the heating season

Few calculations, using the fixed pressures approach, were performed also for the heating season operation, aiming at better understanding the heat pump operation and check the results obtained.

The sets of measurements analysed in this brief overview come from the past years, considering for instance 2019, while the fixed pressures approach was preferred with respect to the variable pressures one because of the higher number of on/off switching of the compressor experienced during the heating period.

Indeed, the variable pressures approach, originally designed compatibly with the cooling operation previously analysed, suffers from numerous on/off transients, as the pressures profiles present wider oscillations linked with higher DeltaLcompr deviations. In that way, all the measurements close to these events would lead to less reliable results, affected by the numerous deviation peaks.

Regarding the MATLAB script, it was adapted to the different configuration of the sensors installed on the heat pump (heating operation in section 4.3), while the main structure mentioned in the previous sections remained almost the same.

The data recordings used for the calculations were derived from an experimental campaign which took place in the period ranging between October 24th and November 20th 2019, also treated in previous thesis works as those of Filippo Sterrantino and Raffaele Rondina.

However, the time span considered for this section did not involve the full experimental campaign, but a briefer period ranging between October 25th-30th (more precisely, each set of 24h measurements started at 14:52:27 of the mentioned day, ending at 14:52:02 of the following one), compatibly with the data available.

Additional information concerned the delivery temperature to the user, set to 45°C and the configuration of the ground heat exchangers, that involved the series arrangement of the three circuits.

The active cooling start, and so the compressor switch on, was set once the cumulative of DM (degree minutes) reaches -60°Cmin.

11.1 COP and power calculation

The COP and power calculation followed procedures analogous to those presented respectively in section 8.1 and 8.2, even if in that case the indoor unit and the outdoor one are reversed.

$$COP = \frac{Q_{cond}}{L_{compr}} = \frac{q_{cond,R407C}}{l_{compr,R407C}}$$

The COP definition for the heating operation differs by the numerator, as the useful effect becomes the heat provided to the final user, while the work spent is again that required by the compressor.

$$q_{cond,R407C} = h_{compr,out} - h_{sat,liq}$$

$$l_{compr,R407C} = h_{compr,out} - h_{compr,in}$$

The hypotheses assumed for the summer operation (as no subcooling), and especially the measures adopted for the fixed pressures approach were still considered for the winter operation.
That was the case, for instance, of the location of the compressor inlet/outlet working points, which must not belong to the biphasic region to avoid liquid compression problems. Again, it was adopted the same monitoring process concerning the temperatures recorded by BT14 and BT17 (their position did not change) and the selected pressure levels for the two branches of the refrigerant circuit.
As the pressure levels were not calculated by an external algorithm, the values selected must be additionally checked in terms of the number of measurements discarded, avoiding too high percentages which could undermine the calculation of the desired average quantities.
The manual selection of the pressure levels also eliminated the need for any correction factor, as with the fixed pressures approach both the heat exchanged and the compression work were calculated by means of the enthalpy change involved.

In that way, the calculation of the specific heat for the compressor inlet/outlet was not required, and the direct use of the enthalpies involved errors below 1,5%, as previously reported for the summer operation.
Similarly to the cooling case, the water/glycol flow rate within the primary circuit was assumed as constant, even if the old value was not valid anymore, as higher mass flow rates were involved.
Again, no measures recorded by the flow meters were available, but the GP1 and GP2 pumps reported a 100% working condition, so the value assumed was the nominal one of 0,650 m³/h.

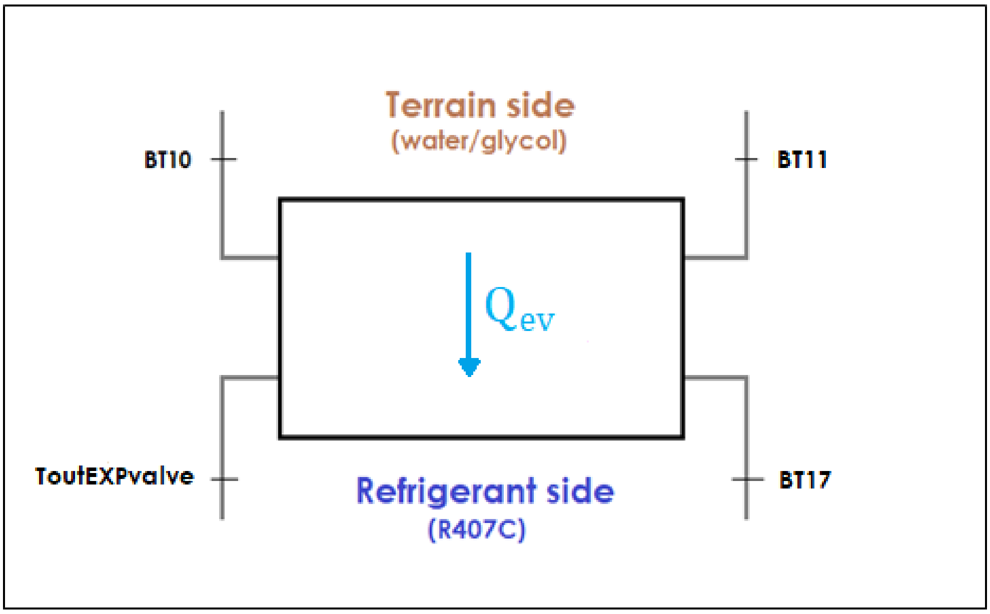

Figure 96: Evaporator simplified scheme

Once fixed, the water/glycol flow rate within the primary circuit, together with the temperature values recorded by the sensors BT10 and BT11, was used to derive the refrigerant mass flow rate in the heat pump circuit.

$$Q_{ev} = \dot{m}_{w/g} \cdot c_{p_{w/g}} \cdot (T_{BT10} - T_{BT11}) = \dot{m}_{R407C} \cdot q_{ev_{R407C}}$$

$$\dot{m}_{R407C} \cdot q_{ev_{R407C}} = \dot{m}_{R407C} \cdot \left(q_{cond_{R407C}} - l_{compr_{R407C}}\right)$$

$$\dot{m}_{R407C} = \frac{\dot{m}_{w/g} \cdot c_{p_{w/g}} \cdot (T_{BT10} - T_{BT11})}{q_{cond_{R407C}} - l_{compr_{R407C}}}$$

As for the cooling operation, the refrigerant mass flow rate obtained for each set of measurements was then multiplied by the specific quantities calculated by the MATLAB script (qev, qcond and lcompr) to obtain the expected extensive ones. Again, through the application of the first law of thermodynamics for open systems, also the water/glycol flow rate in the secondary circuit was derived:

$$Q_{cond} = \dot{m}_{R407C} \cdot q_{cond_{R407C}} = \dot{m}_{w/g} \cdot c_{p_{w/g}} \cdot (T_{BT12} - T_{BT3})$$

$$\dot{m}_{w/g\ (sec)} = \frac{Q_{cond}}{c_{p_{w/g}} \cdot (T_{BT12} - T_{BT3})}$$

11.2 Discussion of the results

Proceeding with the fixed pressures approach, similarly to what was performed in section 8.4, the main idea for that last part of the thesis is that of observing the system behaviour during the heating season too, then arranging the results in the form of graphs.
To do so, the couple of pressures 16/7 bar was selected to assess the winter performances, as it provided suitable results (Rondina, 2020), thus checking for the main effects of the strong intermittent behaviour of the heat pump on the system parameters.

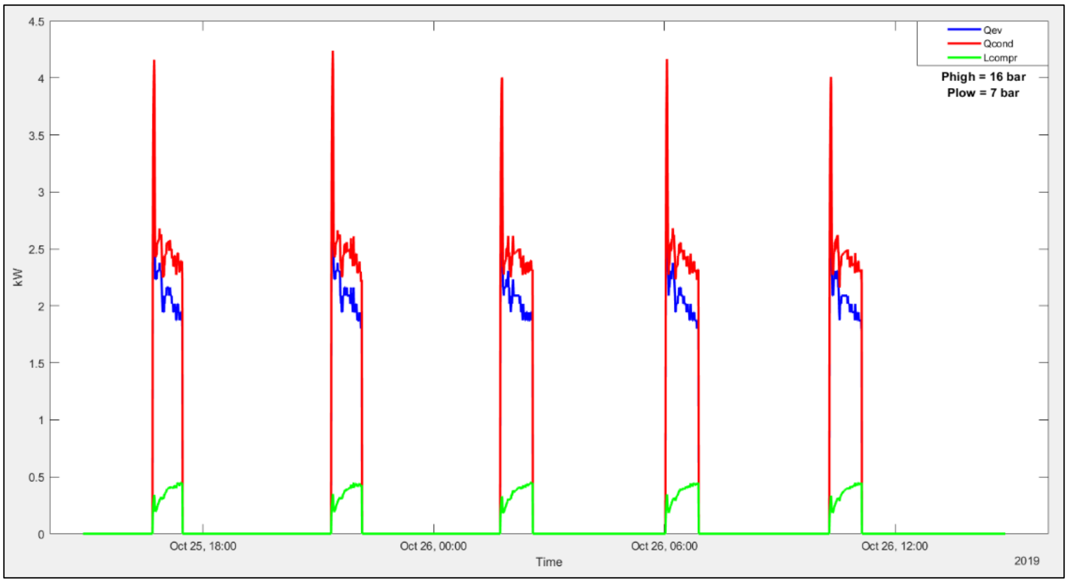

Figure 97: Qev, Qcond, Lcompr vs Time (MATLAB), 16/7 bar, October 25th 2019

From *Figure 97*, can be observed the first differences with respect to the summer operation previously discussed, as in that case the number of peaks, associated with the compressor switch on, was much higher.
The general trend for the thermal power exchanged both at the condenser and at the evaporator involves a first huge peak, followed by a stabilization towards lower values until the following switch off.
Again, these initial peaks are linked with the high temperature difference that is established once the compressor is turned on after an off period.
Considering the hypothesis of no subcooling, the working point representing the condenser outlet lays on the saturated curve, hence the related temperature is not that recorded by the sensor B15 but a function of only the pressure (Phigh).

Because of this assumption, once the high pressure level is fixed, the temperature at the condenser outlet (on the refrigerant side) assumes the value of the saturated liquid temperature at the pressure Phigh, so the temperature difference is a function of only the values recorded by BT14.

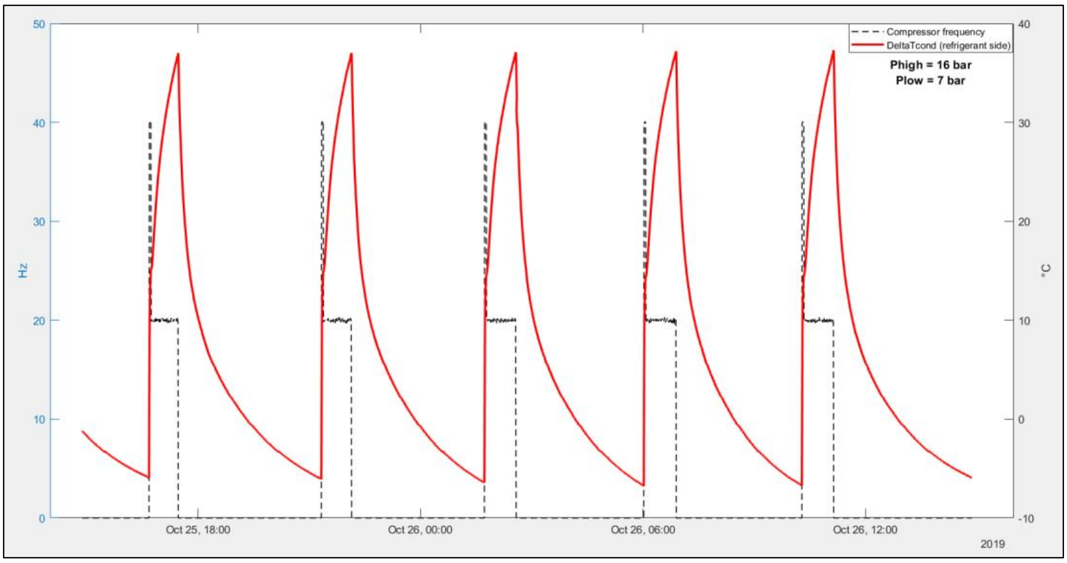

Figure 98: DeltaLcompr (refrigerant side) vs Time (MATLAB), 16/7 bar, October 25th 2019

In *Figure 98* the DeltaT variation in relation to the compressor frequency can be noted, highlighting the incurrence of the growing trend in correspondence of the compressor switch on.

In that way the energy stored in the refrigerant fluid is transferred to the secondary circuit, causing a peak too in BT12 trend, which represents the delivery temperature to the user.

Indeed, because of the heat pump settings, it should reach the target value of 45°C, presenting then an oscillating trend managed by the heat pump switch on/off.

Regarding instead the effects that can be perceived on the other temperatures recorded by the BT sensors, they are analogous to those found for the summer operation, even if that time the ground is used as a heat source.

The heat extracted by the outdoor unit (the evaporator) is thus upgraded by the heat pump operation, to be then provided to the secondary circuit of the fan coil, now thermally connected with the condenser.

The data reported in *Figure 97* were used to calculate the COP of the system point by point, always excluding the set of measurements with the compressor off or those involving liquid compression phenomena.

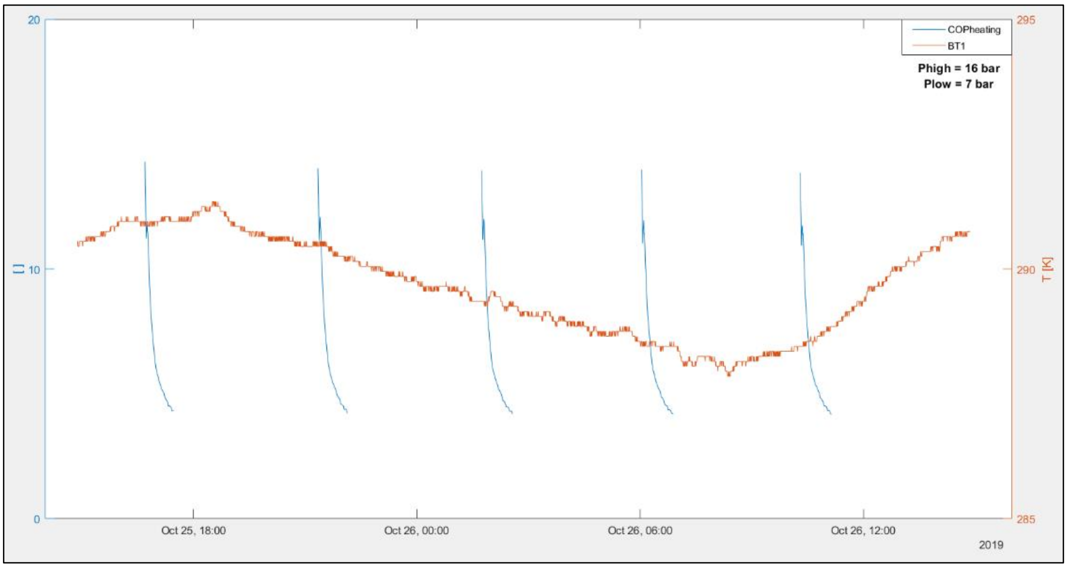

Figure 99: COP vs Time (MATLAB), 16/7 bar, October 25th 2019

The COP trend reported in *Figure 99* underlines other important differences with respect to the June 2022 cooling operation, which not only consist in the occurrence of peaks, but also involve huge discontinuities in the pattern.
After performing many tests, to better assess the situation, it was noted that these missing points were mostly due to the operating time of the heat pump, corresponding to the situation of the compressor switched off.
Considering for instance the case of October 25th reported above, roughly 82,7% of the measurements belonging to the set were discarded because of this problem, then considering also an additional little percentage of measures involving liquid compression (1%), discarded too.
This situation made the point-by-point representation, widely used in the previous sections, quite inefficient, as mostly of the COP values reported above were still affected by the switch on events.
In that way, details such as the effect of the outdoor temperature on the COP could not be noted easily, so the results were directly considered on daily basis, "cleaning" the values obtained from those immediately close to the switch on events, similarly to what was done for June 2022 experimental campaign (considering the set of measurements reporting a compressor switch off/on).

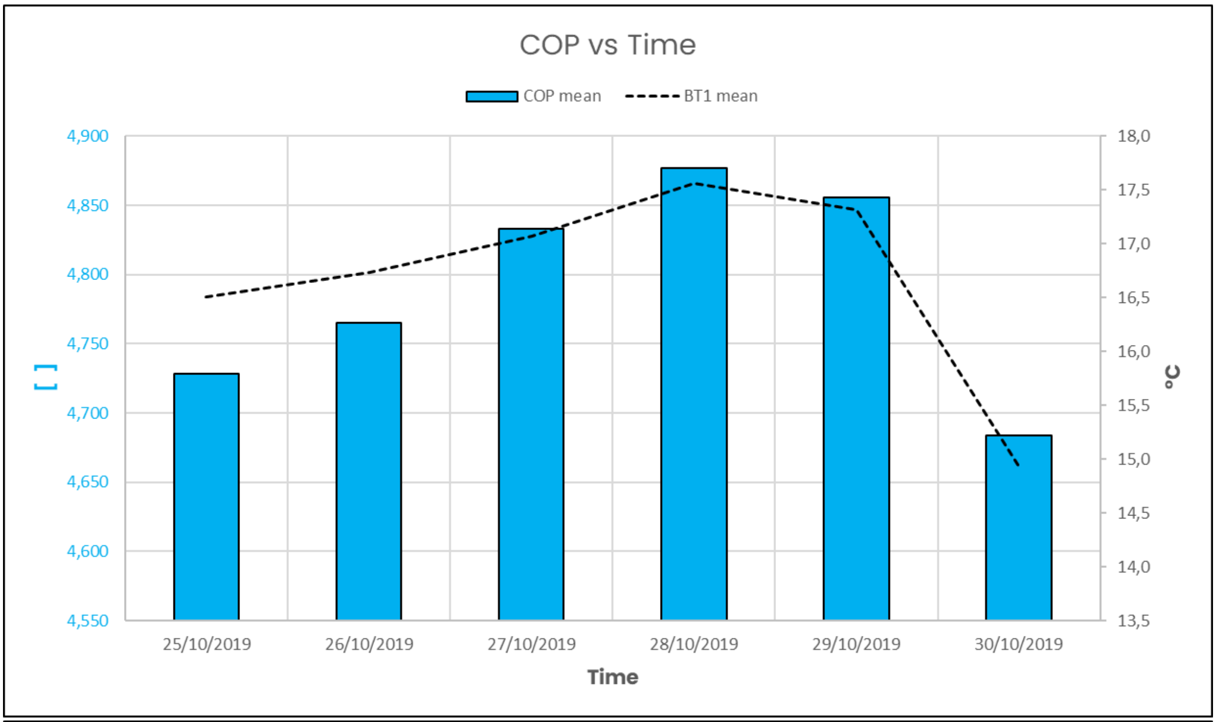

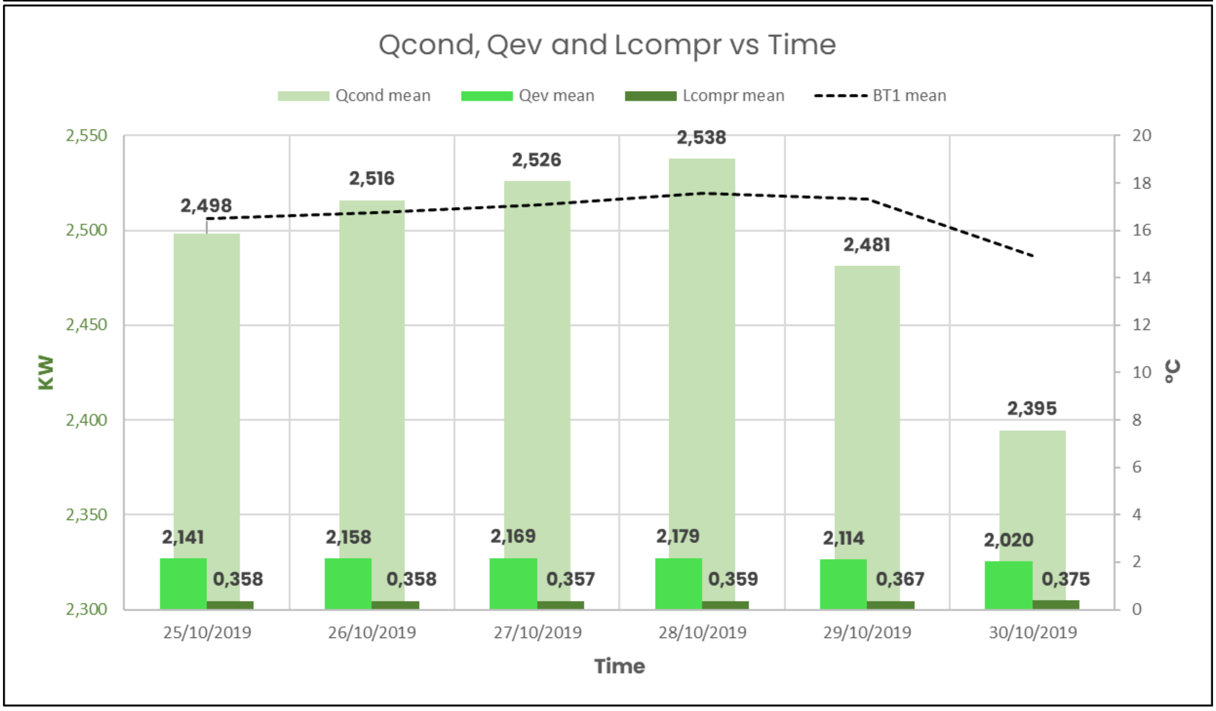

Figure 100: COP vs Time (Excel), 16/7 bar, October 25th-30th 2019

Figure 101: Qcond, Qev and Lcompr vs Time (Excel), 16/7 bar, October 25th-30th 2019

Grouping the results on a longer basis, the expected trends for the main thermodynamic quantities were the expected ones, presenting some differences with respect to the summer operation.

For instance, looking at *Figure 100*, this time the COP trend follows the pattern of the outdoor temperature, as it reached higher values during warmer days.

This occurred because in that case the aim was no more that of removing heat from the indoor environment, but keep it warm, indeed the higher compression work is reported for the coldest days (October 29th and 30th).
Unlike the cooling operation, now a countercheck for the COP values could be represented by the fact that the lowest values occurred in correspondence of the coldest day of the list, October 30th.
In summary, the results obtained in this heating campaign, relatively to the pressure levels adopted, seem as good as those obtained for the cooling season, with COP values that ranges between 4 and 5.

12. Conclusions

Starting from the huge amount of data recorded by the heat pump system, together with the indispensable help of MATLAB to process all the deriving calculations, it has been possible to assess the performances of the GeothermSkin system installed in the experimental field at the Energy Center for the cooling season, for which very few data were available. Indeed, as already mentioned, the start of this Master Thesis work has slightly anticipated the occurrence of the summer season, allowing to study a period which has not been the subject of other studies.

From this basis, the system was analysed resorting to the post processing of the data recorded from the system sensors, which provided the values of temperature needed to build the thermodynamic cycle of the heat pump.

In this perspective, the methods analysed for the estimation of the pressure levels (with the implementation of the pressure calculation algorithm) were also important to define the inlet/outlet conditions of the main components of the refrigerant circuit, allowing the calculation of the required thermodynamic properties to determine the power exchanged and the COP.

Indeed, the choice to dedicate few sections to the pressure levels determination was motivated by the fact that they represent one of the most relevant deficiencies within the monitoring systems, in view of a complete determination of the heat pump cycle. Anyway, the different approaches explored led to the calculation of the results expected.

Finally, the analysis of these results provided a general framework of the system operation, compatibly with the hypothesis assumed, which was the main goal expected from the energy assessment performed.

Regarding the future, other projects may be carried out running new experimental campaigns, for different periods of the year, considering the implementation of pressure sensors too, even if their installation within the heat pump circuit could be not so simple. Otherwise, the same path could be taken choosing to refine the approach adopted in this thesis for the determination of the pressure levels or considering some scenarios with different fixed values (similarly to what has been done in thesis such as those of Rondina and Sterrantino).

At the same time, an additional concept could be studied even for the heating season, trying to compensate for the higher number of on/off transients which represent a significant issue in the calculation of the thermodynamic quantities, causing many peaks in the COP trend for instance, and so moving much further from a stationary situation.

Nevertheless, the results obtained for the cooling season, together with those regarding the heating one, suggest a quite great potential for the GeothermSkin energy system, with COP values ranging between 4-5 and a useful effect around 2,5 kW for both the operation modes ($\mathrm{Q_{ev}}$ for cooling and $\mathrm{Q_{cond}}$ for heating) considering a power consumption between 0,3-0,6 kW ($\mathrm{L_{compr}}$).

This means that the GeothermSkin energy system possesses the numbers to become more than a prototype, considering that these results are also accompanied by a sustainable investment for the geothermal heating field, without involving the huge depths required for the high potential geothermal systems. Indeed, the system is conceived to minimize costs and is characterized by a negligible horizontal area occupation, together with the possibility to be installed during both building construction or refurbishment.

13. Bibliography

REN21 (2022), Renewable 2022 Global status report

Papurello D. (2022), Slides of "Laboratori di impianti energetici" course

Lo Russo S. (2021), Slides of "Geothermal energy" course

Cattoni E. (2020), Le geo-strutture energetiche: una sfida per il futuro. From https://www.rinnovabili.it/energia/geotermia/geo-strutture-energetiche-sfida-futuro/

Nowak T. (2021), Heat pumps – a renewable energy technology?. From REHVA Journal

International Energy Agency (2020), Tracking Heat Pumps 2020. From https://www.iea.org/reports/tracking-heat-pumps-2020

Thermal Control Business Update (2019), Heat pumps: The new kid on the block in energy efficiency. From https://thermalcontrolmagazine.com/behind-the-scenesdesign/heat-pumps-the-new-kid-on-the-block-in-energy-efficiency/

Refrigera industriale, PROGETTAZIONE TERMO-FLUIDO-DINAMICA DI VALVOLA A SFERA DI INVERSIONE A 4-VIE. From https://www.refrigera.eu/it/cases/thermo-fluid-dynamic-design-of-a-4-way-reversing-valve

The Engineering Mindset (2017), Reversing valve - Heat Pump. How it works, Operation. From https://youtu.be/r8n1_6qmsKQ

Mecobat. From https://mecobat.com/it/home/

SWEP, Brazed plate heat exchangers. From https://www.swep.net/technology/brazed-plate-heat-exchangers/

Baralis M. (2020), Optimisation of geothermal resources in urban areas. Doctoral Dissertation

Rondina R. (2020), Analisi sperimentale di una pompa di calore geotermica in ambito residenziale. Master’s thesis.
Sterrantino F. (2021), Analisi energetica di una pompa di calore geotermica in ambito residenziale. Master’s thesis

Enea (2019). From https://www.efficienzaenergetica.enea.it/servizi-per/cittadini/interventi-di-efficienza-e-risparmio-energetico-nelle-abitazioni/impianti/raffrescamento/tecnologie-e-etichetta-energetica-raffrescamento/dimensionamento.html

Viessmann (2021), Come scegliere la potenza di un climatizzatore. From https://residenziale.viessmannitalia.it/come-scegliere-un-climatizzatore-in-base-ai-metri-quadri

Consulente energia, COME CALCOLARE LA POTENZA FRIGORIFERA NECESSARIA PER UN CLIMATIZZATORE. From http://www.consulente-energia.com/ba-dimensionamento-di-un-climatizzatore-calcolo-della-potenza-in-btu-ora-o-kw-per-mq-di-superficie-o-per-mq-di-volume-dei-climatizzatori.html

Capozzoli A. (2018), Educational material from the course “Energetica dell’edificio. Thermophysics section

AGC Yourglass. From http://www.yourglass.com

14. Appendix

```
function[Plow,Phigh,Pressures,err]=PressuresCalc(BT14,BT17)


% Plg = P low guesses  [Pa]
% Phg = P high guesses  [Pa]

m = 40;                          %Number of elements for the pressures arrays

Plg = linspace(400000,750000,m);
Phg = linspace(800000,1600000,m);
%different ranges have been investigated for both Phigh and Plow

eps = 0.20;                      %Max tolerance for Deltalcompr (the algorithm searches then the smallest value)
n = size(BT14,1);
N = m*m;                         %Number of combinations between the two arrays

Pressures = zeros(n,2);          %Matrix containing the Plow-Phigh couples
delta = zeros(N,n);              %Indicates the difference between lcomprA and lcomprB
err = zeros(n,1);                %Error associated with the pressures determination
lcomprAA = zeros(n,1);
lcomprBB = zeros(n,1);

Klow=0.95;                       %Coefficient introduced to match the values of Cplow calculated with CoolProp and CoolPack

%% Creation of the matrix of the possible combinations among the elements of Plg and Phg

i = 0;
Pairs = zeros(N,2);              %Matrix where the couples of pressures are saved

for val1 = Plg
    for val2 = Phg
        i = i + 1;
        Pairs(i,1) = val1;
        Pairs(i,2) = val2;
    end
end


%% CODE OF THE ITERATIVE PROCEDURE

for j=1:n

val=1;                           %counter used to find the minimum delta

for k=1:N

    %Verification that the point does not fall in the biphasic region
    TsatBP=py.CoolProp.CoolProp.PropsSI('T', 'P', Pairs(k,1),'Q', 1, 'R407C');
    TsatAP=py.CoolProp.CoolProp.PropsSI('T', 'P', Pairs(k,2),'Q', 1, 'R407C');

    if BT17(j)>TsatBP && BT14(j)>TsatAP

    Phigh = Pairs(k,2)/1e5;
    Plow = Pairs(k,1)/1e5;

    %lcompr calculation way A
    CPlow = py.CoolProp.CoolProp.PropsSI('C', 'P', Pairs(k,1),'T', BT17(j), 'R407C')*Klow;
    CPhigh = py.CoolProp.CoolProp.PropsSI('C', 'P', Pairs(k,2),'T', BT14(j), 'R407C');
    CPm = (CPhigh+CPlow)/2;
    lcomprA = CPm*(BT14(j)-BT17(j));

    %lcompr calculation way B
    Hlow = py.CoolProp.CoolProp.PropsSI('H', 'P', Pairs(k,1),'T', BT17(j), 'R407C');
    Hhigh = py.CoolProp.CoolProp.PropsSI('H', 'P', Pairs(k,2),'T', BT14(j), 'R407C');
    lcomprB = Hhigh-Hlow;


    delta(k,j) = abs(lcomprA-lcomprB)/max([lcomprA lcomprB]);

    if delta(k,j) < eps && delta(k,j) < val

    Pressures(j,1) = Pairs(k,1);
    Pressures(j,2) = Pairs(k,2);
    val = delta(k,j);
    lcomprAA(j) = lcomprA;
    lcomprBB(j) = lcomprB;

    end

    end

end

err(j) = val;

end

Plow = Pressures(:,1);
Phigh = Pressures(:,2);
```

Figure A.1: Pressures calculation algorithm script, used in the variable pressures approach